To study the process parameters involved in Tungsten Inert Gas Welding of Austenitic Stainless Steel Alloys SS-310 and SS-316

A THESIS

Submitted in the partial fulfilment of requirement for the award of degree

MASTER OF ENGINEERING

IN

PRODUCTION AND INDUSTRIAL ENGINEERING

Submitted by

SAURABH JETLEY

Regn. No. - 821082004

Under the supervision of

Dr. V.K. SINGLA

Associate Professor

Department of Mechanical Engineering

Thapar University, Patiala

DEPARTMENT OF MECHANICAL ENGINEERING

THAPAR UNIVERSITY

PATIALA - 147004, INDIA

(DECEMBER-2013)

DECLARATION

I hereby declare that the work done in the thesis report entitled **"To study the process parameters involved in Tungsten Inert Gas Welding of Austenitic Stainless Steel Alloys SS-310 and SS-316"** submitted towards partial fulfilment of the requirement for the award of **Master of Engineering** degree(part time) in **Production and Industrial Engineering** in **Mechanical Engineering Department** of **Thapar University, Patiala,** is an authentic record of the work carried out by me under the supervision and guidance of **Dr V.K. Singla, Associate Professor** of **Department of Mechanical Engineering, Thapar University, Patiala.**

The matter embodied in this report has not been submitted in part or full to any other university or institute for the award of any degree.

Saurabh Jetley

SAURABH JETLEY

This is to certify that above declaration made by the student concerned is correct to the best of my knowledge and belief.

03/01/14

Dr. V.K. SINGLA

Associate Professor,

Department of Mechanical Engineering,

Thapar University, Patiala

Countersigned By:

Dr. AJAY BATISH

Professor and Head,

Department of Mechanical Engineering

Thapar University, Patiala

Dr. S. K. MOHAPATRA

Dean of Academic Affairs,

Thapar University, Patiala

ACKNOWLEDGEMENT

I am highly grateful to the authorities of Thapar University, Patiala for providing this opportunity to carry out the thesis work.

I would like to express a deep sense of gratitude and thank profusely to my thesis **guide Dr. V.K. Singla, Associate Professor, Department of Mechanical Engineering, Thapar University, Patiala,** for his invaluable guidance, encouragement and suggestions which inspired me to submit this thesis work in the present form.

I am extremely thankful to our Head of the Department **Dr. Ajay Batish**, for providing us an opportunity to learn in a very nice working environment having state of art facilities.

I would also like to express my sincere thanks to staff members **Mr. M.Suri, Mr. Surinder, Mr. Rath and Mr. Roshan** who motivated me and provided valuable technical assistance.

Very special thanks to my friends **Mr. Inderjeet Singh, Mr. Paras Ralhan and Mr. Narender** for offering me a helping hand whenever needed.

I would also like to thanks all employees and members belonging to Mechanical Engineering department for their everlasting support.

Last but not least, I would like to thanks my **parents** for their kind moral support that kept my spirit up always.

Saurabh Jetley

SAURABH JETLEY

Regn. No.-821082004

ABSTRACT

The purpose of carrying out the present study was to investigate the effects of various process parameters of tungsten inert gas welding on austenitic stainless steel SS-310 and SS-316. Four parameters namely welding current, type of gas, gas flow rate and included angle of weld plates during butt joint were varied at three levels. Orthogonal array L9 is used as per Taguchi Design of Experiments to finalise number of samples to be made for carrying out experimentation. Various welding tests like measuring the geometry of weld bead, bulk hardness test, dye penetration test, impact test, tensile test, micro-hardness test and chemical composition test of weld bead have been carried out on both materials to optimise best combination of process parameters in practice. The weld bead width for both materials depends on welding current and the type of shielding gas used in which current is most significant factor. On the other hand for weld bead height, the grove angle act as the most significant factor contributing to the result in a particular way and current is also having sub-significant effect. Dye penetration test shows that no major defects were found over effective length of the welded plates besides negligible amount of defects at corners. Rockwell hardness test carried out on both material shows that there is no considerable variation in the values of hardness in the defined zone in comparison to base metal. The result of Charpy impact test for both materials at room temperature as well as at -20^{o} C temperature shows that the value of toughness depends mainly on current and type of the gas used. The value of toughness decreases with decrease in surrounding temperature for both materials. The maximum toughness of SS 310 obtained was112.7 J (210A, argon, 9 L/min and 75^{o}) at room temperature and 105.35 J (210A, argon, 9 L/min and 75^{o}) was obtained at -20^{o} C. The maximum toughness of SS 316 obtained 105.35 J (210A, argon, 9 L/min and 75^{o}) at room temperature and 102.9 J (210A, argon, 9 L/min and 75^{o}) was obtained at -20^{o} C. Microhardness test on both SS 310 and SS 316 shows that the current is the most significant factor affecting the microhardness. Chemical composition result analysis for both material shows that there is a slight decrease in percentage composition of chromium because of formation of any compound in the welded region on account of tremendous heat generated during welding.

TABLE OF CONENTS

LIST OF FIGURES

LIST OF TABLES

ABBREVIATIONS

S NO.	ABBREVIATION	DESCRIPTION
1	TIG	Tungsten Inert Gas
2	GTAW	Gas Tungsten Arc Welding
3	HVN	Vicker's Hardness Number
4	HRC	Rockwell Hardness Number (C-Scale)
5	DPT	Dye Penetration Test
6	AWS	American Welding Society
7	DC	Direct Current
8	AC	Alternating Current
9	DCEN	Direct Current Electrode Negative
10	DCEP	Direct Current Electrode Positive
11	HAZ	Heat Effected Zone
12	ANOVA	Analysis Of Variance
13	S/N	Signal to Noise
14	DOF	Degree Of Freedom
15	SS	Sum Of Squares
16	PC	Percentage Contribution

CHAPTER 1 INTRODUCTION

1.1 WELDING PROCESS

Welding is type of fabrication process which is used for joining several metal parts by causing them to coalesce locally with each other for the purpose of fabricating the desired structure. This is done often by melting the workpieces and adding filler material to form a weld pool with or without application of pressure. Cooling of the joint so formed makes a permanent strong bond between both workpieces. Permanent joint so formed cannot be separated easily unless broken. This process is found to be most efficient and economical means of making permanent joints, finds applications even in space and underwater. The source of heat may be an electric arc, friction, chemical reaction, electric resistance or radiation of high intensity.

1.1.1 DEFINITION:

"Welding is defined as localised coalescence of metals, wherein coalescence is obtained by heating to a suitable temperature, with or without the application of pressure and with or without use of filler metal."[1]

1.2 HISTORY OF GTAW

The TIG welding process was invented during the Second World War due to the need of the American aircraft industry for a method of joining magnesium and aluminium. "Russell Meredith" demonstrated the first TIG process for the welding of magnesium using a Tungsten electrode and helium gas in the late 1930´s. TIG welding or GTAW (Gas Tungsten Arc Welding which is the common name in North America) uses a non-consumable tungsten electrode protected by an inert gas. The electrode is either made of pure tungsten or tungsten, mixed with small amounts of oxides (thorium-oxide, zirconium-oxide) improving the stability of the arc and makes it easier to strike. Since the process uses a non-consumable electrode, extra filler material is usually added. TIG is a trade name of the Linde Company. The Linde Company, a division of Union carbide, developed the process for welding difficult types of material, e.g. aluminium and magnesium. Linde, along with others, developed a wide range of air-cooled and water-cooled torches, gas lenses to improve shielding and other accessories that increased the use of the process. Initially, the electrode overheated quickly and, despite tungsten's high melting temperature, particles of tungsten were transferred to the weld. To address this problem, the polarity of the electrode was changed from positive to negative, but

the change made it unsuitable for welding many non-ferrous materials. Finally, the development of alternating current units made it possible to stabilize the arc and produce high quality aluminium and magnesium welds. The use of TIG today has spread to a variety of metals like stainless, mild and high tensile steels. Earlier the trade name given to GTAW was "Heliarc" since helium was used as shielding gas but the process is most popularly give name "TIG." Development within the GTAW process has continued as well, and today a number of variations exist. Among the most popular are the pulsed-current, manual programmed, hot-wire, dabber, and increased penetration GTAW methods. [2]

1.3 TUNGSTEN INERT GAS WELDING

Gas tungsten arc welding (GTAW) also known as tungsten inert gas (TIG) welding, is an arc welding process that uses a non-consumable tungsten electrode to produce the weld. The weld area is protected from atmospheric contamination by an inert shielding gas (argon or helium) and a filler metal is normally used though some welds, known as autogenous welds, do not require it. A constant-current welding power supply produces energy which is conducted across the arc through a column of highly ionized gas and metal vapors known as plasma. The necessary heat for Gas Tungsten Arc Welding (TIG) is produced by an electric arc maintained between a non-consumable tungsten electrode and the part to be welded. The heat-affected zone, the molten metal, and the tungsten electrode are all shielded from the atmosphere by a blanket of inert gas fed through the GTAW torch. Inert gas is that which is inactive, or deficient in active chemical properties. The shielding gas serves to blanket the weld and exclude the active properties in the surrounding air. It does not burn, and adds nothing to or takes anything from the metal. Inert gases such as argon and helium do not chemically react or combine with other gases. They possess no odour and are transparent, permitting the welder maximum visibility of the arc. In some instances a small amount of reactive gas such as hydrogen can be added to enhance travel speeds.

GTAW is most commonly used to weld thin sections of stainless steel and non-ferrous metals such as aluminium, magnesium, and copper alloys. The process grants the operator greater control over the weld than competing processes such as shielded metal arc welding and gas metal arc welding, allowing for stronger, higher quality welds. However, GTAW is comparatively more complex and difficult to master, and furthermore, it is significantly slower than most other welding techniques. Tungsten is used as non-consumable electrode because of its highest melting point of all metals. It is also a strong emitter of electrons which help to

ionize the path of arc and thus generates a concentrated and stable arc. In order to provide stable arc with ease of starting, tungsten electrodes are alloyed with Thoria and Zirconia. The TIG welds are strong, ductile and corrosion-resistant with virtually no cleanup required, making it popular for welding of surgical, medical and foodservice equipment, especially on stainless-steel. When the workpiece or weldment is connected to the positive (+) terminal of a direct current power supply, the operating mode is referred to as direct current straight polarity (DCSP) or direct current electrode negative (DC –ve or DCEN). When the workpiece is connected to the negative terminal of a direct current power supply, the operating mode is referred to as direct current reverse polarity (DCRP) or direct current electrode positive (DC +ve or DCEP). In DCSP, electrons are emitted from the tungsten electrode and accelerated to very high speeds and kinetic energies while travelling through the arc. These high-energy electrons collide with the workpiece, give up their kinetic energy, and generate considerable heat in the workpiece. Consequently, DCSP results in deep penetrating, narrow welds, but with higher workpiece heat input. About two-thirds of the net heat available from the arc (after losses from various sources) enters the workpiece. High heat input to the workpiece may or may not be desirable, depending on factors such as required weld penetration, required weld width, workpiece mass, susceptibility to heat-induced defects or degradation, and concern for distortion or residual stress.

In DCRP, on the other hand, the heating effect of the electrons is on the tungsten electrode rather than on the workpiece. Consequently, larger water-cooled electrodes holders are required, shallow welds are produced, and workpiece heat input can be kept low. This operating mode is good for welding thin sections or heat-sensitive metals and alloys. This mode also results in a scrubbing action on the workpiece by the large positive ions that strike its surface, removing oxide and cleaning the surface. This mode is thus preferred for welding metals and alloys that oxidize easily, such as aluminium or magnesium. The DCSP mode is much more common with non-consumable electrode arc processes than the DCRP mode. There is, however, a third mode, employing alternating current or AC. The AC mode tends to result in some of the characteristics of both of the DC modes, during the corresponding half cycles, but with some bias toward the straight polarity half-cycle due to the greater inertia (i.e., lower mobility) and, thus, greater resistance of large positive ions. During this half-cycle, the current tends to be higher due to the extra emission of electrons from the smaller, hotter electrode versus larger, cooler workpiece.

In the AC mode, reasonably good penetration is obtained, along with some oxide cleaning action. In modern welding power supplies designed specifically for GTA welding, there is the added capability for square-wave AC and for wave balancing. In square-wave AC, solid-state electronic devices reshape the sinusoidal wave provided as input to the power supply from line voltage to give it a square shape; positive for half a cycle and negative for half a cycle. This shape turns out to be advantageous during the transition from one half-cycle to the other, where the voltage and resulting current pass through zero. The effect of the much more rapid (essentially instantaneous) reversal with a square wave is to avoid possible momentary loss and subsequent difficulty of re-establishing the arc.

1.4 TIG WELDING SETUP

In its simplest manual form the standard equipments required for tungsten inert as welding comprises of a source for power supply, a welding torch, the welding leads or cables for connection, shielding gas supplying source and hoses for gas supplies. In TIG welding the tungsten electrode is non-consumable whereas shielding gas and filler wires are major consumables.

Figure 1.1: TIG Setup (Courtesy: Thapar Univ. Patiala)

1.4.1 POWER SOURCE

TIG welding can be carried out using DC for Stainless Steel, Mild Steel, Copper, Titanium, Nickel Alloys etc and AC for Aluminium and its Alloys and Magnesium. Further information

on the TIG Welding Process follows information on equipment used in this document. The Power Source is of a transformer design with or without a rectifier, with a drooping characteristic (constant current power source). The output is generally controlled by either a moving core within the main transformer of the power source or by using electronic control of power thyristors. DC power sources could be of 1-phase or 3-phase design, with an inductor to provide a smooth output. AC and AC / DC Power Sources are of a single phase design. The power source used for tungsten inert gas welding has constant current characteristics. The advantage of using constant current characteristic is that the current remains unchanged or constant when ever arc length gets varied over several millimetres in manual welding process moreover this helps to have limited short circuit current at time of arc initiation by touch start method hence the life of electrode is not adversely affected. As a result of all these during manual welding, there is a little effect on weld consistency. A typical TIG power source may operate within a range of 5-300A current value, 10-35 volts at 60% duty cycle.

There are three choices of welding current. Each of these has its own applications, advantages, and disadvantages. The type of current used will have a great effect on the penetration pattern as well as the bead configuration. Types of welding current used for tungsten inert gas welding are:

1.4.1.1 TIG WELDING WITH DCSP:

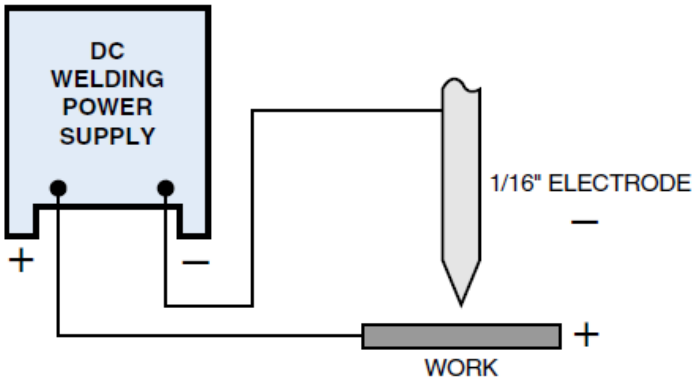

Figure 1.2: Direct current electrode negative (courtesy: TIG handbook by Miler)

TIG welding with **DCSP** (direct current straight polarity) produces deep penetration because it concentrates the heat in the joint area. It has been observed that out of total heat generated the 70% of heat is at workpiece and 30% is at electrode. This means the tungsten will run a lot cooler than DCRP. The resulting weld will have good penetration and a narrow profile. No

oxide cleaning action occurs with this polarity. For steel welding, direct polarity (negative electrode) is always used with argon as the shielding gas.

1.4.1.2 TIG WELDING WITH DCRP:

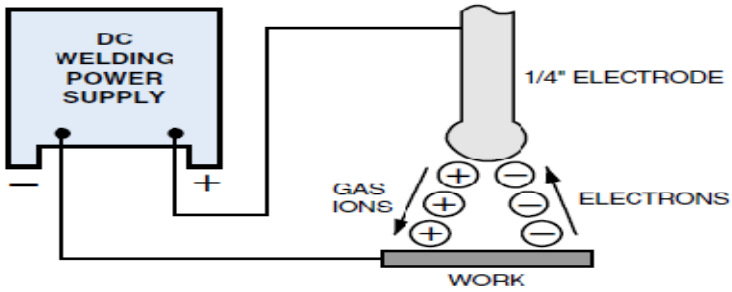

Figure 1.3: Direct current electrode positive (courtesy: TIG handbook by Miler)

TIG welding with **DCRP** (direct current reverse polarity) produces good cleaning action as the argon ions flowing towards the work strike with sufficient force to break up oxides on the surface. In this case it has been observed that 30% of heat is generated at workpiece and remaining 70% heat is generated at electrode. This type of connection is used very rarely because most heat is on the tungsten, thus the tungsten can easily overheat and burn away. DCRP produces a shallow, wide profile and is mainly used on very light material at low amps.

1.4.1.3 ALTERNATING CURRENT

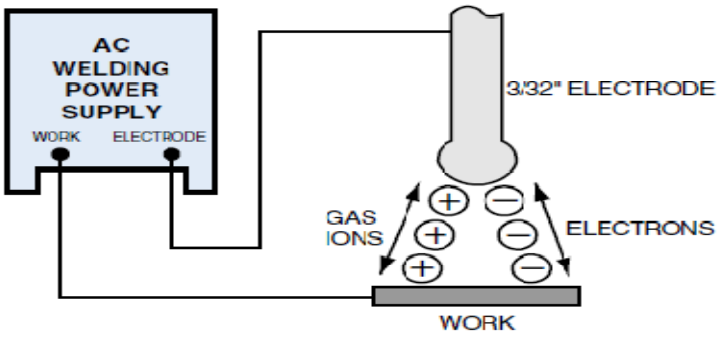

Figure 1.4: Alternating Current (courtesy: TIG handbook by Miler)

Alternating Current is the preferred welding current for most white metals, e.g. aluminium and magnesium. The heat input to the tungsten is averaged out as the AC wave passes from one side of the wave to the other. On the half cycle, where the tungsten is positive electron welding current will flow from base material to the tungsten. This will result in the lifting of any oxide skin on the base material. This side of the wave form is called the cleaning half. As the wave

moves to the point where the tungsten becomes negative the electrons (welding current) will flow from the welding tungsten to the base material. This side of the cycle is called the penetration half of the AC wave-form. Because the AC cycle passes through a zero point the arc goes out. The penetration achieved is medium as 50% of heat is developed at electrode and remaining 50% at workpiece.

With the advent of modern electricity AC welding machines can now be produced with a wave form called Square Wave. The square wave has the benefit of a lot more control and each side of the wave can be, in some cases, controlled to give a more cleaning half of the welding cycle, or more penetration. Once the welding current gets above a certain amperage (often depends on the machine) the HF can be turned off, allowing the welding to be carried on with the HF interfering with anything in the surrounding area. Square wave machines allow us to change the amount of time within each cycle. It is also known as balance control. Incorporation of fast switching electronics enables current to switch fifty thousand times per second thus allowing the power source to be much more responsive to our requirements. Moreover now these days with advancement in technology, the positive and negative amplitudes of the wave forms can be controlled independently.

1.4.2 TIG WELDING TORCH

The TIG torch can be air cooled or water cooled and of vastly different shapes and sizes dependant on access to the area to be welded and welding current required. TIG torch for use on equipment without an electric operated valve (normally scratch start systems) can have a finger operated gas valve fitted to the torch head. If the operator is using a foot control unit, the torch will not need a switch fitted. For welding in difficult to get to areas, a flexible head torch can be used and bent to the best position for welding. In water cooled torches, the current cable is a bore copper conductor within a water carrying hose; this means the conductor can be greatly reduced in size and weight. An air cooling system is incorporated for applications requiring low current values usually up to 200 amperes, whereas water cooling systems are required for higher amperage values

The function of the TIG torch is to:

1) Hold the electrode tungsten

2) Deliver welding current to the tungsten via a welding power cable

3) Deliver shielding gas to the TIG torch nozzle. The nozzle then directs the shielding gas to cover the weld pool protecting it from contamination from the surrounding air.

The TIG torch is made up of following parts:

- **Collets:** The welding electrode is held in the torch by means of collet. It is usually made of copper or copper alloy. It secures the grip on electrode when the torch cap is tightened in place. Good electrical contact between the collet and tungsten electrode is essential for good current transfer.
- **Collet Body:** The collet body screws into the torch body. It is replaceable and is changed to accommodate various sized tungsten electrodes and their respective collets.
- **Leads:** The lead will be set up for either air-cooled or water-cooled. It will be at a length suitable to do the job, e.g. 4 metre, 8 metre, etc. The lead will be made up of a power cable, gas hose and water leads in and out if the TIG torch is water-cooled. The lead may also include a control lead.
- **Nozzles -** The nozzle's job is to direct the correct gas flow over the weld pool. Its size depends on amount of area to be shielded from atmospheric air during welding. The nozzles are more often made up of heat resistant materials like ceramics. Nozzles can be made of ceramic, metal, metal-jacketed ceramic, glass, or other materials. Ceramic is the most popular, but are easily broken and must be replaced often. Nozzles used for automatic applications and high amperage situations often use a water-cooled metal design.

- **Back Caps -** The back cap is the storage area for excess tungsten. They can come in different lengths depending on the space the torch may have to get into (e.g. long, medium and short caps).[3]

1.4.3 SHIELDING GASES:

The shielding gases are those inert gases which are often used during welding process with a purpose of protecting the weld region from moisture and various gases present in atmosphere. If such is not done, it may result in several defects like weld brittlement, pin holes etc. The type of gas used has profound effect on weld properties and bead appearance. Oxygen present in atmosphere is the most reactive as it combines with other elements present in the metal and forms undesirable oxides. Nitrogen gas causes more serious problem when welding steel.

Because of its solubility in iron at elevated temperature, the nitrogen precipitates out and forms detrimental metal nitrides which causes increased yield strength, weld cracks and hardness. Such properties are undesirable because such a welding lacks the ductility. The most commonly used gas for TIG welding is argon which can be used on all metals. Argon - Hydrogen mixtures containing 2 - 5 % Hydrogen are frequently used for stainless steel and nickel-base alloys having the advantage of producing cleaner welds, giving deeper penetration. Helium - Argon mixtures give deeper penetration, greater heat input and therefore faster welding because of the higher arc voltage than pure Argon, but arc striking may be more difficult than in Argon. These mixtures can be used for Aluminium and Copper Alloys. The shielding gases must have high purity for welding operations. The effectiveness of shielding gas depends on gas density.

1.4.3.1 PROPERTIES OF SOME COMMONLY USED SHIELDING GASES:

Argon (Ar)

Argon is one of the most popular shielding gases thanks to its suitable properties. As an inert gas it has no chemical interaction with other materials. Therefore it is suitable for sensible materials such as aluminum and stainless steel. At MIG welding of mild steel an addition of C02 or a small amount of oxygen will increase the welding properties, especially for short arc welding. Contents of up to 20 % C02 improves the penetration (limits the risk of lack of fusion) while 5-8 % will give reduced spatter. Argon is superior for welding metals. It operates at a higher arc voltage, makes the arc start more easily, and is commonly used to weld mild steel, aluminium and titanium.

Helium (He)

Helium like argon is an inert gas. It gives more heat input to the joint. Mixed with argon it increases welding speed and is advantageous for the penetration in thick-walled aluminium or copper where it compensates for the high heat conduction. Drawback with helium is a high cost and the low density. At TIG welding, high contents of helium will reduce the ignition properties. It is used for high speed welding of mild steel and titanium. Helium offers a smaller heat affected zone and therefore, penetrates metals deeply. It also can increase the welding speed up to 40%. Helium is also commonly used to weld stainless steel and copper.

Carbon dioxide (C02)

Pure carbon dioxide (C02) can be used for short arc welding. It is a cheap gas; it has good properties for welding of galvanised steel and gives better safety against lack of fusion than argon based gases. Drawbacks are a higher amount of spatter and the fact that the gas cannot be used for spray arc.

Hydrogen (H2)

Small additions of hydrogen can be used to increase heat input and welding speed in the same manner as helium, but it is much cheaper. Because of the risk of cracks, hydrogen can only be used for welding of austenitic stainless steel. It actively reduces the oxides and is therefore also used in root gases.

1.4.3.2 APPLICATIONS OF DIFFERENT SHIELDING GASES:

Steel:

Argon is generally used for TIG welding of unalloyed steels, low-alloyed steels and stainless steels. For welding of all these metals, the shielding gas used can be argon, or its mixture with hydrogen or helium. A small addition of nitrogen may be used when welding duplex stainless steels in order to ensure the correct ferritic-austenitic balance. When making quality welds with TIG, it is also very common to use a root gas in order to protect the root side of the weld against oxidation. This is particularly important in the case of stainless steels or when welding easily-oxidised materials. The root gas is often a mixture of nitrogen hydrogen, or pure argon.

Aluminium and its alloys:

The shielding gas used for aluminium and its alloys is usually argon, possibly with the addition of helium. Helium improves the amount of heat transfer, and is used when welding thicker sections. The welding current is normally AC or, at low current levels, it may be DC with the electrode connected to the positive. Under certain conditions, horizontal and horizontal-vertical welds can be welded with DC if pure helium is used as the shielding gas and the electrode is connected to the negative. The higher arc voltage that results from the use of helium supplies more heat to the base material and thus increases the rate of welding. This higher heat input also means that butt joints can be made in thicker sections. The use of argon as the shielding gas causes oxide breakdown hence promotes clean welding region.

Copper and its alloys:

Argon is suitable for welding copper in all positions, and gives excellent results when welding metal thicknesses up to about 6 mm. The high thermal conductivity of the metal generally requires preheating. It is experimentally proved that for welding the workpieces having more than 6 mm thickness is helium, or helium containing 35 % argon is preferable.

Titanium

Welding of Titanium requires an extremely high purity of shielding gas, not less than **99.99** %. Either helium or argon can be used, although argon is generally preferred for metal thicknesses up to about 3 mm due to its higher density and good shielding performance. The use of pure helium is recommended when welding thick sections, due to the resulting higher heat content of the arc.

1.4.3.3 SHIELDING GAS COMPARISON [3]:

Table 1.1: Comparison chart of the gases used in present study

Characteristics	Argon	Argon-helium mixture	Helium
Travel speed	Reduced travel speed	Improved travel speed over 100 % Argon	Faster travel speed
Penetration	Reduced penetration	Improved penetration	Increased penetration
Cleaning effect	Good cleaning action	Cleaning properties closer to Argon	Less cleaning action
Arc starting	Easier	Improved arc starting over 100 % Helium	Difficult arc starting
Arc stability	Good	Improved arc stability over 100 % Helium	Less stability at low amperage
Arc cone	Focussed	More focussed than helium	Flared arc cone
Arc voltage requirement	Lower	Between 100% Argon and Helium	Higher
Gas flow rate requirement	Lower	Higher flow rates	Higher flow rates
Cost	Lower cost	Cost is higher than pure Argon	Highest cost as compared to argon and argon-helium mixtures.

In the present study work, three shielding gases namely pure argon, pure helium and mixture Ar+He (50:50) are used; the table above gives a clear comparison of various characteristics of all these gases.

1.4.4 WELDING ELECTRODE:

A non-consumable tungsten electrode is used for establishing and maintaining the arc during welding process. Tungsten is preferred material for the process because it is having highest melting point temperature among all other metals. Some burn-off is usually associated with tungsten but it remains non-consumable. A great care must be taken so that tungsten may not come in contact with weld pool as it gets contaminated and hence weld integrity is adversely affected. The tungsten electrode comes in standard sizes having diameters varying from 1/100" to 1/4" and length usually varies from 3" to 24". The most commonly used length is 7".

On basis of the chemical alloying element the tungsten electrode is classified into nine types as shown in table below.

Table 1.2: Tungsten electrode classification.

S No.	Classification	Composition Element	Colour Code
1	EWP	100 % Tungsten	Green
2	EWCe-2	2 % Cerium	Orange
3	EWLa-1	1% Lanthanum	Black
4	EWLa-1.5	1.5 % Lanthanum	Gold
5	EWLa-2	2 % Lanthanum	Blue
6	EWTh-1	1 % Thorium	Yellow
7	EWTh-2	2 % Thorium	Red
8	EWZr-1	1 % Zirconium	Brown
9	EWG	Unspecified alloy	Gray

- The letter "E" designates the electrode
- The letter "W" designates the chemical element Tungsten
- The letter "P" designates pure tungsten
- The numbers "1", "1.5", "2" with classification indicates percentage of alloy element added.

1.5 WELDING PARAMETERS

Regardless of the technology, efficiency or variability, these are the list of parameters that affect the quality and outcome of the weld. When these parameters are improperly configured or out of range for the equipment or materials, this can lead to a variety of problems.

1.5.1 CURRENT

Too much current can lead to splatter and workpiece damage. In thin materials, it can lead to a widening of the material gap. Too little current can lead to sticking of the filler wire. This can also lead to heat damage and a much larger weld affected area, as high temperatures must be applied for much longer periods of time in order to deposit the same amount of filling materials. Current limiting helps to prevent spatter when the tungsten tip accidentally comes too close or in contact with the workpiece. Fixed current mode will vary the voltage in order to maintain a constant arc current. In the pulsed-current mode, the welding current rapidly alternates between two levels. The higher current state is known as the pulse current, while the lower current level is called the background current. During the period of pulse current, the weld area is heated and fusion occurs. Upon dropping to the background current, the weld area is allowed to cool and solidify. Pulsed-current has a number of advantages, including lower heat input and consequently a reduction in distortion and warpage in thin workpieces. In addition, it allows for greater control of the weld pool, and can increase weld penetration, welding speed, and quality.

1.5.2 WELDING VOLTAGE

This can be fixed or adjustable depending on the equipment. Some metals require a specific voltage range to be able to work. A high initial voltage allows for easy arc initiation and allows for a greater range of working tip distance. Too large voltage, however, can lead to greater variability in workpiece quality (depending on the workpiece distance and a greater variation in power and heat delivered to the work-area).

1.5.3 GAS FLOW AND COMPOSITION

Various welding or shielding gasses are available including mixtures of argon, carbon dioxide, oxygen, nitrogen, helium, hydrogen, nitric oxide, sulfur hexafluoride and dichlorodifluoromethane. The choice of gas is specific to the working metals and affects the

production costs, electrode life, weld temperature, arc stability, welder control complexity, molten weld fluidity, weld speed, and spatter. Most importantly it also affects the finished weld penetration depth and subsurface profile, surface profile, composition, porosity, corrosion resistance, strength, ductility, hardness and brittleness.

The correct flow rate is an adequate amount to shield the molten weld pool and protect the tungsten electrode. Any greater amount than this is wasted. Generally speaking, when the welding current, nozzle diameter, or electrode sickout is increased, the flow rate should be increased. When welding in the AC mode the current reversals have a disturbing affect on the shielding gas and flow should be increased by 25%. And of course when welding in a drafty situation, flow rate should be doubled. When welding corner or edges, excessive flow rates can cause air entrapment. In this situation, the effectiveness of the shielding gas can be improved by reducing the gas flow by about 25%.

The shielding gas is pre-flowed and post-flowed in the process. The purpose of both pre-flow and post flow is to prevent contamination of both the weld pool and the tungsten electrode by the surrounding atmosphere. When the torch is not in use, air will enter the system through the nozzle. Moisture in the air can condense inside the nozzle and gas hose and then cause hydrogen contamination during initial stages of the weld. The shielding gas pre-flow will clear the air and moisture from the torch and prevent this contamination. Post-flow works a little differently. Immediately after the welding arc is extinguished, the weld bead, filler rod and the tungsten electrode remain hot enough to cause a chemical reaction with oxygen in the atmosphere. The result of this oxidization is quite obvious when it occurs because it causes the weld bead, filler rod and tungsten to turn black. Proper post flow will prevent oxidization from occurring by shielding the hot electrode and weld area, and by speeding up the cooling process. It should be remembered that tungsten that has discoloured because of oxidization must be properly removed. Usually, in the TIG welding of stainless steels with argon shielding, full penetration welding is restricted to joints of a maximum thickness of 3 mm and to relatively low welding speed. The welding speed can be increased substantially (up to 160%) when helium or hydrogen is used as part of the shielding gas mixture.

1.6 APPLICATIONS

TIG is applied in all industrial sectors but is especially suitable for high quality welding. In manual welding, the relatively small arc is ideal for thin sheet material or controlled

penetration (in the root run of pipe welds). Because deposition rate can be quite low (using a separate filler rod) MMA or MIG may be preferable for thicker material and for fill passes in thick-wall pipe welds. While the aerospace industry is one of the primary users of gas tungsten arc welding, the process is used in a number of other areas. Many industries use GTAW for welding thin workpieces, especially nonferrous metals. It is used extensively in the manufacture of space vehicles, and is also frequently employed to weld small-diameter, thin-wall tubing such as those used in the bicycle industry. In addition, GTAW is often used to make root or first pass welds for piping of various sizes.

In maintenance and repair work, the process is commonly used to repair tools and dies, especially components made of aluminium and magnesium. Because the weld metal is not transferred directly across the electric arc like most open arc welding processes, a vast assortment of welding filler metal is available to the welding engineer. In fact, no other welding process permits the welding of so many alloys in so many product configurations. Filler metal alloys, such as elemental aluminium and chromium, can be lost through the electric arc from volatilization. This loss does not occur with the GTAW process. Because the resulting welds have the same chemical integrity as the original base metal or match the base metals more closely, GTAW welds are highly resistant to corrosion and cracking over long time periods, GTAW is the welding procedure of choice for critical welding operations like sealing spent nuclear fuel canisters before burial

TIG welding is often used for jobs that demand high quality welding such as for instance:

- The offshore industry
- Combined heat and power plants
- The petrochemical industry
- The food industry
- The chemical industry
- The nuclear industry

1.7 STAINLESS STEEL

In metallurgy, stainless steel, also known as inox steel, is a steel alloy with a minimum of 10.5% to 11% chromium content by mass. Stainless steel is a generic name for a number of different steels used primarily due to their corrosion resistance characteristic. The chromium

present in stainless steel has great affinity for oxygen and forms a film of chromium oxide on the surface. Stainless steel does not readily corrode, rust or stain with water as ordinary steel does, but despite the name it is not fully stain-proof, most notably under low oxygen, high salinity, or poor circulation environments. It is also called corrosion-resistant steel or CRES when the alloy type and grade are not detailed, particularly in the aviation industry. Stainless steel differs from carbon steel by the amount of chromium present. Unprotected carbon steel rusts readily when exposed to air and moisture. This iron oxide film (the rust) is active and accelerates corrosion by forming more iron oxide, and due to the greater volume of the iron oxide this tends to flake and fall away. Stainless steels contain sufficient chromium to form a passive film of chromium oxide, which prevents further surface corrosion and blocks corrosion from spreading into the metal's internal structure, and due to the similar size of the steel and oxide ions they bond very strongly and remain attached to the surface.

Stainless steel is used where both the properties of steel and resistance to corrosion are required. Stainless steel base metals are grouped primarily into three classes depending on their crystal structure; austenitic (such as 302, 304, 308, 316, etc.), martensitic (such as 410, and 416), and ferritic (such as 409, and 430.). Austenitic grades are also available with a lowered carbon content (designated with an "L", such as 304L or 316L). These have in general, a higher resistance to corrosion in some definite environment, as well as a higher resistance to scaling at high temperature. Stainless Steel is iron-based alloy containing a minimum of 10.5% Chromium with or without other alloying elements. Based on the alloy content and the micro structure, stainless steels are classified into following three major categories:

Austenitic

This category of stainless steel contains 16 to 26% Chromium and 6 to22% Nickel. They are non- magnetic in annealed condition and have excellent corrosion resistance. They are not hardenable by heat treatment. However, they can develop high strength on cold working. They have excellent weldability, formability, hygiene factor and cryogenic properties. . On cold working they exhibit different degrees of magnetism. They are identified in the AISI 300 series.

Ferritic

This category of stainless steel contains 10.5 to 30% chromium without any Nickel. They are Ferro magnetic in nature and generally not hardenable by heat treatment. These steels possess

good resistance to stress corrosion cracking and moderate weldability &formability. They are identified in the AISI 400 series.

Martensitic

This group contains 11 to 14% chromium without any nickel, but with a higher carbon content compared to the Austenitic and ferritic stainless steels. They are ferro-magnetic in nature and are hardenable by heat treatment. They possess moderate corrosion resistance and are identified in the AISI 400 series. Generally Stainless steels are alloys of iron, chromium, nickel, manganese, molybdenum, titanium, niobium, carbon and others just to mention the most important ones. Stainless steels include all the types of steel which are made corrosion-resistant by alloying the steel with different alloying elements. TIG welding is an economically advantageous to welding of thinner stainless steels. It makes clean, smooth welds without porosities and craters possible even without welding from the backside. Welding is done in DC with negative polarity on the electrode.

Ideally, austenitic stainless steels exhibit a single-phase, the face-centered cubic (F.C.C) structure, that is maintained over a wide range of temperatures. This structure results from a balance of alloying additions, primarily nickel, that stabilize the austenite phase from elevated to cryogenic temperatures. Because these alloys are predominantly single phase, they can only be strengthened by solid-solution alloying or by work hardening. Precipitation-strengthened austenitic stainless steels will be discussed separately below.

The austenitic stainless steels were developed for use in both mild and severe corrosive conditions. Austenitic stainless steels are used at temperatures that range from cryogenic temperatures, where they exhibit high toughness, to elevated temperatures, where they exhibit good oxidation resistance. Because the austenitic materials are nonmagnetic, they are sometimes used in applications where magnetic materials are not acceptable.

The most common types of austenitic stainless steels are the 200 and 300 series. Within these two grades, the alloying additions vary significantly. Furthermore, alloying additions and specific alloy composition can have a major effect on weldability and the as-welded microstructure. Because of their physical properties, the welding behaviour of austenitic stainless steels is different than the ferritic, martensitic, and duplex stainless steels. For example, the thermal conductivity of austenitic alloys is roughly half that of ferritic alloys.

Therefore, the weld heat input that is required to achieve the same penetration is reduced. In contrast, the coefficient of thermal expansion of austenite is 30 to 40 percent greater than that of ferrite, which can result in increases in both distortion and residual stresses, due to welding. The molten weld pool of the austenitic stainless steels is commonly more viscous, or sluggish, than ferritic and martensitic alloys. This slows down the metal flow and wet ability of welds in austenitic alloys, which may promote lack-of-fusion defects when poor welding procedures are employed.

1.7.1 AUSTENITIC STAINLESS STEEL

Austenitic stainless steels have been used widely by the fabrication industry owing to their excellent high temperature and corrosion resistance properties. Some of the typical applications of these steel include their use as nuclear structural material for reactor coolant piping, valve bodies, vessel internals, chemical and process industries, dairy industries, petrochemical industries etc. Out of 300 series grade of these steels type 304 SS is extensively used in industries due to its superior low temperature toughness and corrosion resistance. One of the typical applications of type 304 SS include storing and transportation of liquefied natural gas (LNG), whose boiling point is 162 ^{0}C under 1 atmosphere.

1.7.2 APPLICATIONS OF AUSTENITIC STAINLESS STEEL

SS 301:

An austenitic stainless steel, it has the ability to attain high strength with some sacrifice of ductility through moderate or severe cold working. It can be used where high strength to weight ratio is required with good general corrosion resistance. By varying chemical composition within ASTM limits and temper rolling broad range of magnetic & mechanical properties can be achieved for a variety of applications. The susceptibility to carbide precipitation during welding restricts its use in many applications in favour of 304 grades. Transportation cars such as railway coaches, wagons, subway cars, electrical equipment and endless belts are some of the major applications where SS 301 is preferred.

SS 301 L

A Cr-Ni austenitic stainless steel, similar to SS301 with lower carbon (0.03%) and higher Nitrogen (0.20%), it has the ability to attain high strength without much sacrifice of ductility

through moderate or severe cold working. It can be used where high strength to weight ratio is required with good general corrosion resistance & weldability. Broad range of mechanical properties with good weldability can be achieved by temper rolling.

SS 304

The most widely used austenitic stainless steel with a nominal composition of 18% Chromium & 8% Nickel it has excellent general corrosion resistance and forming characteristics. It finds application in transport, chemical, petrochemical and fertilizers industries, dairy, food processing, pharmaceutical industries, hospital equipment, cryogenic vessels, households as utensils & appliances, heat exchangers, machinery in paper, pulp, textile and beverage industries. In architectural applications it is used for panels, curtain walls, roofing etc. The weld ability of this grade is very good; it can be used in work hardened condition for uses requiring high strength.

SS 304L

An austenitic stainless steel similar to SS 304 but has lower carbon level (0.03% max). It is used in place of SS 304 for improved resistance to Intergranular corrosion and excellent Weldability. It is used for parts and structures which cannot be heat treated after welding. It has fewer tendencies to work hardened by cold working.

SS-308

Typical applications include stainless steel piping in refineries, oil and gas industries, and chemical plants. AISI Type 308 is an Austenitic Standard grade Stainless Steel. It is commonly called AISI Type 308 Chromium-Nickel steel or UNS S30800. It has increased chromium and nickel contents, thus increased corrosion resistance as compared to SS-304.

SS 310

This is an austenitic stainless steel with a higher Chromium and Nickel content. The restricted Carbon helps in better welding and formability. Because of their relatively high creep strength and mechanical properties at higher temperatures, these grades find applications where higher temperature and severe service conditions exist. They have high temperature scaling resistance but not good for high sulphur environments. Used for air heaters, annealing boxes, ovens,

carburizing boxes, fire box sheets, furnace linings, furnace stacks and dampers, gas turbine parts, heat exchangers, kiln linings, nozzle diaphragm assemblies for turbo jet engines, oil burner parts, paper mill equipment, oil refinery equipment and recuperater.

SS 316

It is a type of austenitic stainless steel with 2 to 3% Molybdenum to have improved corrosion resistance, particularly apparent for pitting and crevice corrosion resistance in chloride environment. This grade has good oxidation resistance. Continuous use at 425-860 ^{0} C is not recommended due to carbide precipitation. Typical applications include architectural trims, marine exteriors, chemical processing equipment, food processing equipment, petroleum refining equipment, pharmaceuticals equipment, photographic equipment, pulp & paper processing equipment and textile finishing equipment.

It has superior corrosion resistance as compared to other chromium-nickel steels when exposed to many types of chemical corrodents such as sea water, brine solutions etc. It is the second most common grade (after 304); the addition of molybdenum prevents specific forms of corrosion. It is used in the manufacturing and handling of food and pharmaceutical products where it is desirable to minimize metallic contamination. Type 316 is considerably more resistant to solutions of sulphuric acid, chlorides, bromides, iodides and fatty acids at high temperature.

SS 316L

This steel is similar to SS 316 with lower carbon level (0.03%) to have better corrosion resistance and Weldability. Low carbon content also reduces work hardening and improves ductility for cold forging, drawing etc., Low hot strength than SS316. Typical applications include food processing, chemical and petrochemical equipment, brewery equipment, coastal architectural panelling, laboratory equipments, heat exchangers, mining screens, chemical transportation containers etc.

CHAPTER 2 LITERATURE REVIEW

2.1 A REVIEW ON LITERATURE

The TIG welding process (or GTAW) is used when a good weld appearance and a high quality of the weld are required. A lot of research has been done in the field of TIG welding which can be broadly categorized as follows:

1. Effect of parameters on the properties of materials
2. Optimization of the process
3. TIG-Pulse welding
4. Comparative studies done on TIG and any other welding process
5. Studies related to use of activated fluxes and their effects
6. Effect of shielding gas on quality of weld

The subsections of this chapter describes literature review base on above classifications.

2.1.1 EFFECT OF PARAMETERS ON THE PROPERTIES OF MATERIALS

Wang et al.(2011) investigated the effects of TIG Welding Parameters on Morphology and Mechanical Properties of Welded Joint of Ni-base Super alloy. The effect of welding parameters on the tensile strength and fracture were analyzed. Materials for experiments were plates of Ni-base super alloy; grade GH99, with a thickness of 1.2 mm and 1.5 mm respectively. The welding parameters were as follows: welding current 55~165A, welding speed 19-29cm/mm, impulse frequency 2~5Hz. Results show that the increase of welding current and the decrease of welding speed bring about the large amount of heat input in the welding pool and the enlargement of width and deepness of the welding pool. It was found that the root of welding joint is un-welded when the welding current is lower, so that the strength and elongation of welded joint are inferior. And the more welding defects in the welding zone and the more hard and brittle phase precipitates in the overheated zone when the welding current is too high. Consequently, the strength and plasticity go up first and then go down, i.e. they have a peak value with welding current increasing. [5]

Kumar, Shahi (2011) studied the influence of heat input on the microstructure and mechanical properties of gas tungsten arc welded 304 stainless steel. Three heat input combinations

designated as low heat (2.563 kJ/ mm), medium heat (2.784 kJ/mm) and high heat (3.017 kJ/mm) were selected from the operating window of the gas tungsten arc welding process (GTAW) and weld joints made using these combinations were subjected to micro-structural evaluations and tensile testing so as to analyze the effect of thermal arc energy on the microstructure and mechanical properties of these joints. The base material used were AISI 304 SS plates of sizes 200 mm x 100 mm x 6mm which were cut from a rolled sheet and the filler was 308 SS solid electrode of 3.15 mm diameter. The results of this investigation indicate that the joints made using low heat input exhibited higher ultimate tensile strength (UTS) than those welded with medium and high heat input. Significant grain coarsening was observed in the heat affected zone (HAZ) of all the joints and it was found that the extent of grain coarsening in the heat affected zone increased with increase in the heat input. For the joints investigated in this study it was also found that average dendrite length and inter-dendritic spacing in the weld zone increases with increase in the heat input which is the main reason for the observable changes in the tensile properties of the weld joints welded with different arc energy inputs.[6]

Goyal et al. (2009), studied the metallography of the aged and tested material was through optical, scanning and transmission electron microscopy. The effect of transformation of d-ferrite to sigma phase and carbides in the weld metal on low cycle fatigue behaviour was evaluated. Thermal ageing was done for 10,000 h at 823 and 873 K. Total strain controlled low cycle fatigue tests were conducted at a constant strain rate of $3x10^{-3}$ s^{-1} with strain amplitudes in the range ±0.25% to ±0.6% at 823 and 873 K. Weld metal exhibited initial hardening followed by cyclic softening prior to failure. The fatigue life of the aged material was inferior to that of the unaged material due to the higher stress response and cracking at the sigma austenite interface. However, fatigue life of the aged weld metal was found to lie in the scatter band of the design curve for weld metal in the RCC-MR design code. **[7]**

Shanping Lu et al. (2009), investigated the influences of argon and oxygen in helium base shielded GTA welding on the arc ignitability, bead protection and weld penetration by bead-on-plate welding on SUS304 stainless steel. SUS304 stainless steel plates with a sulphur content of 0.002wt% pct and an oxygen content of 0.002wt% pct were used as the substrate with dimensions of 100mm×50mm×10mm. Experimental results show that the critical electrode tip work distance for arc ignition is increased from 1mm under pure He shielding to 5mm under He–50%Ar shielding. Small addition of oxygen content to the He–Ar mixed

shielding can significantly change the weld shape from a wide shallow type to a narrow deep and the weld depth/width ratio can be doubled due to the change in the Marangoni convection from an outward to an inward direction. When the argon content in the He–Ar mixed shielding is below 30%, the shielding gas protection to the weld bead from the atmosphere is poor, and the weld bead surface is dirty and oxidized. Adding argon gas to helium gas can improve the arc ignitability of helium gas and make the arc stable because the Ar ionization energy (15.76 eV) is much lower than the He ionization energy (24.58 eV). [8]

Bayraktar et al. (2006), study was undertaken with the objective of clarifying formability characteristics of welded thin sheet steels, such as Interstitial Free Steels (IFS) and Ferritic Stainless Steels (FSS) based on the LASER, TIG and resistance spot welding (RSW). The characterisation of basic parameters influencing formability of homogeneous; base metal (BMs) and welded parts (WPs) has been carried out. General micro structural observations indicate that a certain proportion of martensite is seen in the LASER welded parts of the non-stabilised grade of 430 and the amount of martensite is higher than that of TIG and RSW processes. The stabilised grades of 409 and 430Ti present entirely ferritic structure with a reasonable grain size. Correlation realized between the transition temperatures and deep drawability can be used for evaluating of the welding conditions and also of the material characteristics. **[9]**

2.1.2 OPTIMIZATION OF THE PROCESS

Dhas J et al. (2012) in his study has done a review on optimization of welding process. According to him optimization of welding process parameters depend upon ability to measure and control the process variables involved in the welding process. An effective control of variables is required to obtain desired output. It is the simulation of welding process through finite element analysis which has made this possibility to measure and control the process variables. DOE is very good approach to conduct experiments in economical way. Taguchi method is extremely good as it is insensitive to variations in environmental conditions and other noise factors. Taguchi method uses special design of orthogonal arrays to study entire process parameters with small number of experiments. To analyse the results, Taguchi method uses a statistical measure of performance called signal to noise ratio, derived from electrical control theory. FEA software like WELDSOFT etc is user friendly to simulate weld conditions.

Multiple regression analysis, artificial neural network, response surface methodology etc are few methods widely used for efficient process control. **[10]**

Nagesh, Datta (2010) explains an integrated method with a new approach for predicting the weld bead geometric descriptors and use of genetic algorithm for optimization of process parameters. The properties of the welded joints are affected by a large number of welding parameters. Modelling of weld bead shape is important for predicting the quality of welds. In an attempt to model the welding process for predicting the bead shape parameters, modelling and optimization of bead shape parameters in tungsten inert gas (TIG) welding process has been carried out. To optimize the process parameters for the desired front height to front width ratio and back height to back width ratio, genetic algorithmic approach has been applied. A two level fractional factorial design and multiple linear regression technique applied on the conventional experimental data have yielded reasonably accurate results. The proposed methods were found to be effective in determining the weld bead geometric descriptors for tungsten inert gas welding process. **[11]**

Benyounis et al. (2008), A comprehensive literature review of the application of various methods like design of experiment (DoE), evolutionary algorithms and computational network are widely used to determine the welding input parameters that lead to the desired weld quality are have been discussed. This review was classified according to the output features of the weld, i.e. bead geometry and mechanical properties of the welds. Combining two optimization techniques, such as GA and RSM, would reveal good results for finding out the optimal welding conditions. The fusion layer should also not be thicker than necessary in order to avoid wasting of energy, edge burn-off, sagging of the weld pool and deep weld end craters. Raveendra and Parmar have built mathematical models using the fractional factorial technique to predict the weld-bead geometry and shape relations (penetration, width, reinforcement height, and width to penetration ratio and percentage dilution). Andersen et al. have explained some concepts related to neural networks and how they can be used to model weld-bead geometry, in terms of equipment parameters, in order to evaluate the accuracy of neural networks for weld modelling. They carried out a number of simulations and they used actual GTAW data for this purpose. The data consisted of values for voltage, current, electrode travel speed and wire feed speed and the corresponding bead width, penetration, reinforcement height and bead cross-sectional area. The performance of neural networks for weld modelling was presented and evaluated using actual welding data. It was concluded that the accuracy of neural

networks modelling is fully comparable with the accuracy achieved by more traditional modelling schemes. **[12]**

Juang, Tarng (2002) presented the selection of process parameters for obtaining an optimal weld pool geometry in the tungsten inert gas (TIG) welding of stainless steel. Basically, the geometry of the weld pool has several quality characteristics, for example, the front height, front width, back height and back width of the weld pool. To consider these quality characteristics together in the selection of process parameters, the modified Taguchi method is adopted to analyze the effect of each welding process parameter on the weld pool geometry, and then to determine the process parameters with the optimal weld pool geometry. Optimization of process parameters is the key step in the Taguchi method to achieving high quality without increasing cost. This is because optimization of process parameters can improve quality characteristics and the optimal process parameters obtained from the Taguchi method are insensitive to the variation of environmental conditions and other noise factors. Results showed the front height, front width, back height and back width of the weld pool in the TIG welding of stainless steel are greatly improved by using these approaches. **[13]**

2.1.3 TIG-PULSE WELDING

Traidia, Roger (2011) described the coupling between the welding arc and the weld pool dynamic in pulsed gas tungsten arc welding. The cathode, arc-plasma and melting anode regions are taken into account. The unified time-dependent model describes the heat transfer, fluid flow and electromagnetic fields in the three regions. To validate the predictions of the model, an Infra-Red camera is used to film the dynamic of the weld pool surface. Then an image processing algorithm permits to get the time evolution of the weld pool width directly from the film. The numerical model was applied to the 304 stainless steel welding, and the computed results show that the predictions are in fair agreement with the experimental results. The numerical results show that the Marangoni effect plays an important role on the weld pool dynamic. By considering a surface tension coefficient variable with both temperature and sulphur activity they explained the formation of different vortices which have a great impact on the time evolution in the dimensions of the weld pool. **[14]**

Correa et al. (2009), investigates the weldability of iron-based powder metal alloys Fe–Ni, Fe–Ni–P alloys) using the pulsed gas tungsten arc welding process (GTAW) with three

different filler metals (AWS R 70S-6, AWS R 309L, AWS R Fe–Ni). Results from this study indicate that powder metal Fe–Ni alloys may be successfully joined by pulsed GTAW with filler metal of Fe–Ni alloy and mild steel in various thickness range (3–7 mm). Concerning to the powder metal Fe–Ni–P alloy, it may be joined by pulsed GTAW but a discerning selection of the filler metal and a careful control over the heat input. No excessive hardening was observed in the weld metal and HAZ of the powder metal Fe–Ni alloy as well as in the powder metal Fe–Ni–P alloy. **[15]**

Balasubramanian et al.(2008), studied the effect of pulsed current Gas Tungsten Arc (GTA) welding parameters on corrosion behaviour of Ti–6Al–4V titanium alloy. Pulsed current gas tungsten arc welding was used to fabricate the joints. To optimize the number of experiments to be performed, central composite design was used. The investigation revealed increase in corrosion resistance with increase in peak current and pulse frequency up to an optimum value of the same and decrease in corrosion resistance beyond that optimum point. An increase in corrosion resistance with grain refinement was also detected. It was observed that effect of pulsing frequency and peak current had two regions with initially decreasing the corrosion rate and then increasing the corrosion rate irrespective of changes in base current and pulse on time. Current pulsing in GTAW lead to relatively finer and more equiaxed grain structure in titanium welds. The grain refinement due to current pulsing has resulted in increase in corrosion resistance. It is shown that out the four pulsed current parameters, peak current and pulse frequency are having predominant effect on corrosion properties. **[16]**

Lothongkum et al. (1999), The TIG pulse welding parameters of 304L stainless steel sheet of 3 mm thickness in flat, vertical and overhead positions were investigated. The shielding gases were Ar, and Ar‡N2 (0±5%, v/v). The base and pulse currents in all welding positions were adjusted to achieve a weld bead contour corresponding to DIN 8563 class AS at 3.4 mm/s welding speed, 1 pulse/s pulse frequency and 55% on-time. In the vertical and overhead positions, gravitational force made the weld pool fall down, leading to undercut after solidification. With the appropriate welding parameters, the gravitational effect can be eliminated. It was found To gain a higher welding rate by increasing the welding speeds to more than 3.4 mm/s simultaneously with increasing pulse frequencies, pulse currents and base currents, was not successful. [17]

2.1.4 COMPARATIVE STUDIES DONE ON TIG

Dongjie Li et al. (2012), in his present study compared double-shielded TIG method with the traditional TIG welding method under different welding parameters (i.e., speed, arc length and current). The strength of the Marangoni convection was calculated to estimate the influence of the welding parameters on the variations in weld pool shapes. The results show that changes in the welding parameters directly impact the oxygen concentration in the weld pool and the temperature distribution on the pool surface. The oxygen content and heat distribution on the weld pool surface are determinants of the pattern and strength of the Marangoni convection. The double-shielded TIG process is an appropriate method for adding an active element, such as oxygen, into the weld pool so as to transform the outward flow of Marangoni convection into an inward flow. Changes in the welding parameters directly change the heat input and the pattern of the Marangoni convection, thus controlling the shape of the molten pool. For the pure-He-shielded TIG process, the outward Marangoni convection was weakened with increasing oxygen content; thus, the D/W ratio increased slightly. [18]

Arivazhagan et al. (2011) carried out investigations to study the microstructure and mechanical properties of AISI 304 stainless steel and AISI 4140 low alloy steel joints by Gas Tungsten Arc Welding, Electron Beam Welding and Friction Welding. For each of the weldments, a detailed analysis was conducted on the phase composition, microstructure characteristics and mechanical properties. The results of the analysis showed that the joint made by EBW has the highest tensile strength (681 MPa) than the joint made by GTAW (635 Mpa) and FRW (494 Mpa). From the fractographs, it could be observed that the ductility of the EBW and GTA weldment were higher with an elongation of 32% and 25% respectively when compared with friction weldment (19%). Moreover, the impact strength of weldment made by GTAW is higher compared to EBW and FRW. [19]

J.J. del Coz Díaz et al.(2010) in this study the thermal stress analyses were performed in the tungsten inert gas (TIG) welding process on two different stainless steel specimens in order to compare their distortion mode and magnitude. The finite element method including the birth and death technique is an efficient procedure to analyze the vertical displacement evolution at different plate locations in the welding process of stainless steels, as well as their angular deformation and longitudinal bending. The use of thermo graphic imaging in the context of TIG welding has been successfully demonstrated on a practical scale and helps to compare the

thermal results in the subsequent numerical simulation at different locations and a specific time. [20]

Cabello Munoz et al. (2008), investigated the comparative micro structural and mechanical characteristics of fusion welds (TIG) and solid-state welds (FSW) of Al–4.5 Mg–0.26 Sc heat-treatable aluminium alloy. Microstructures of base metal and welded zones are analyzed by optical (OM) and transmission electron (TEM) microscopy. Particular emphasis was laid on the evolution of hardening precipitates in welded areas. The corresponding mechanical properties are evaluated through microhardness measurements and uniaxial tensile tests. The effect of a post-weld heat treatment on both microstructure and mechanical properties were also examined. The results suggest that hardening precipitates are comparatively more affected by the TIG than by the FSW process. This results in a substantial reduction of mechanical properties of TIG welds that can be partially recovered through a post-weld heat treatment. It appears that FSW joints exhibit higher mechanical properties than those obtained by A-TIG. Compared to base metal, YS of welded joints decreases by 20% for FSW and 50% for ATIG. This decrease is explained by a loss of strain hardening and a modification of Al3Sc hardening particles. The difference between friction stir welds and fusion welds is explained by a partial preservation of Al3Sc hardening particles in the case of FSW and a complete dissolution in the case of A-TIG. [21]

Squillace et al. (2004) carried out an investigation on microstructure and corrosion resistance of weld butt joints of AA 2024-T3. Two different welding processes were considered: a conventional tungsten inert gas (TIG) process and an innovative solid state welding process known as friction stir welding (FSW). Polarisation curve tests and electrochemical impedance spectroscopy were performed. In FSW joint, instead, lower temperatures involved in process and severe plastic deformations induced by tool motion allow rising of a complex situation: by a general point of view a slight decay of mechanical properties is recorded in nugget zone, flow arm and thermo-mechanically altered zone (TMAZ), while in heat-affected zone (HAZ), due to starting heat treatment of alloy under investigation, a light improvement of such properties is appreciated. In flow arm and in nugget zone, however, a light recovery of hardness, w.r.t. TMAZ zone, is recorded, due to the re-crystallisation of a very fine grain structure. Micro-hardness tests performed through the thickness of FSW joint allow pointing out the great differences among four different main zones: nugget zone (including flow arm), TMAZ, HAZ and unaffected zone (i.e. parent alloy). The first two zones were characterised by a general

drop of mechanical properties, even though the nugget and flow arm zone show a slight recovery due to very fine grain structure, while the third one show a very slight increase. Polarisation curve and EIS tests allow to point out that in both kind of joints parent alloy show evident pitting tendency, while weld bead and HAZ showed a passive behaviour, even though, in case of FSW joint, such differences are less evident. [22]

2.1.5 STUDIES RELATED TO USE OF ACTIVATED FLUXES AND THEIR EFFECTS

Tseng, Hsu (2011), investigated the effect of activated tungsten inert gas (activated TIG) process on weld morphology, angular distortion, delta-ferrite content, and hardness of Type 316L stainless steels. Five kinds of oxide fluxes, MnO2, TiO2, MoO3, SiO2, and Al2O3, were used to study. An autogenous TIG welding was applied to 6 mm thick stainless steel plates through a thin layer of flux to produce a bead-on-plate welded joint. The oxide fluxes used were packed in powdered form. The experimental results indicated that the SiO2 flux facilitated root pass joint penetration, but Al2O3 flux led to the deterioration in the weld depth and bead width compared with conventional TIG process. Activated TIG welding can increase the joint penetration and weld depth to- width ratio, thereby reducing angular distortion of the weldment. To obtain high quality welds and stable weld arc, the activated TIG process requires large diameter electrodes to support a given level of the weld current. Activated TIG welding can increase the joint penetration and weld depth-to-width ratio, significantly reducing the angular distortion of the weldment. It was observed that the activated TIG welding increase the arc voltage thus the amount of heat input per unit length in a weld was also increased, and therefore the delta-ferrite content in weld metal increased. [23]

Huang (2010) A systematic study of the effects of activating flux in the weld morphology, arc profile, and angular distortion and microstructure of two different arc welding processes, namely, Gas Tungsten Arc Welding (GTAW) and Plasma Arc Welding (PAW) was carried out. The results showed that the activating fluxes affected the penetration capability of arc welding on stainless steel. An increase in energy density resulting from the arc constriction and anode spot reduction enhanced the penetration capability. The Depth/Width (D/W) ratio of the weld played a major role in causing angular distortion of the weldment. Also, changes in the cooling rate, due to different heat source characteristics, influenced the microstructure from the fusion line to the centre of the weld. The base material used in this study was austenitic stainless steel (AISI 304) with a chemical composition. The size of each specimen was 150 ×

150 mm with a thickness of 5 mm. The specimens were roughly polished with 400 grit abrasive paper to remove surface impurities, and then cleaned with acetone. The composition of the activating flux was TiO2 (30 wt.%), SiO2 (25 wt.%), Cr2O3 (25 wt.%) and MoO3 (20 wt.%). Before welding, the flux powder was mixed with acetone to produce a paint-like consistency, and then a coating was brushed on the plate surfaces. Increasing the welding current decreased the cooling rate, therefore reducing the δ-ferrite content. Also, conventional GTAW was found to be a very high heat input process, thus exhibiting lower delta-ferrite content in a stainless steel weld. [24]

Xu et al. (2007), the effect of flux on TIG weld shape variations was investigated by application of the heat transfer and fluid flow model. The flux used was Nimonic 263 alloy, TiO, TiO2 and Ti2O3. The arc constriction and the reversed Marangoni convection are considered to be the two main factors for increasing penetration of A-TIG weld pool. And the simulated results show that the latter is the main factor for changing weld shapes. The surface tension temperature coefficient is sensitive to the active elements and affects the pattern of the fluid flow. It was observed that by controlling the type and quantity of the active elements, different kinds of the weld shapes are obtained. The experimental result shows that increase of active flux on the weld bead tends to increase the penetration of the weld pool at first and then decreases steeply because part of the oxide in the flux do not totally decomposed when the flux reaches a critical value. The solid oxide particles in the weld pool act as the obstacles of the fluid flow and reduce the velocity of the flow. [25]

2.1.6 EFFECT OF SHIELDING GAS ON QUALITY OF WELD

Kanga et al. (2009), the effect of alternate supply of shielding gases in austenite stainless steel GTA welding was investigated. Basically two types of experiments were carried out. The former experiment was to measure the welding voltage waveforms to confirm the alternate supply of different gases in apparatus for alternate supply of shielding gases, and the latter one was to find the variations in welding distortion and welding speed with different types of shielding gases and type of gas supply. Discrete alternate supply of shielding gas is a new technology that alternately supplies the different kinds of shielding gases in weld zone. As the new developed methods compared to the previous general welding with a mixing supply of shielding gas, it cannot only increase the welding quality, but also reduce the energy by 20% and the emission rate of fume. As a result, under the same welding conditions, compared with

the welding by supplying pure argon, argon + 67% helium mixture by conventional method and the welding by supplying alternately pure argon and pure helium by alternate method showed the increased welding speed. Also, the alternate method showed the same welding speed with argon + 67% helium mixture without largely deteriorating of weld penetration. The alternate method with argon and helium compared with the conventional methods of pure argon and argon + 67% helium mixture produced the lowest degree of welding distortion. Argon (Ar) gas is the most commonly used shielding gas for GTA (gas tungsten arc) welding for aluminium and stainless. Helium (He) gas causes a high heat input due to high arc energy and thermal conductivity, and thus supports increasing welding speed and weld penetration. The alternate method with Ar and He presented the possibility of solving the problem of the increase in gas cost and welding distortion with the use of He in stainless steel welding. [26]

Durgutlu (2004), the effect of hydrogen in argon as shielding gas was investigated for tungsten inert gas welding of 316L austenitic stainless steel. The microstructure, penetration and mechanical properties were examined. Pure argon, 1.5%H2–Ar and 5%H2–Ar were used as shielding gas. The highest tensile strength was obtained from the sample which was welded under shielding gas of 1.5%H2–Ar. After bending test cracks, tearing and surface defects were not observed on the samples welded under all three shielding media. Mean grain size in the weld metal increased with increasing hydrogen content. Additionally, weld metal penetration depth and its width increased with increasing hydrogen content. [27]

Ming Gao et al. (2007), a detailed experiment of CO2 laser-TIG hybrid welding with different shielding gas methods, is carried out on the 316L stainless plate. The results demonstrate that full weld penetration denoting efficient synergetic effect only can be obtained under the appropriate shielding gas parameters. The weld penetration of hybrid welding was determined by the plasma shape varying with the shielding gas parameters, especially the plasma height interacting with incident laser. The full penetrated weld cannot be generated by pure TIG torch method, but can be reached by the hybrid protecting method. The weld penetration of hybrid welding varies with the plasma shape determined by the shielding gas parameters, especially the plasma height interacting with incident laser. The higher the plasma height interacting with incident laser is the shallower is the weld penetration. [28]

2.2 **GAPS IN LITERATURE**

- Although many researchers have done testing and analysis on stainless steel grade SS310 and SS 316 but less work is done on optimization of parameters for TIG welding which is proposed in the present thesis work.

- Less work has been reported in the area of studying the effect of pure helium, argon-helium mixture (50-50) and pure argon on the mechanical properties and bead geometry which is carried out in the present work.

- Identification of surface defects along with mechanical tests like Bulk hardness test, impact tests, Micro hardness (Vickers), weld bead geometry (bead width and bead height) etc have not been investigated.

- Chemical composition analysis of welded joint has not been investigated in depth as due to high temperature there may be chances of dissociation or formation of new compounds in weld bead**.**

CHAPTER 3 PROBLEM FORMULATION AND METHODOLOGY

3.1 OBJECTIVES

1. To study the affect of various process parameters on SS-310 and SS-316
2. To optimize the parameters by using Taguchi D.O.E. and ANOVA in order to get quality in welding specimens
3. To investigate the effect of pure helium, argon-helium mixture (50-50) and pure argon on the mechanical properties and bead geometry
4. To find out best combination of parameters so that maximum tensile strength is obtained in actual working conditions
5. To carry out various confirmatory experiments

3.2 PROBLEM FORMULATION

In this present work the following input parameters are varied and their affect is analyzed by some experimental testing.

Input Parameters:

- Welding current
- Shielding gas type
- Gas flow rate
- Groove angle

Output Parameters:

- Weld Bead geometry (Bead width and bead height)
- Bulk Hardness test
- Micro-hardness (Vickers) test
- Dye-Penetration test for identification of surface cracks
- Impact test (at room temperature and -20 ^{0}C)
- Chemical composition analysis of weld joint
- Tensile testing

3.3 METHODOLOGY

3.3.1 D.O.E APPROACH:

In general usage, design of experiments (DOE) or experimental design is the design of any information-gathering exercises where variation is present, whether under the full control of the experimenter or not. In the design of experiments, the experimenter is often interested in the effect of some process or intervention (the "treatment") on some objects (the "experimental units"). Design of Experiments techniques enables designers to determine simultaneously the individual and interactive effects of many factors that could affect the output results in any design. DOE also provides a full insight of interaction between design elements; therefore, it helps turn any standard design into a robust one. DOE begins with determining the objectives of an experiment and selecting the process factors for the study.

An Experimental Design is the laying out of a detailed experimental plan in advance of doing the experiment. Well chosen experimental designs maximize the amount of "information" that can be obtained for a given amount of experimental effort. It is common to begin with a process model of the `black box' type, with several discrete or continuous input factors that can be controlled-that is, varied at will by the experimenter and one or more measured output responses. The output responses are assumed continuous. Experimental data are used to derive an empirical (approximation) model linking the outputs and inputs. Obtaining good results from a DOE involves these seven steps:

1. Set objectives
2. Select process variables
3. Select an experimental design
4. Execute the design
5. Check that the data are consistent with the experimental assumptions
6. Analyze and interpret the results
7. Use/present the results [4]

3.3.2 **ANOVA**

ANOVA method was applied in order to determine significant and non-significant parameters. ANOVA is basically a statistical technique which can infer some important conclusions based on analysis of the experimental data. The method is very useful for revealing the level of

significance of influence of factor(s) or interaction of factors on a particular response. It separates the total variability of the response (sum of squared deviations about the grand mean) into contributions rendered by each of the parameter/ factor and the error. In analysis of variance, a continuous response variable, known as a dependent variable, is measured under experimental conditions identified by classification variables, known as independent variables. It is also used to determine the percent contribution of each factor for results of the experiment. It calculates parameters known as sum of squares (SS), pure SS, degree of freedom (DOF), variance, F-ratio and percentage of each factor. Since the procedure of ANOVA is a very complicated and employs a considerable of statistical formulae, only a brief description of is given as following.

The Sum of Squares (SS) is a measure of the deviation of the experimental data from the mean value of the data.

Let '*A*' be a factor under investigation

$$SS_T = \sum_{i=1}^{N} (y_i - \overline{T})^2$$

Where N = Number of response observations,

$\overline{T}$ is the mean of all observations y_i is the i th response

Factor Sum of Squares (SS_A) - Squared deviations of factor (A) averages from overall average

$$SS_A = \left[\sum_{i=1}^{k_A} \left(\frac{A_i^2}{n_{Ai}} \right) \right] - \frac{T^2}{N}$$

Where

Average of all observations under A_i level = A_i/n_{Ai}

T = sum of all observations

T Average of all observations = *T* / *N*

n_{Ai} = Number of observation under A_i level

Error Sum of Squares (SS_e) - Squared deviations of observations from factor (A) averages

$$SS_e = \sum_{j=1}^{k_A} \sum_{i=1}^{n_{Ai}} \left(y_i - \overline{A}_j \right)^2$$

Sum of Squares (SS_{AxB}) for interactions

$$SS_{A\times B} = \left[\sum_{i=1}^{c} \left(\frac{(A\times B)_i^2}{n_{(A\times B)i}} \right) \right] - \frac{T^2}{N} - SS_A - SS_B$$

The parameters that influence the output can be categorized in two categories, controllable factors and uncontrollable factors. The control factors that may contribute to reduced variation can be quickly identified by looking at the amount of variation present in response. The uncontrollable factors are the sources of variation often associated with operational environment. For this experimental work, response characteristics have given in the Table 3.1

Table 3.1: Responses studied and the desired characteristics

S. No.	**Dependent variables**	**Response characteristic desired**
1	Bead Width	Smaller-the-better
2	Bead Height	Smaller-the-better
3	Toughness at room temperature	Larger-the-better
4	Toughness at -20^{o} C	Larger -the-better
5	Microhardness	Larger -the-better

CHAPTER 4 EXPERIMENTAL DESIGN

The proposal for present study was carried out by finding gaps in the literature and future scope. In this present study four parameters namely welding current, shielding gas, gas flow rate and groove angle were varied at three levels. The type of joint was butt welding joint. Tungsten inert gas welding was carried out by welding machine setup (Make: "Techno Weld, MDX-300, India") available at Thapar University, Patiala on SS 310 and SS 316 materials. The shielding gases used for this purpose were pure argon, pure helium and Argon-Helium mixture. The size of plates welded for both SS-310 and SS-316 was 160 X 100 X 6 mm. The filler wires used were of same material as that of base metal, having 2.5 mm diameter. Maximum value up to which parameters on welding machine that can be varied are:

Table 4.1: Welding Machine specifications

S. No.	PARAMETERS	Maximum Value
1	Welding Current	up to 500 amperes
2	Tungsten electrode diameter	up to 3 mm
3	Gas flow rate	up to 25 L/min.

Pilot study was carried out to finalise the process parameters. Following table shows four parameters varied at three levels:

Table 4.2: Variation of welding parameters and levels of variations

Welding Parameters	Symbol used	Levels		
		1	2	3
Current	I	130 A	170A	210A
Angle	Ɵ	60 ^{o}	75 ^{o}	90 ^{o}
Gas Type	G	Ar	He	Ar + He
Gas flow rate	F	9 L/min.	12 L/min.	15 L/min.

Pilot study was carried out to find out effect of nature of gases on welding speed. The results are shown below in table 4.3. It can be concluded that if helium is used then 25.78 % of time is saved and if mixture of both gases is used then 11.78 % of time is saved for welding same length of 100mm. Since in case of manual TIG welding speed of welding cannot be controlled so welding speed cannot be considered a parameter.

Table 4.3: Study of time consumption by each gas during welding of 100 mm length

Gas type	Time consumed (sec)	Welding speed (mm/sec)	Time consumed w.r.t argon
Argon	45.86	2.180	100
Helium	34.04	2.937	74.22
Argon + Helium	40.46	2.471	88.22

4.1 RAW MATERIAL:

The raw material includes all those consumables or non-consumables which go into the tungsten inert gas welding process.

4.1.1 STAINLESS STEEL PLATES

Stainless steel plates of grade SS-310 and SS-316 were obtained from Bombay Metal and Alloys, Ludhiana in the form of plates of sizes 160 X 100 X 6 mm as shown in figure.

Figure 4.1: Flat plates (a) SS-310 (b) SS-316

4.1.2 FILLER WIRE

The filler wires are main consumables supplied from outside to compensate for loss of metal. The filler wire is fed manually into the arc striking between non-consumable tungsten electrode and workpiece. For welding of SS-310 and SS-316, same filler wires were used with same parent metal. The filler wires were obtained from Shree Chintpurni charan industries, Ludhiana. The size of filler wire was ⌀ 2.5 X 1000 mm.

Figure 4.2: Filler wires (a) ER-310 (b) 316-LER

4.1.3 SHIELDING GASES

In the present study work, three type of shielding gases were used namely, Pure Argon, Pure Helium and Argon-Helium mixture (50:50). These gases were obtained from Dwarka Mai Gases, Jalandhar. The gas flow rate was varied at three levels as discussed earlier.

Figure 4.3: Shielding gas cylinders

4.2 CHEMICAL COMPOSITION

The following table shows various chemical constituents present in stainless steel grades SS 310 and SS 316 and percentage of these constituents:

Table 4.4: Chemical composition of the base material

Base Metal	Chemical Constituents									
	Fe	**C**	**Si**	**Mn**	**P**	**S**	**Cr**	**Mo**	**Ni**	**Cu**
SS 310	51.4	0.25	1.50	2.0	0.045	0.03	24.4	-	19.1	0.258
SS 316	62.2	0.08	0.749	2.0	0.045	0.03	17.4	2.54	12.6	0.218

4.3 PROCESS PARAMETER SELECTION

A pilot study was carried out after doing extensive study on literature to identify value of current on both SS 310 and SS 316 material, as suggested in literature review the current was to be varied between 100 -300 amperes for quality welding. So initially a weld bead was formed at 100 amperes without use of any filler and then raised in steps of 50 amperes till 250 amperes. The main purpose of carrying out such a study was to find penetration of heat energy on the down side of plate. So on basis of that the values of current chosen for present study were 130 A, 170 A, 210 A.

As per literature review gas flow rate must be varied between 9-16 L/min and included angle for butt weld joint to be varied within $60\text{-}90^0$ for quality weld. The selection of process parameters within this range gives best possible results. Gas flow affects the finished weld penetration, depth, surface profile, composition, porosity, corrosion resistance, strength, ductility, hardness and brittleness [2]. The electrode size is selected according to plate thickness. For larger diameter size of filler, larger values of current is required to get sufficient penetration as larger diameter filler wires result in to wider but less deep penetrating weld bead. In the present study, filler wire diameter used was 2.5 mm. Non- consumable Thoriated

Tungsten electrode having 3 mm diameter was used to establish arc with workpieces and hence to weld. The figure shows weld bead on both plates on up and down side.

Figure 4.4 Result of pilot study on both SS 310 and SS 316 showing up and down side

4.4 ORTHOGONAL ARRAY SELECTION

Orthogonal Arrays are often employed in experiments to study the effect of several control factors. The main benefit of using orthogonal array designed by Taguchi is that its use make analysis easy and reduces the number of experiments to be carried out in order to get result. In order to define an orthogonal array, one must define number of factors to be studied, levels of each factor to be varied and degree of freedom. The degrees of freedom are defined as the number of comparisons between process parameters that need to be made to determine which level is better and specifically how much better it is. In this study, L9 orthogonal array was used which permitted to carry out only nine experiments for each material used for study purpose. The degree of freedom of each parameter is obtained by subtracting 1 from number of levels i.e.

Degree of freedom = no. of levels-1

In this case total degree of freedom comes out to be 8 as shown in following table

Table 4.5: Allocation of degree of freedom to all parameters under study

S. No.	Parameters	DOF
1	Welding Current	2
2	Shielding gas type	2
3	Groove angle	2
4	Gas flow rate	2
	Total	**8**

The Table 4.5 shows the orthogonal array as suggested by Taguchi D.O.E method used in the present study for both SS 310 and SS 316.

Table 4.6: Orthogonal array for experimentation on both SS 310 and SS316

Exp. No.	Parameter's abbreviation	Current (A)	Gas	Gas flow rate (L/min.)	Groove angle (Θ^0)
1	I_1,G_1,F_1,Θ_1	130	Ar	9	60
2	I_1,G_2,F_2,Θ_2	130	He	12	75
3	I_1,G_3,F_3,Θ_3	130	Ar+He	15	90
4	I_2,G_1,F_2,Θ_3	170	Ar	12	90
5	I_2,G_2,F_3,Θ_1	170	He	15	60
6	I_2,G_3,F_1,Θ_2	170	Ar+He	9	75
7	I_3,G_1,F_3,Θ_2	210	Ar	15	75
8	I_3,G_2,F_1,Θ_3	210	He	9	90
9	I_3,G_3,F_2,Θ_1	210	Ar+He	12	60

4.5 WELDING OF STAINLESS STEEL PLATES

4.5.1 EDGE PREPARATION OF SPECIMENS:

In common welding practices, the welding surface needs to be prepared to ensure the strongest weld possible. Preparation is needed for all forms of welding and all types of joints. Filler metal, in the form of welding rod, is almost always used in making square butt welds. It is seldom possible to make a satisfactory, full-strength weld by merely butting the pieces tight together, without spacing, and then melting the edges together. When welding, contact is established only at a few points in the surface therefore the strength attained will be only a fraction of the full strength. Also, the irregular surface may not be very clean, being contaminated with adsorbed moisture, oxide film, grease layer etc.

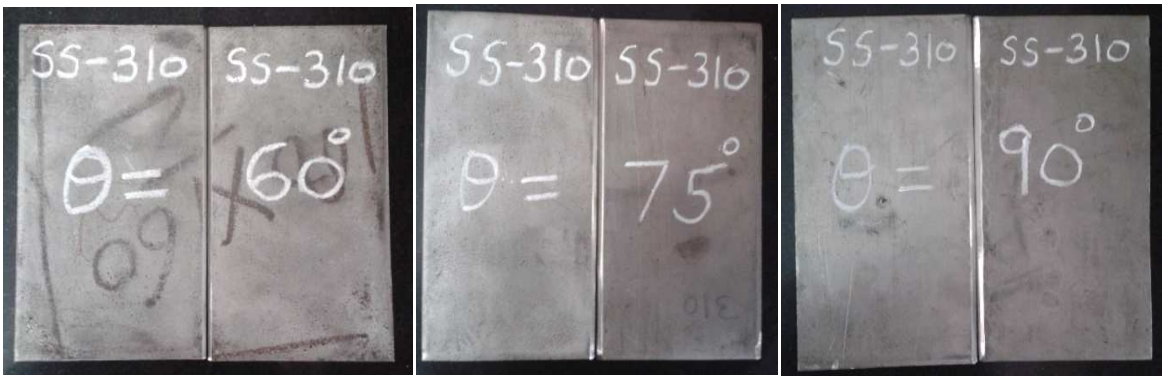

Figure 4.5: Groove angles on SS 310 welding specimens

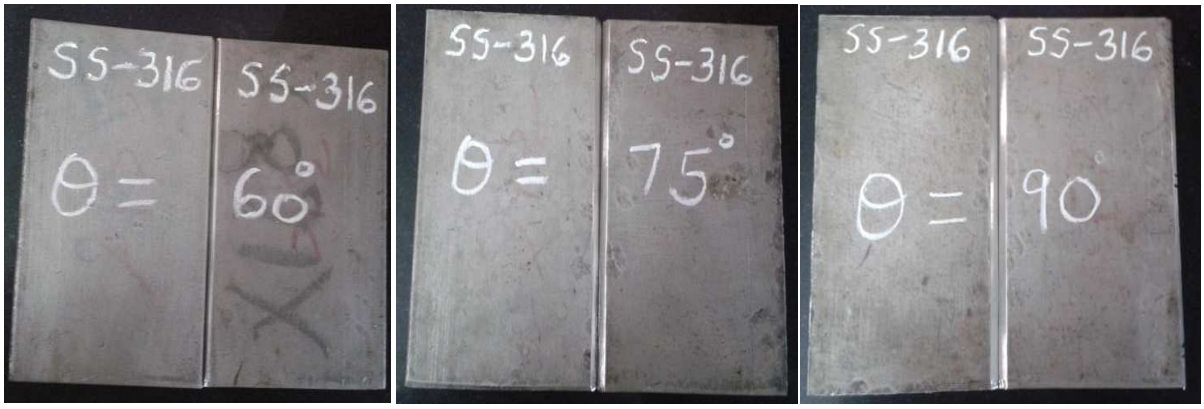

Figure 4.6: Groove angles on SS 316 welding specimens

4.5.2 TACKING AND CLAMPING OF WELDING SPECIMENS

Figure 4.7: Tacking and clamping of samples welded

4.5.3 WELDING OF SPECIMENS

The welding of stainless steel specimens were carried out as per orthogonal array decided earlier with all necessary precautions and the pieces were cooled naturally in open air. The figure ahead shows welded pieces immediately after welding.

(1) **(2)** **(3)**

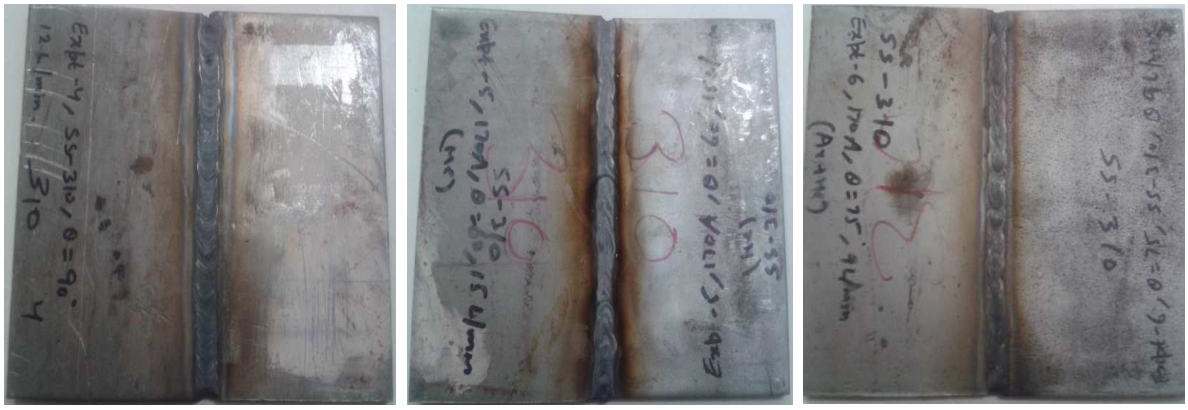

(4) **(5)** **(6)**

(7) **(8)** **(9)**

Figure 4.8: Specimens (1-9) of stainless steel grade 310 after welding with filler wire of same grade.

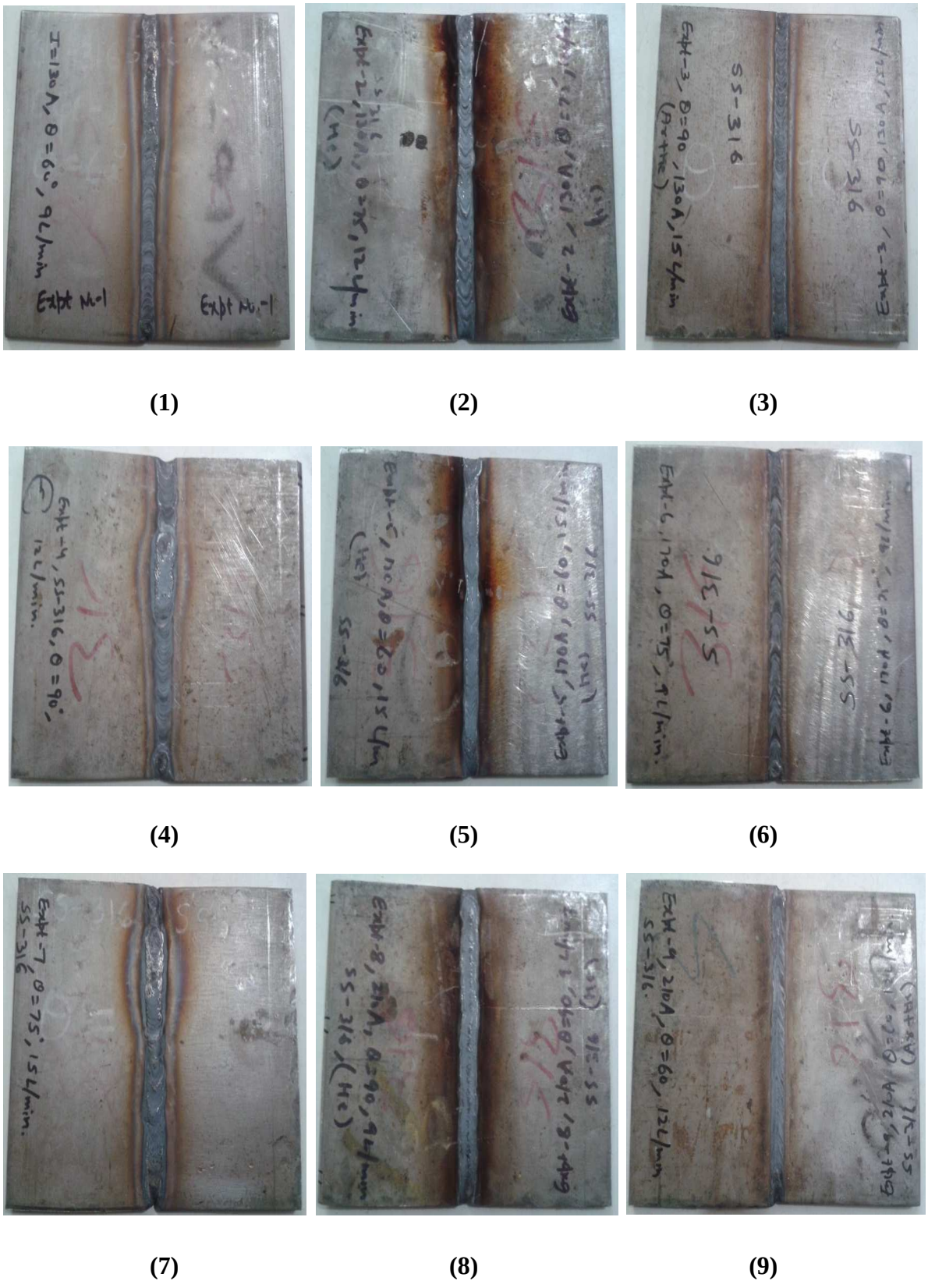

(1) **(2)** **(3)**

(4) **(5)** **(6)**

(7) **(8)** **(9)**

Figure 4.9: Specimens (1-9) of stainless steel grade 316 after welding with filler wire of same grade.

After welding process as per orthogonal array decided earlier, the weld bead was cleaned thoroughly with clean cloth and acetone. After this, bead width and bead height were measured on individual samples, the results are discussed later.

4.5.4 CUTTING OF WELDED SPECIMEN FOR VARIOUS TESTING

The following figure shows the plan according to which welded specimens were cut on chop saw cutting machine. A margin of 2 mm is already included during cutting of specimens. The specimens were grinded to make them of exact sizes. The shaper machine tool was used to make a V-notch having 45^{o} included angle for impact test specimens.

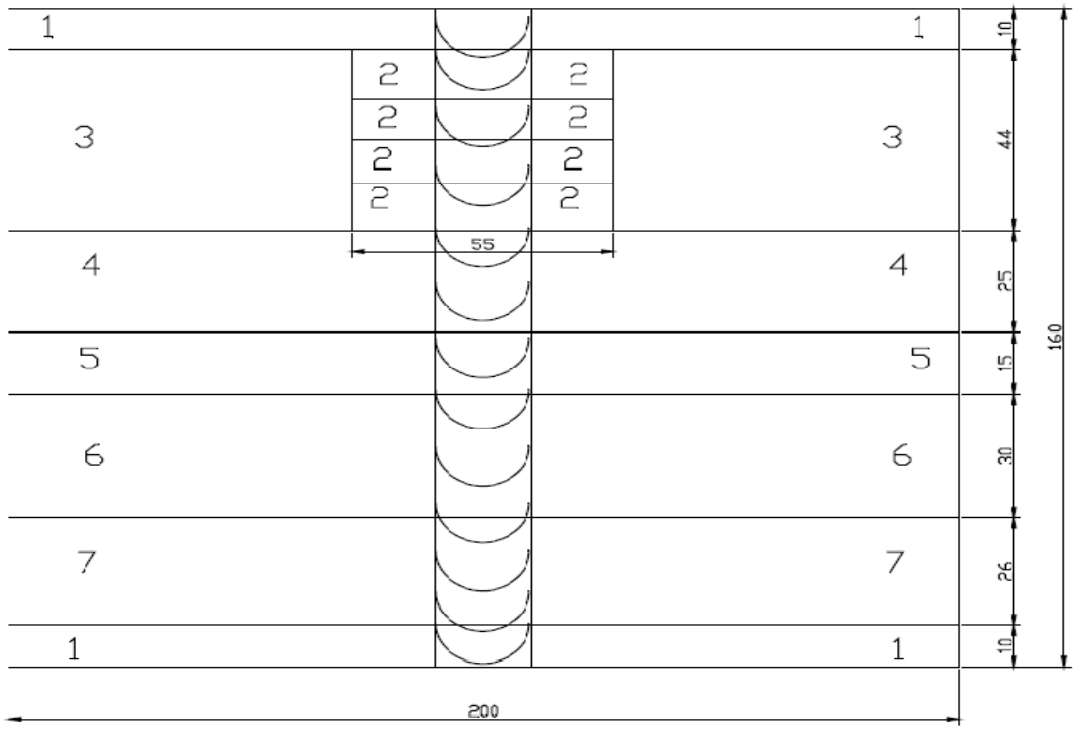

Figure 4.10: Marking and cutting plan of welded specimens (all dimensions in mm)

Table 4.7: Description of various marked portions for both SS 310 and SS 316 grade

Marking on welded specimen	Usage for particular test measurement
1-1, 3-3	Rejected portion of welded pieces
2-2	Four specimen for carrying out impact testing
4-4	One specimen for Tensile testing
5-5	One specimen for bulk-hardness testing
6-6	Specimen for micro-hardness testing
7-7	Specimen for chemical composition analysis of weld bead

4.6 TESTING OF STAINLESS STEEL WELD SPECIMEN

As decided earlier following various output parameters were tested and measured on welded specimens:

- Weld Bead geometry
- Dye Penetration test
- Bulk Hardness test
- Impact test
- Micro-hardness test
- Weld bead chemical composition analysis
- Tensile Test

4.6.1 WELD BEAD GEOMETRY:

In the fabrication of welded steel joints using arc welding methods, several process parameters influence the weld bead geometry and weld joint characteristics. The weld bead shape is a very important factor determining the quality of welds. The knowledge of how welding process parameters affect weld bead geometry is important because it can be applied in automatic and semiautomatic control of arc welding processes where optimal selection of input parameters is required for high productivity and cost effectiveness. Theoretically, an extremely thin fused layer might be sufficient for connecting the parts to be joined. The fusion layer should also not be thicker than necessary in order to avoid wasting of energy, edge burn-off, sagging of the weld pool and deep weld end craters. Control of weld-bead shape is essential as the mechanical properties of welds are affected by the weld-bead shape.

Generally, all welding processes are used with the aim of obtaining a welded joint with the desired weld-bead parameters, excellent mechanical properties with minimum distortion. In the present study, readings of bead width and height were measured at five different points with help of Digital Vernier Calliper (Make: Mitutoyo, Japan having least count=0.02mm) and Vernier height gauge (Make: Starrett-723, American having least count= 0.01mm) respectively at C.E.C, Landran workshop. The pieces were kept on surface plate as shown in figure ahead.

Figure 4.11: Measurement of bead height (Courtesy: workshop at C.E.C, Landran)

4.6.2 DYE PENETRATION TEST:

In order to detect the presence of surface cracks and porosities the dye penetration test is carried out. Dye penetrant inspection (DPI), also called liquid penetrant inspection (LPI) or penetrant testing (PT), is a widely applied and low-cost inspection method used to locate surface-breaking defects in all non-porous materials (metals, plastics, or ceramics). The penetrant may be applied to all non-ferrous materials and ferrous materials; although for ferrous components magnetic-particle inspection is often used instead for its subsurface detection capability. LPI is used to detect casting, forging and welding surface defects such as hairline cracks, surface porosity, leaks in new products, and fatigue cracks on in-service components.

DPI is based upon capillary action, where a low surface tension fluid penetrates into clean and dry surface-breaking discontinuities. Penetrant may be applied to the test component by dipping, spraying, or brushing. After adequate penetration time has been allowed, the excess penetrant is removed and a developer is applied. The developer helps to draw penetrant out of the flaw so that an invisible indication becomes visible to the inspector.

The main advantages of DPI are the speed of the test and the low cost. It produces a flaw indication that is much larger and easier for the eye to detect than the flaw itself. Many flaws are so small or narrow that they are undetectable by the unaided eye (a person with a perfect vision cannot resolve features smaller than 0.08 mm). It improves the detectability of a flaw due to the high level of contrast between the indication and the background which helps to make the indication more easily seen (such as a red indication on a white background for visible penetrant or a penetrant that glows under ultraviolet light for fluorescents penetrant).

Disadvantages include the detection of only surface flaws, skin irritation, and the inspection should be on a smooth clean surface where excessive penetrant can be removed prior to being developed. Conducting the test on rough surfaces, such-as "as-welded" welds, will make it difficult to remove any excessive penetrant and could result in false indications. Water-washable penetrant should be considered here if no other option is available. Also, on certain surfaces a great enough color contrast cannot be achieved or the dye will stain the workpiece. Limited training is required for the operator although experience is quite valuable. Proper cleaning is necessary to assure that surface contaminants have been removed and any defects present are clean and dry. General steps of Liquid Penetrant Testing are:

- Surface Preparation: One of the most critical steps of a liquid penetrant testing is the surface preparation. The surface must be free of oil, grease, water, or other contaminants that may prevent penetrant from entering flaws.
- Penetrant Application: Once the surface has been thoroughly cleaned and dried, the penetrant material is applied by spraying, brushing, or immersing the part in a penetrant bath.
- Penetrant Dwell: The penetrant is left on the surface for a sufficient time to allow as much penetrant as possible to be drawn from or to seep into a defect. Penetrant dwell time is the total time that the penetrant is in contact with the part surface. Dwell times are usually recommended by the penetrant producers or required by the specification being followed. The times vary depending on the application, penetrant materials used, the material, the form of the material being inspected, and the type of discontinuity being inspected for. Minimum dwell times typically range from five to 60 minutes. Generally, there is no harm in using a longer penetrant dwell time as long as the penetrant is not allowed to dry.
- Excess Penetrant Removal: This is the most delicate part of the inspection procedure because the excess penetrant must be removed from the surface of the sample while removing as little penetrant as possible from defects. Depending on the penetrant system used, this step may involve cleaning with a solvent, direct rinsing with water, or first treating the part with an emulsifier and then rinsing with water.
- Developer Application: A thin layer of developer is then applied to the sample to draw penetrant trapped in flaws back to the surface where it will be visible. Developers come in a variety of forms that may be applied by dusting (dry powders), dipping, or spraying (wet developers).

- Indication Development: The developer is allowed to stand on the part surface for a period of time sufficient to permit the extraction of the trapped penetrant out of any surface flaws. This development time is usually a minimum of 10 minutes. Significantly longer times may be necessary for tight cracks.
- Inspection: Inspection is then performed under appropriate lighting to detect indications from any flaws which may be present.
- Post Cleaning Surface: The final step in the process is to thoroughly clean the part surface to remove the developer from the parts that were found to be acceptable.

Figure 4.12: Orion's cleaner, penetrant and developer for DPT of welded specimen.

For performing of dye penetration test, three solutions (Make: The oriental chemical works (P) LTD, Kolkata) namely Orion 115PR (penetrant remover), Orion115P (red dye penetrant) and Orion115D (developer) were used.

4.6.3 BULK HARDNESS TEST:

Rockwell hardness testing is a general method for measuring the bulk hardness of metallic and polymer materials. Although hardness testing does not give a direct measurement of any performance properties, hardness of a material correlates directly with its strength, wear resistance, and other properties. Hardness testing is widely used for material evaluation because of its simplicity and low cost relative to direct measurement of many properties. Hardness is a measure of how resistant solid matter is to various kinds of permanent shape change when a force is applied. Macroscopic hardness is generally characterized by strong intermolecular bonds, but the behaviour of solid materials under force is complex; therefore,

there are different measurements of hardness: scratch hardness, indentation hardness, and rebound hardness. Indentation hardness measures the resistance of a sample to material deformation due to a constant compression load from a sharp object they are primarily used in engineering and metallurgy fields. Smooth parallel surfaces, free of coatings, scale and gross contamination, are required for testing.

To start the test, the indenter is set into the sample at a prescribed minor load. A major load is then applied and held for a set time period. The force on the indenter is then decreased back to the minor load. The Rockwell hardness number is calculated from the depth of permanent deformation of the indenter into the sample, i.e. the difference in indenter position before and after application of the major load. The minor and major loads can be applied using dead weights or springs. The indenter position is measured using an analog dial indicator or an electronic device with digital readout.

Figure 4.13: Rockwell Hardness Testing machine (Courtesy: solid mechanics lab, Thapar University, Patiala)

Bulk hardness of the weld specimen for both materials was found by using Rockwell Hardness Testing Machine (Make: Avery, England). For this purpose the scale chose was C-scale which makes use of a diamond indenter. Markings were made on sample and hardness was measured at centre of weld bead, 2 mm away from mean, 5 mm away from mean 10 mm away from mean and so on in both directions along weld bead. In order to nullify any chance of error, three readings were taken at each position marked earlier and then average was taken.

4.6.4 IMPACT TEST:

It is a method for determining behaviour of material subjected to shock loading in bending, tension, or torsion. The quantity usually measured is the energy absorbed in breaking the specimen in a single blow, as in the Charpy Impact Test, Izod Impact Test. Materials behave quite differently when they are loaded suddenly than when they are loaded more slowly as in tensile testing. Because of this fact, impact test is considered to be one of the basic mechanical tests (especially for ferrous metals). Impact testing is about resisting impact. This is often called a material's toughness. It's the amount of energy a material can absorb before fracturing or breaking). It becomes of engineering importance when the ability of a material to withstand an impact load without fracturing is considered. Charpy test was performed on impact testing machine (Make: Alfred J Amsler and Co. Switzerland). The range of this testing machine is 0-300 Kgm. In the present study, the specimens were prepared having size 10 X 6 X 55 mm. As per ASTM standard A-370 if thickness of plate is less than 11 mm then undersize test specimen can be used to carry out impact test. Impact test conditions were chosen to represent those most severe relative to the potential for fracture like room temperature condition and temperature below room temperature(-20^{o} C). Liquid nitrogen was used to create artificial test conditions of -20^{o} C temperature.

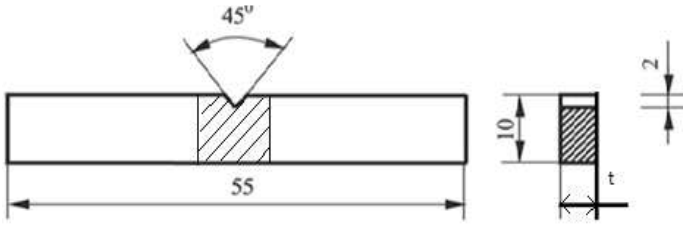

Figure 4.14: Impact Test specimen as per ASTM A-370 standard

4.6.5 MICRO-HARDNESS (VICKERS) TEST

The Vickers hardness test method consists of indenting the test material with a diamond indenter, in the form of a right pyramid with a square base and an angle of 136 degrees between opposite faces. The advantages of the Vickers hardness test are that extremely accurate readings can be taken, and just one type of indenter is used for all types of metals and surface treatments. The samples were grounded on belt grinder and then rubbed with emery paper size number 400, 600, 800, 1000 and then polished on polishing wheel. The two diagonals of the indentation left in the surface of the material after removal of the load were

measured using a microscope and their average value is provided. The microhardness of weld region was determined with microhardness tester (Make: Metatech Industries, Pune, India). Software named 'Quantimet' was used to measure the indents so formed at forty times magnification. For getting an indentation, load applied to indenter was 1000 grams with 20 second dwell time.

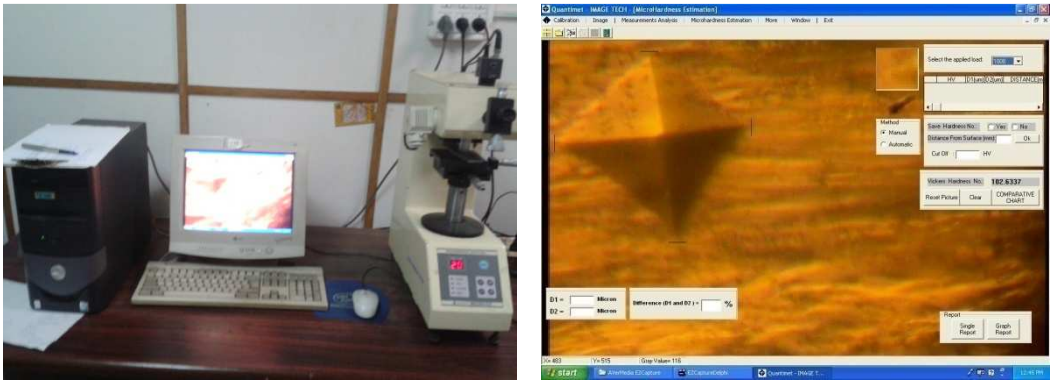

(a) **(b)**

Figure 4.15: (a) Microhardness testing equipment (courtesy Thapar Univ. Patiala) and (b) indentation on one of the sample

4.6.6 CHEMICAL COMPOSITION OF WELD BEAD:

Atomic absorption spectroscopy (AAS) is an analytical technique that measures the concentrations of elements. Atomic absorption is so sensitive that it can measure down to parts per billion of a gram in a sample. The technique makes use of the wavelengths of light specifically absorbed by an element. They correspond to the energies needed to promote electrons from one energy level to another. Atomic absorption spectroscopy has many uses in different areas of chemistry.

In AAS the atomized sample is converted into ground state free atoms in the vapour state and a beam of electromagnetic radiation emitted from excited lead atoms is passed through the vaporized sample. Some of the radiation is absorbed by the lead atoms in the sample. The greater the number of atoms there is in the vapour, the more radiation is absorbed. The amount of light absorbed is proportional to the number of lead atoms. Spectroscopy is the study of matter and its properties by the use of spectra. Each chemical element, when heated so that it gives off light, yields a different series of lines in a spectrum. The position of the lines and the patterns they form in the spectrum of a particular substance can yield many kinds of

information about the substance. Spectroscopy is not limited to the visible-light spectrum, but includes the spectra of other forms of electromagnetic radiation, such as X rays, infrared radiation, and radio waves. The surface of specimen should be free from contaminants and polished. Now a source of light is required which emits light towards a source of heat flame or spark. This source of heat comprises of vaporised atoms of metal surface being analysed in ground state. There is absorption of some part of light during this process. This is passed through a focussing lens and then on to the prism which further divide the light into different sections. This is then aimed on to a device called photomultiplier which provide us the reading. It is with the help of atomic emission spectroscopy we can analyse the types of alloying elements but to know their composition, atomic absorption spectrometry principle is used.

The chemical composition of base metal and welded bead was found by making use of atomic absorption spectrometer (Make: Foundry Master). The software named Worldwide Analytical System was used by the interface which tells about chemical composition. The argon gas was discharged at flow rate of 60 L/min for forming a shielding atmosphere during the time sparking occurs between specimen and electrode during finding out the chemical composition.

Figure 4.16: Atomic Absorption spectrometer (Courtesy: Metrology lab, Thapar University, Patiala)

4.6.7 TENSILE TEST

The basic test for determination of material behaviour is the tensile test. A specimen is ruptured by a test machine while the actual force and the elongation of the specimen is measured. With these measurement values, tension σ and strain ε are calculated. Normally, if steel with a bcc lattice structure is tested, a curve with a clear yield point is obtained. Steels with a fcc lattice

structure show a curve without yield point. Tensile test specimen has enlarged ends or shoulders for gripping. The important part of the specimen is the gauge section. The cross-sectional area of the gauge section is reduced relative to that of the remainder of the specimen so that deformation and failure will be localized in this region. The gauge length is the region over which measurements are made and is centered within the reduced section. The tensile test was performed on all the specimens for both materials. The shape and size of the specimen chosen was in accordance with ASTM specification E8/E8M-11

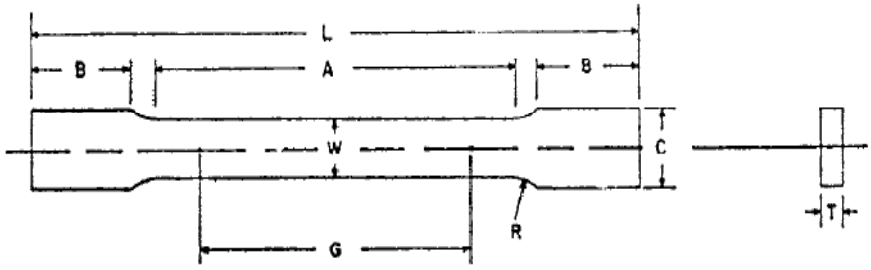

Figure 4.17: Tensile test specimen as per ASTM E8/E8M-11

Nine specimens were prepared from both stainless steel grades, one each from particular specimen as decided in orthogonal array for tensile testing. Tensile test was carried out at a constant speed of 8 mm/min. The shape of the specimen was rectangular bar and all dimensions are shown in Table 4.8 as follows.

Table 4.8: Shape and size specification of tensile test specimens

INDICATION	NOTATION	SIZE (mm)
A	Length of reduced section	57
B	Length of grip section	50
C	Width of grip section	20
G	Gauge length	50
L	Overall length	200
R	Radius of fillet	12.5
T	Thickness of plate	6
W	Width	12.5

CHAPTER 5 RESULTS OF BEAD GEOMETRY

The weld bead shape is a very important factor determining the quality of welds. Weld bead width is directly proportional to arc current, welding voltage and electrode diameter and indirectly proportional to the welding speed. Weld bead height is the crown height of the weld bead from the base plate. It increases with the increase in wire feed rate. Increase of reinforcement with increase of welding filler wire feed rate is mainly due to the larger amount of metal deposited per unit length. As discussed earlier, bead width and bead height were measured and the result of measurement are shown hereunder:

5.1 RESULT OF BEAD GEOMETRY FOR SS 310

Table 5.1: Weld bead width and bead height observations of SS 310

Expt. No.	Bead Width Observations (mm)	Average Bead width (mm)	Bead Height Observations (mm)	Average Bead Height (mm)
1	8.34, 8.36, 8.38, 8.36, 8.37	8.362	0.94,0.96,1.0,1.0,0.98	0.976
2	8.88,8.85,8.87,8.89,8.89	8.876	0.92,0.94,0.88,0.92,0.94	0.92
3	8.28,8.26,8.28,8.28,8.26	8.272	0.9,0.92,0.92,0.88,0.9	0.904
4	8.66,8.67,8.68,8.67,8.68	8.672	0.94,0.96,0.96,0.94,0.94	0.948
5	10.75,10.74,10.76,10.73,10.73	10.742	1.04,1.06,1.04,1.04,1.06	1.048
6	8.38,8.36,8.37,8.39,8.4	8.38	0.82,0.84,0.84,0.86,0.86	0.844
7	9.78,9.79,9.77,9.79,9.79	9.784	1.08,1.06,1.04,1.06,1.08	1.064
8	11.65,11.64,11.66,11.67,11.65	11.654	0.92,0.94,0.92,0.96,0.96	0.94
9	10.42,10.45,10.42,10.46,10.47	10.444	1.2,1.22,1.22,1.24,1.22	1.22

The graphical representation of bead width and height are shown in figures 5.1 and 5.2 ahead showing the variations in all welded samples for stainless steel grade SS 310

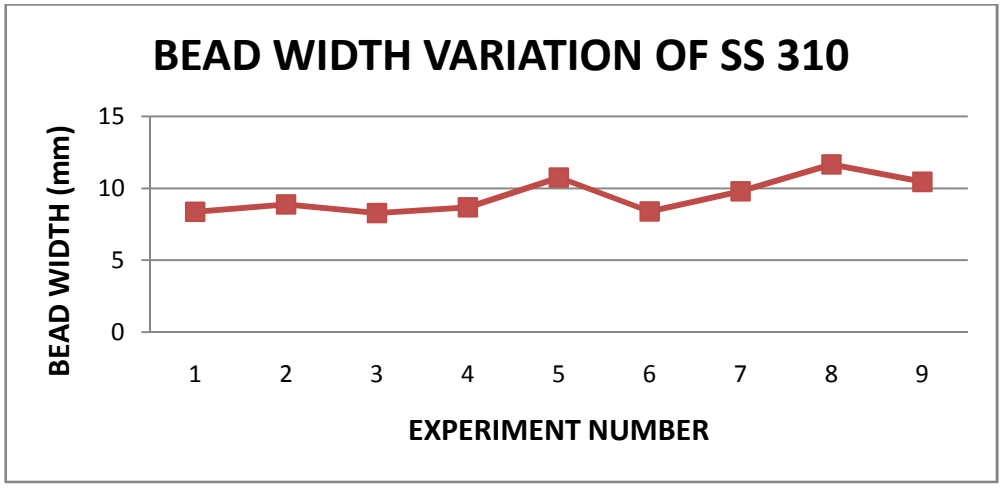

Figure 5.1: Graphical representation of bead width variation of SS 310

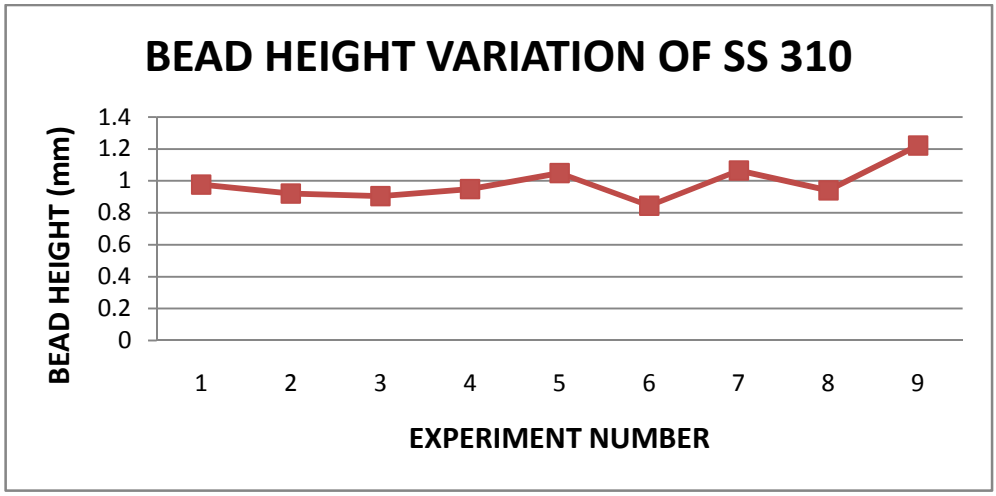

Figure 5.2: Graphical representation of bead height variation of SS 310

5.1.1 ANOVA TABLE FOR SS 310 ON BEAD WIDTH

The results for weld bead width were analysed by using ANOVA in order to identify the significant factors affecting the performance measures. Average value of bead width for all the specimens is shown in Table 5.1 along with its graphical representation in figure 5.1. The minimum value of bead width of SS 310 is 8.27 mm at current value 130A. It is clear from results so obtained from table 5.2 to table 5.5 that current is the most important parameter having the most significant affect on the bead width and then shielding gas type has sub-significant affect, whereas flow rate and groove angle have almost negligible effect on the same. Plot for main effects in figure 5.3 shows that with increase in current the value of bead width increases which is not desirable. Among all gases, argon helps to keep bead width minimum.

Table 5.2 Analysis of variance for SN ratio of weld bead width of SS 310

Source	DOF	SS	Variance	F ratio	F (critical)	PC
Current	2	5.659	2.829	65.668	19	56.940
Gas type	2	3.228	1.614	37.462	19	32.105
Flow rate	2	0.086	0.043	1	19	3.523
Grove angle	2	0.813	0.406	9.440	19	7.432
Total	8	9.787				100
Error pooled	2	0.086	0.043			3.523

Table 5.3: Response table for SN ratio of weld bead width of SS 310

Level	Current	Gas type	Flow rate	Grove angle
1	-18.59	19.01	-19.41	-19.82
2	-19.28	-19.07	-19.37	-19.08
3	-20.51	-20.31	-19.59	-19.48
Delta	1.92	1.30	0.23	0.74
Rank	1	2	4	3

Table 5.4: Analysis of variance for Means of weld bead width of SS 310

Source	DOF	SS	Variance	F ratio	F (critical)	PC
Current	2	6.949	3.474	64.313	19	55.726
Gas type	2	4.149	2.074	38.402	19	32.920
Flow rate	2	0.108	0.054	1	19	3.523
Grove angle	2	1.069	0.534	9.897	19	7.831
Total	8	12.277				100
Error pooled	2	0.108	0.054			3.523

Table 5.5: Response table for Means of weld bead width of SS 310

Level	Current	Gas type	Flow rate	Grove angle
1	8.503	8.939	9.465	9.850
2	9.265	9.032	9.331	9.013
3	10.628	10.424	9.599	9.533
Delta	2.124	1.485	0.268	0.836
Rank	1	2	4	3

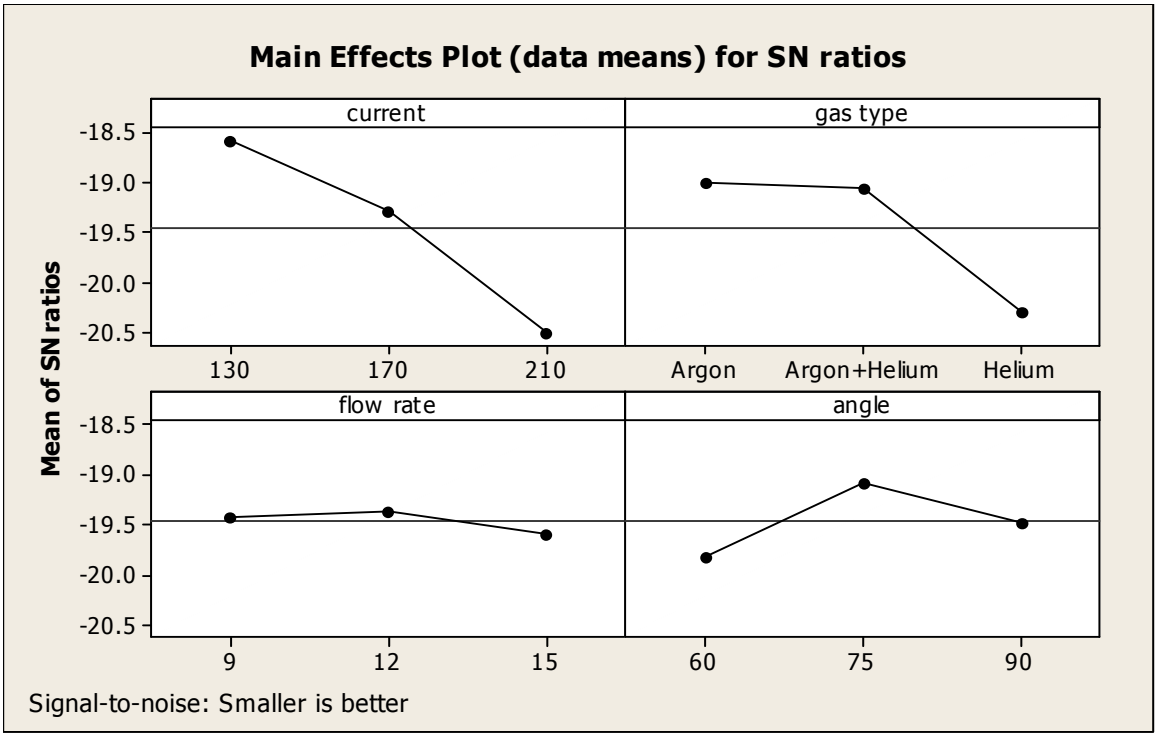

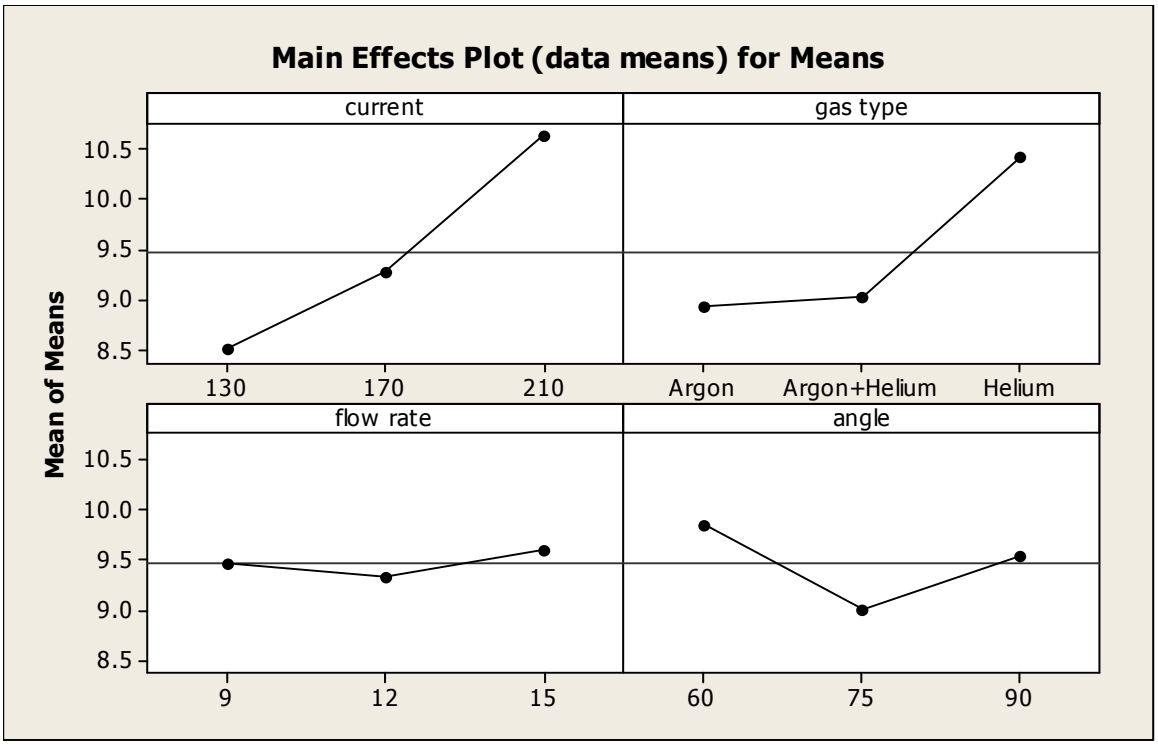

Figure 5.3: Main effect plot for SN ratios and means of Weld Bead width of SS 310

5.1.1.1 OPTIMAL DESIGN FOR BEAD WIDTH OF SS 310

It is clear from ANOVA table for means (table 5.4) that the F value of current and type of gas is greater than F critical. Main effect plot shows that bead width is minimum for first level

current value i.e. 130 A and first level gas type i.e. argon. The confidence interval predict with 95 % confidence so that the value of bead width for SS 310 would be 7.977 ± 0.745 mm.

Mean value of bead width is given by:

$\mu I_1G_1 = \overline{I_1} + \overline{G_1} - \overline{Y}$

$= 8.503 + 8.939 - 9.465$

$= 7.977$ mm

Confidence Interval around the Estimated Mean width

$$CI_1 = \sqrt{\frac{F_{\alpha,v_1,v_2} V_e}{n_{eff}}}$$

Where $F\alpha V_1V_2 = F0.05:1:2 = 18.51$

α = Risk (0.05), Confidence = 1-α

V_1 = DOF for mean which is always = 1

V_2 = DOF for error = Ve = 2

η_{eff} = Number of tests under that condition using the participating factors

$\overline{Y}$ = Average bead width

$\eta_{eff} = N / (1+ DOFI_1G_1) = 9/ 1+2+2 = 1.80$

CI = 0.745

So the confidence interval around the Estimated Mean width is given by 7.977 ± 0.745mm

5.1.2 ANOVA TABLE FOR SS 310 ON BEAD HEIGHT

The observations on variations of bead height and its average value for SS 310 are given in table 5.1. The minimum value of bead height is 0.904 mm which was obtained at 130A current. The results for weld bead height were analysed by using ANOVA in order to identify the significant factors and are shown in tabular form compiled from table 5.6 to table 5.9. It is clear from main effect plot in figure 5.4 that among all values, grove angle of 90^O and gas flow rate of 9 l/min gives the minimum value of bead height. The grove angle is the most significant factor affecting the bead height in a particular way as shown in results followed by current which is ranked second. The bead height increases with increase in value of current. The helium gas was found to be contributing in obtaining minimum bead height.

Table 5.6 Analysis of variance for SN ratio of weld bead height of SS 310

Source	DOF	SS	Variance	F ratio	F (critical)	PC
Current	2	2.578	1.289	28.802	19	34.787
Gas type	2	0.089	0.044	1	19	5.006
Flow rate	2	1.451	0.725	16.215	19	19.0378
Grove angle	2	3.035	1.517	33.902	19	41.169
Total	8	7.156				100
Error pooled	2	0.089	0.044			

Table 5.7: Response table for SN ratio of weld bead height of SS 310

Level	Current	Gas type	Flow rate	Grove angle
1	0.601	0.044	0.738	-0.642
2	0.509	0.206	-0.180	0.551
3	-0.577	0.283	-0.023	0.624
Delta	1.179	0.239	0.919	1.267
Rank	2	4	3	1

Table 5.8: Analysis of variance for Means of weld bead height of SS 310

Source	DOF	SS	Variance	F ratio	F (critical)	PC
Current	2	0.036	0.018	31.605	19	35.531
Gas type	2	0.001	0.0005	1	19	4.644
Flow rate	2	0.019	0.009	17.138	19	18.735
Grove angle	2	0.042	0.021	36.394	19	41.090
Total	8	0.099				100
Error pooled	2	0.001	0.0005			4.644

Table 5.9: Response table for Means of weld bead height of SS 310

Level	Current	Gas type	Flow rate	Grove angle
1	0.933	0.996	0.920	1.081
2	0.946	0.989	1.029	0.942
3	1.074	0.969	1.005	0.930
Delta	0.141	0.026	0.109	0.150
Rank	2	4	3	1

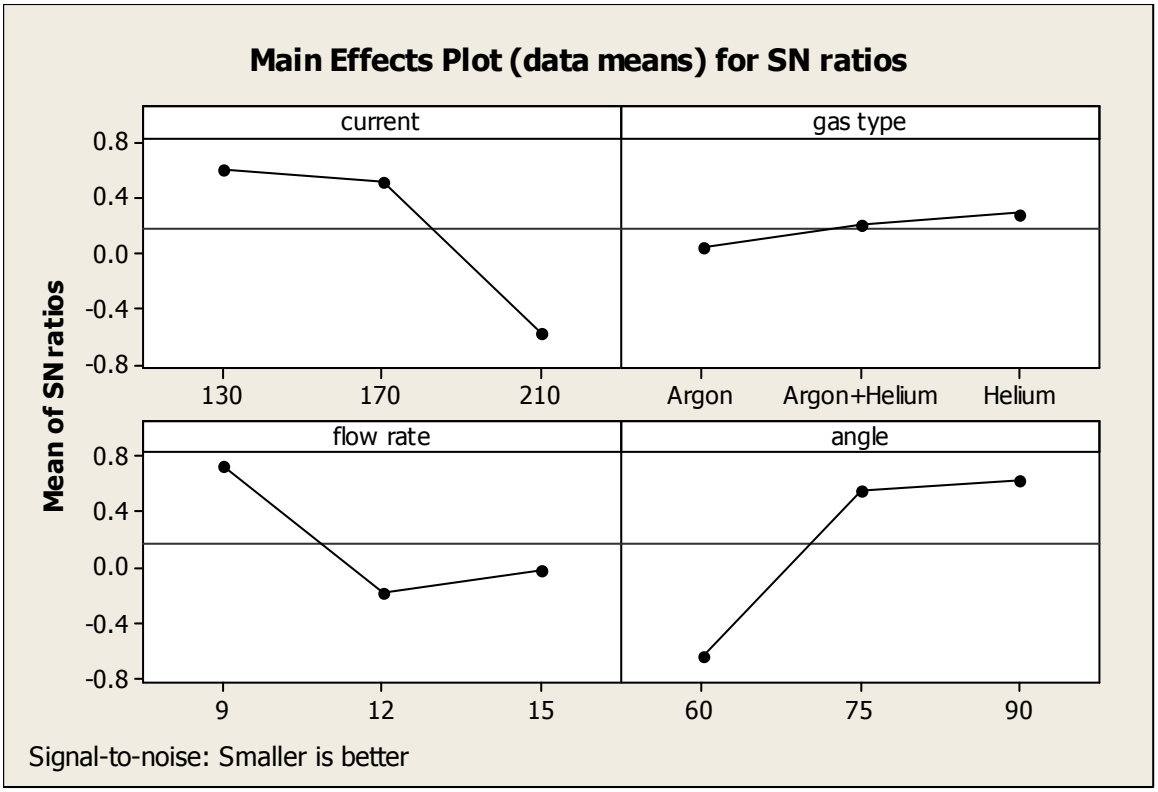

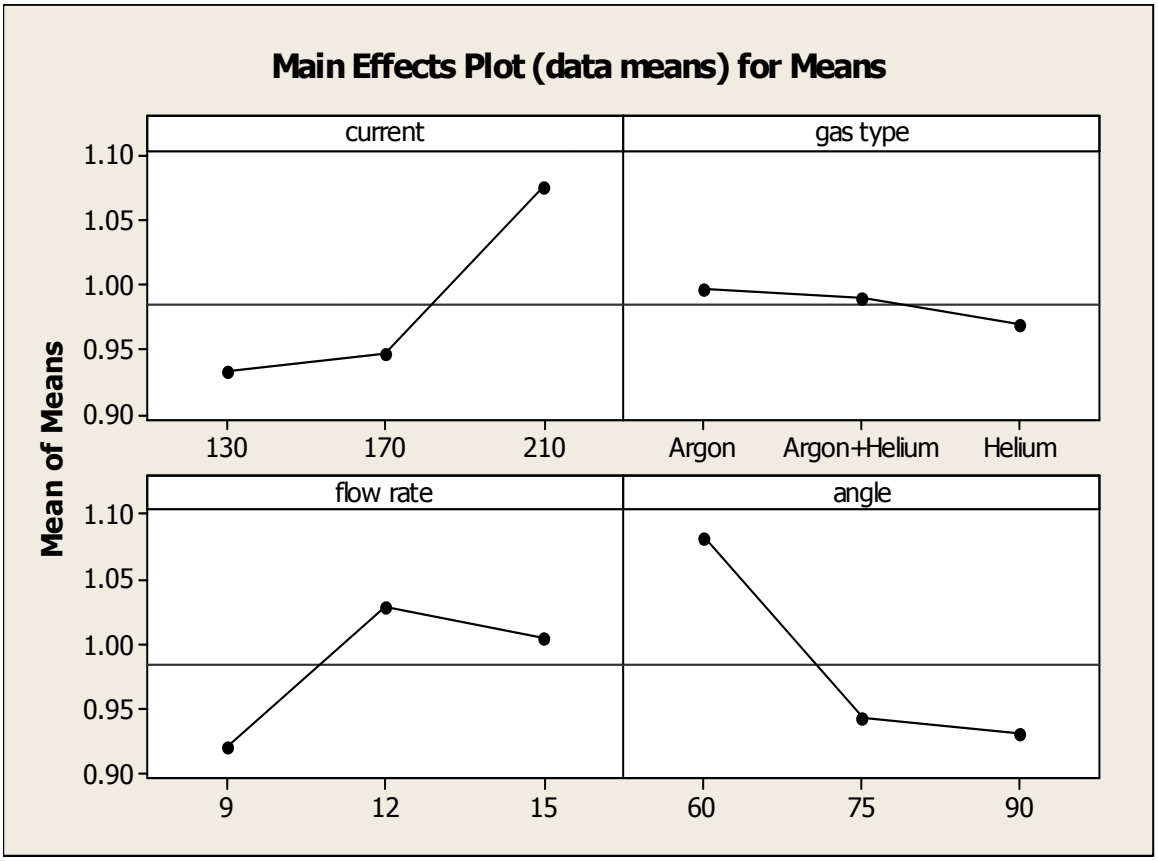

Figure 5.4: Main effect plot for SN ratios and means of Weld Bead height of SS 310

5.1.2.1 OPTIMAL DESIGN FOR BEAD HEIGHT OF SS 310

It is clear from ANOVA table for means (table 5.8) that the F value of grove angle and current is greater than F critical. Main effect plot shows that bead width is minimum for first level current value i.e. 130 A and third level grove angle i.e. 90^o. The confidence interval predict with 95 % confidence so that the value for SS 310 would be 0.880 ± 0.077 mm.

Mean value of bead height is given by:

$\mu\ I_1\Theta_3 = \overline{I_1} + \overline{\Theta}_3 - \overline{Y}$

$= 0.9333 + 0.9307 - 0.984$

$= 0.880$ mm

Confidence Interval around the Estimated Mean width

$$CI_1 = \sqrt{\frac{F_{\alpha,v_1,v_2} V_e}{n_{eff}}}$$

Where $F\alpha,V_1,V_2 = F0.05:1:2 = 18.51$

α = Risk (0.05), Confidence = 1-α

V_1 = DOF for mean which is always = 1

V_2 = DOF for error = Ve = 2

$\overline{Y}$ = Average bead height

η_{eff} = Number of tests under that condition using the participating factors

$\eta_{eff} = N / (1+ DOF\mathbf{I_1G_1}) = 9/ 1+2+2 = 1.80$

CI = 0.077

So the confidence interval around the Estimated Mean height is given by 0.880 ± 0.077 mm

5.2 RESULT OF BEAD GEOMETRY FOR SS 316

Table 5.10: Weld bead width and bead height observations of SS 316

Expt. No.	Bead Width Observations (mm)	Average Bead width (mm)	Bead Height Observations (mm)	Average Bead Height (mm)
1	8.24,8.26,8.25 8.28,8.27	8.26	0.96,0.94,0.94,0.96,0.94	0.972
2	8.98,8.95,8.94,8.96,8.96	8.958	0.98,1.04,1.04,1.0,1.0	0.936
3	8.18,8.16,8.18,8.16,8.16	8.168	0.74,0.76,0.76,0.74,0.76	0.908
4	8.56,8.57,8.58,8.59,8.58	8.576	0.58,0.56,0.56,0.58,0.56	0.976
5	10.92,10.9,10.88,10.9, 10.92	10.906	1.1,1.12,1.12,1.1,1.12	1.02
6	8.48,8.46,8.37,8.45,8.44	8.44	1.08,1.06,1.04,1.04,1.04	0.86
7	9.68,9.64,9.67,9.69,9.66	9.668	1.0,1.02,1.0,1.02,1.02	1.008
8	11.85,11.84,11.88,11.87,11.85	11.858	0.84,0.86,0.84,0.88,0.88	0.96
9	10.32,10.35,10.32,10.36,10.34	10.338	0.7,0.68,0.68,0.68,0.68	1.232

The graphical representation of bead width and height are shown in figures ahead showing the variations in all welded samples for stainless steel grade SS 316

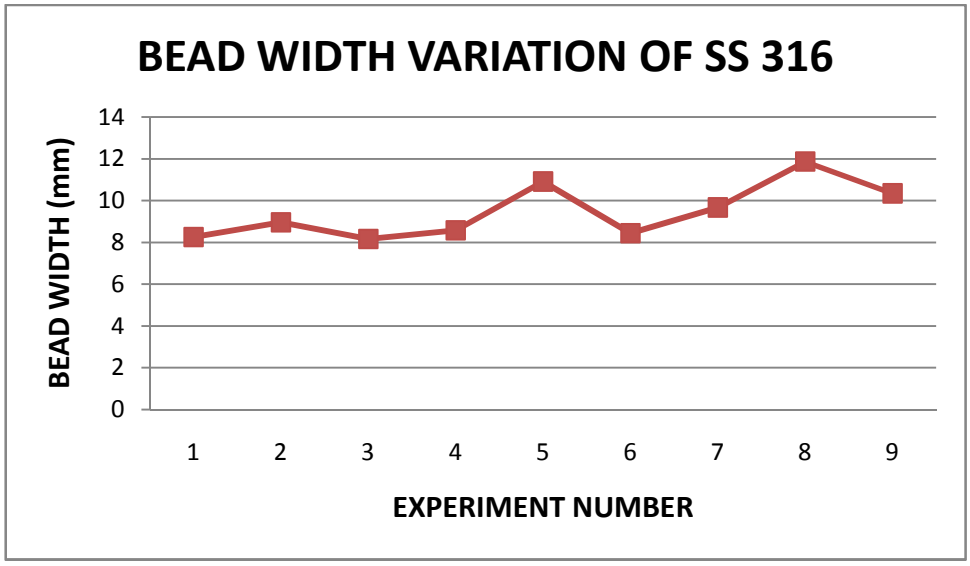

Figure 5.5: Graphical representation of bead width variation of SS 316

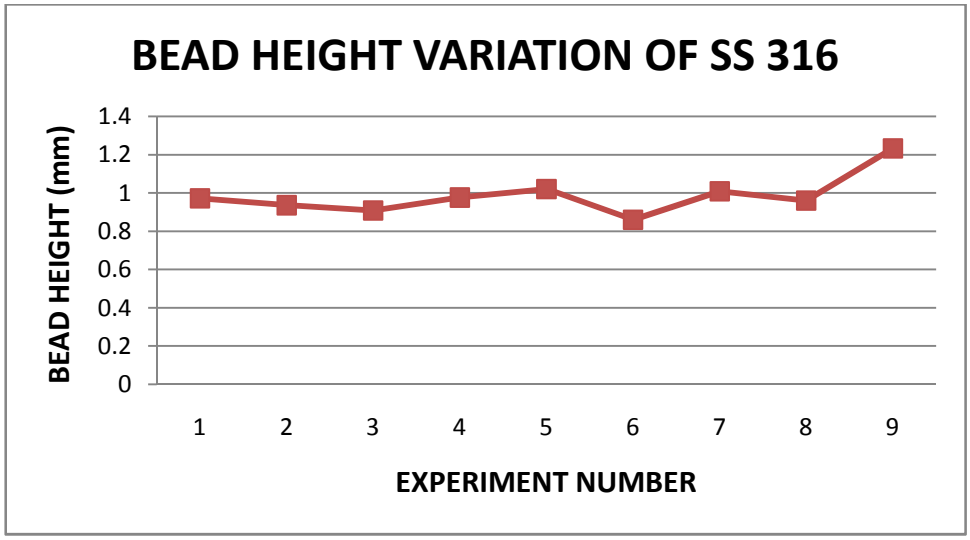

Figure 5.6: Graphical representation of bead height variation of SS 316

5.2.1 ANOVA TABLE FOR SS 316 ON BEAD WIDTH

The results for weld bead width were analysed by using ANOVA in order to identify the significant factors affecting the performance measures. Average value of bead width for all the specimens is shown in Table 5.10. The minimum value of bead width of SS 316 is 8.16 mm at current value 130A. It is clear from results so obtained from table 5.11 to table 5.14 that current is the most important parameter having the most significant affect on the bead width and then shielding gas type has sub-significant affect, whereas flow rate and groove angle have almost negligible effect on the same. Plot for main effects in figure 5.7 shows that with increase in current the value of bead width increases which is not desirable. Among all gases, argon results into minimum bead width along with intermediate flow rate of 12 L/min.

Table 5.11 Analysis of variance for SN ratio of weld bead width of SS 316

Source	DOF	SS	Variance	F ratio	F (critical)	PC
Current	2	5.7842	2.89211	70.077	19	52.245
Gas type	2	4.3080	2.15401	52.193	19	38.718
Flow rate	2	0.0825	0.04127	1	19	3.028
Grove angle	2	0.7384	0.36920	8.945	19	6.009
Total	8	10.9132				100
Error pooled	2	0.0825	0.04127			3.028

Table 5.12: Response table for SN ratio of weld bead width of SS 316

Level	Current	Gas type	Flow rate	Grove angle
1	-18.54	-18.90	-19.45	-19.79
2	-19.32	-19.02	-19.33	-19.09
3	-20.49	-20.43	-19.57	-19.46
Delta	1.95	1.52	0.23	0.70
Rank	1	2	4	3

Table 5.13: Analysis of variance for Means of weld bead width of SS 316

Source	DOF	SS	Variance	F ratio	F (critical)	PC
Current	2	7.103	3.551	50.684	19	50.321
Gas type	2	5.581	2.790	39.822	19	39.320
Flow rate	2	0.140	0.070	1	19	4.052
Grove angle	2	1.013	0.506	7.227	19	6.307
Total	8	13.838				100
Error pooled	2	0.140	0.070			4.052

Table 5.14: Response table for Means of weld bead width of SS 316

Level	Current	Gas type	Flow rate	Grove angle
1	8.462	8.835	9.519	9.835
2	9.307	8.982	9.291	9.022
3	10.621	10.574	9.581	9.534
Delta	2.159	1.739	0.290	0.813
Rank	1	2	4	3

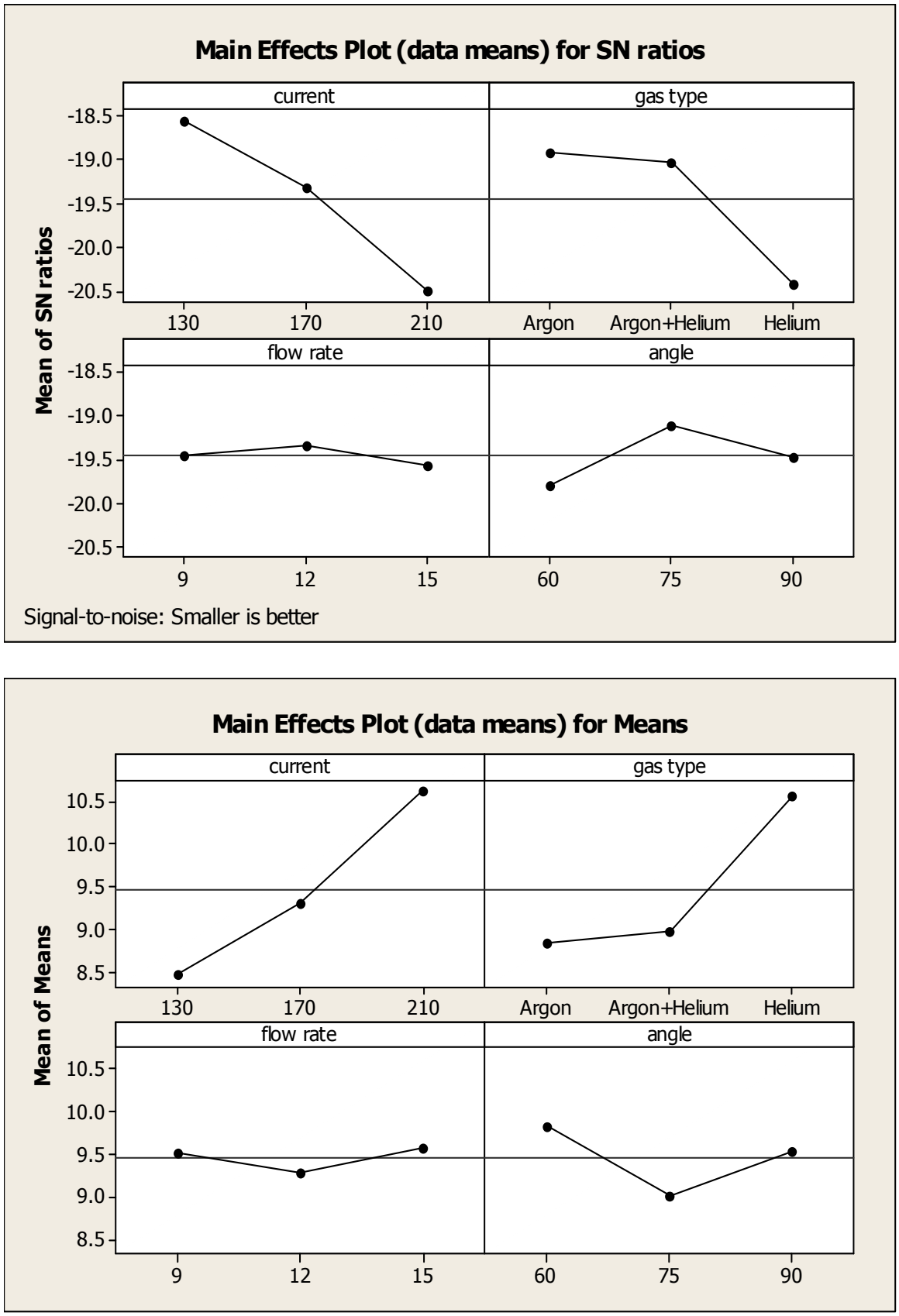

Figure 5.7: Main effect plot for SN ratios and means of Weld Bead width of SS 316

5.2.1.1 OPTIMAL DESIGN FOR BEAD WIDTH OF SS 316

It is clear from ANOVA table for means (table 5.13) that the F value of current and type of gas is greater than F critical. Main effect plot shows that bead width is minimum for first level current value i.e. 130 A and first level gas type i.e. argon. The confidence interval predict with 95 % confidence so that the value of bead width for SS 316 would be 7.834 ±0.848 mm.
Mean value of bead width is given by:

$\mu I_1G_1 = \overline{I_1} + \overline{G_1} - \overline{Y}$

$= 8.462 + 8.835 - 9.463$

$= 7.834$ mm

Confidence Interval around the Estimated Mean width

$$CI_1 = \sqrt{\frac{F_{\alpha,v_1,v_2} V_e}{n_{eff}}}$$

Where $F\alpha V_1V_2 = F0.05:1:2 = 18.51$

α = Risk (0.05), Confidence = 1-α

V_1 = DOF for mean which is always = 1

V_2 = DOF for error = Ve = 2

η_{eff} = Number of tests under that condition using the participating factors

$\overline{Y}$ = Average bead width

$\eta_{eff} = N / (1+ DOF\mathbf{I_1G_1}) = 9/ 1+2+2 = 1.80$

CI = 0.848 mm

So the confidence interval around the Estimated Mean width is given by 7.834 ±0.848 mm.

5.2.2 ANOVA TABLE FOR SS 316 ON BEAD HEIGHT

The observations on variations of bead height and its average value for SS 316 are given in table 5.10. The minimum value of bead height is 0.908 mm which was obtained at 130A current. The results for weld bead height were analysed by using ANOVA in order to identify the significant factors and are shown in tabular form compiled from table 5.15 to table 5.18. It is clear from main effects plot in figure 5.8 that among all values, grove angle of 75^O and gas flow rate of 9 l/min gives the minimum value of bead height. The grove angle has most significant affect on the bead height of SS 316 followed by current. It is clear from the plot for means that bead height goes on increasing with increase in current which is not desirable.

Table 5.15: Analysis of variance for SN ratio of weld bead height of SS 316

Source	DOF	SS	Variance	F ratio	F (critical)	PC
Current	2	2.056	1.028	58.598	19	33.409
Gas type	2	0.035	0.017	1	19	2.322
Flow rate	2	1.444	0.722	41.144	19	23.285
Grove angle	2	2.515	1.257	71.658	19	40.984
Total	8	6.051				100
Error pooled	2	0.035	0.017			2.322

Table 5.16: Response table for SN ratio of weld bead height of SS 316

Level	Current	Gas type	Flow rate	Grove angle
1	0.5522	0.1286	0.6364	-0.5796
2	0.4488	0.1112	-0.3430	0.6041
3	-0.5097	0.2515	0.1980	0.4669
Delta	1.0618	0.1403	0.9794	1.1837
Rank	2	4	3	1

Table 5.17: Analysis of variance for Means of weld bead height of SS 316

Source	DOF	SS	Variance	F value	F (critical)	PC
Current	2	0.0297	0.014	25.263	19	32.577
Gas type	2	0.001	0.0005	1	19	5.375
Flow rate	2	0.020	0.010	17.753	19	22.493
Grove angle	2	0.035	0.017	30.460	19	39.555
Total	8	0.087				100
Error pooled	2	0.001	0.0005			5.375

Table 5.18: Response table for Means of weld bead height of SS 316

Level	Current	Gas type	Flow rate	Grove angle
1	0.938	0.985	0.930	1.074
2	0.952	1.000	1.048	0.934
3	1.066	0.972	0.978	0.948
Delta	0.128	0.028	0.117	0.140
Rank	2	4	3	1

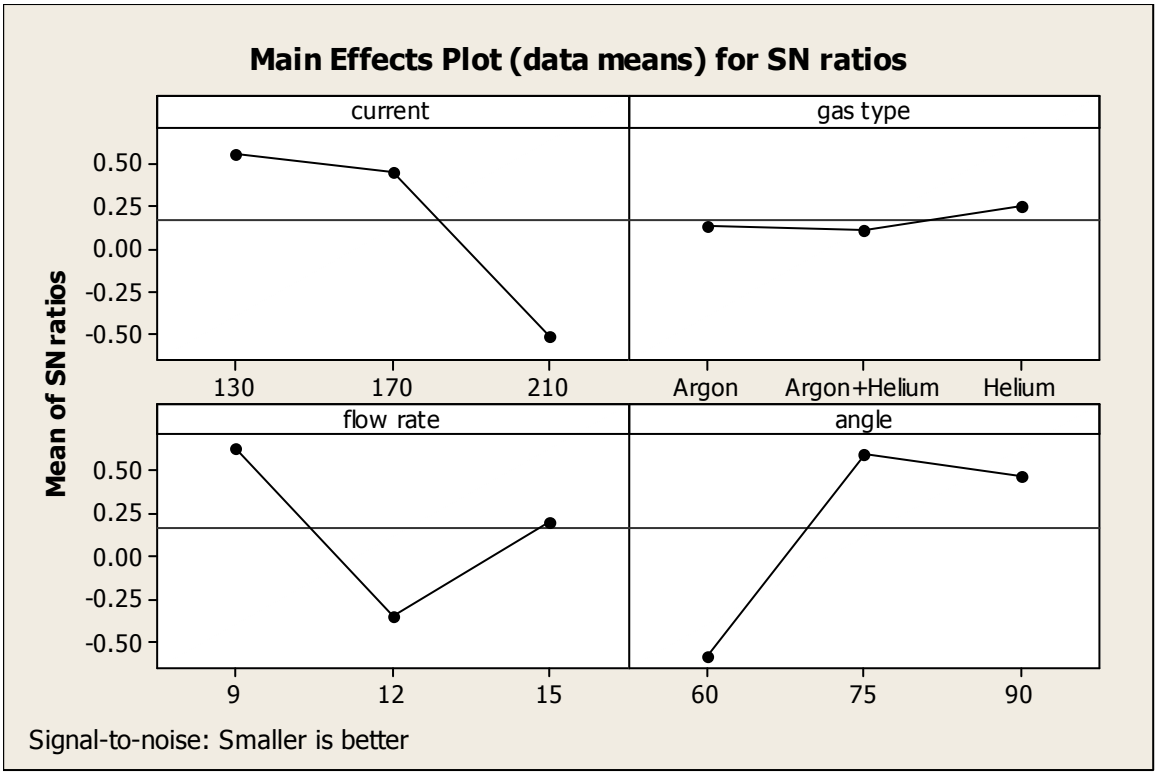

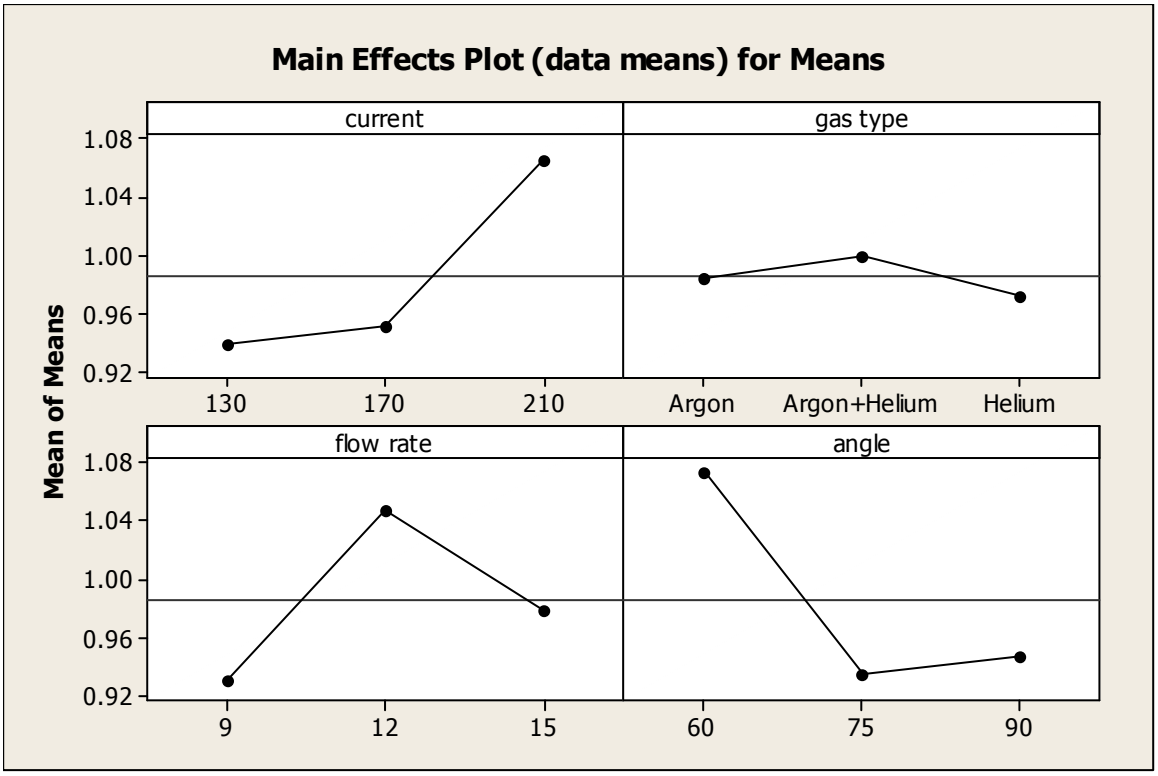

Figure 5.8: Main effect plot for SN ratios and means of Weld Bead height of SS 316

5.2.2.1 OPTIMAL DESIGN FOR BEAD HEIGHT OF SS 316

It is clear from ANOVA table for means (table 5.13) that the F value of current and type of gas is greater than F critical. Main effect plot shows that bead height is minimum for first level current value i.e. 130 A and second level angle type i.e. 75. The confidence interval predict with 95 % confidence so that the value of bead height for SS 316 would be 0.887 ±0.077 mm. Mean value of bead height is given by:

$\mu I_1\Theta_2 = \overline{I_1} + \overline{\Theta_2} - \overline{Y}$

$= 0.9387 + 0.9347 - 0.9857$

$= 0.887$ mm

Confidence Interval around the Estimated Mean height

$$CI_1 = \sqrt{\frac{F_{\alpha,v_1,v_2} V_e}{n_{eff}}}$$

Where $F\alpha V_1V_2 = F0.05:1:2 = 18.51$

α = Risk (0.05), Confidence = 1-α

V_1 = DOF for mean which is always = 1

V_2 = DOF for error = Ve = 2

η_{eff} = Number of tests under that condition using the participating factors

$\overline{Y}$ = Average bead height

$\eta_{eff} = N / (1 + DOF\mathbf{I_1G_1}) = 9/ 1+2+2 = 1.80$

CI = 0.077 mm

So the confidence interval around the Estimated Mean height is given by 0.887 ±0.077 mm.

CHAPTER 6 RESULTS OF DYE PENETRATION TEST

The photographs of dye penetration test performed on all welding specimen of both materials SS 310 and SS 316 are shown below.

6.1 RESULT OF DYE PENETRATION TEST ON SS 310

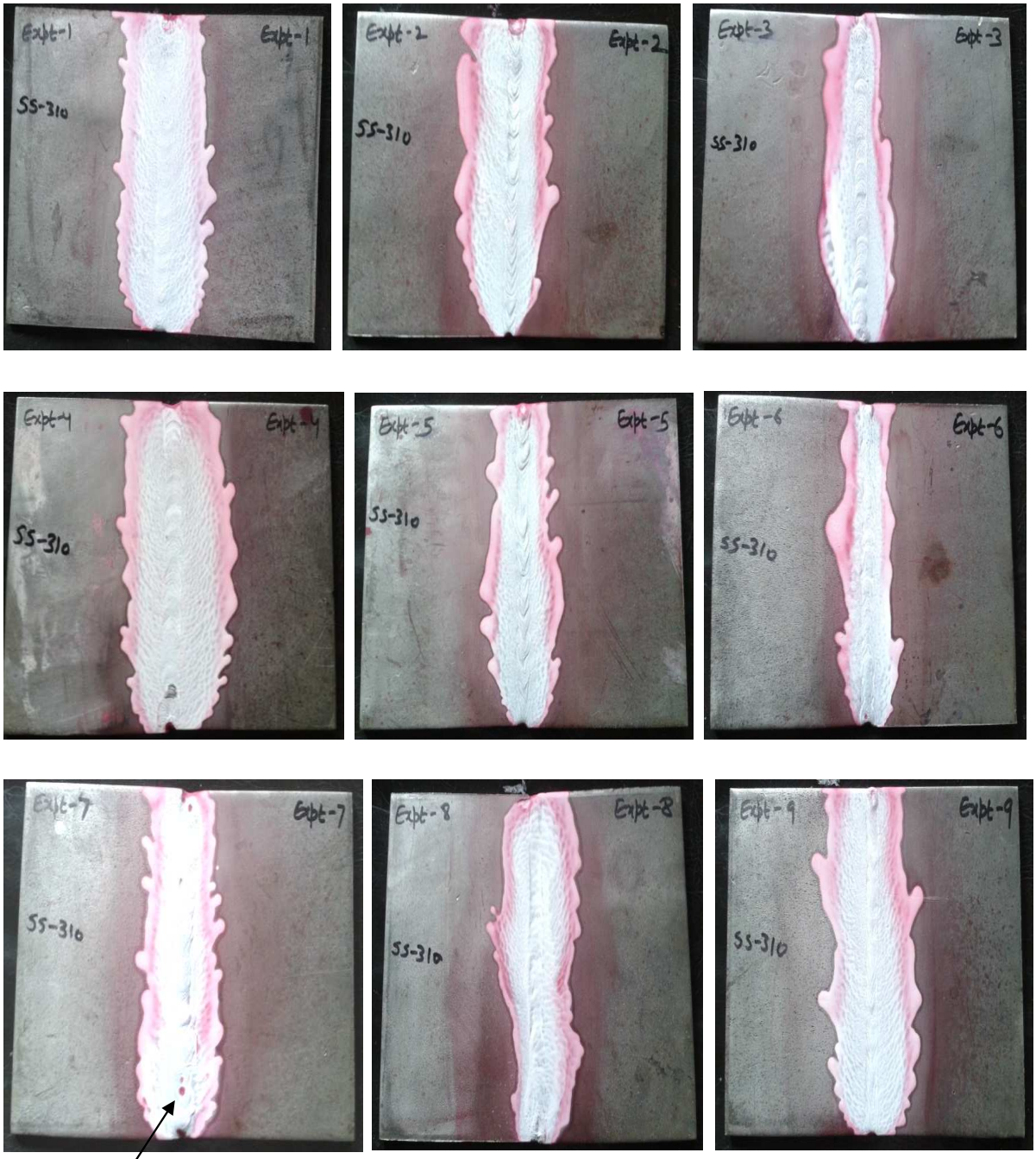

Figure 6.1: Result of dye penetration test on SS 310 specimens

Surface defect

6.2 RESULT OF DYE PENETRATION TEST ON SS 316

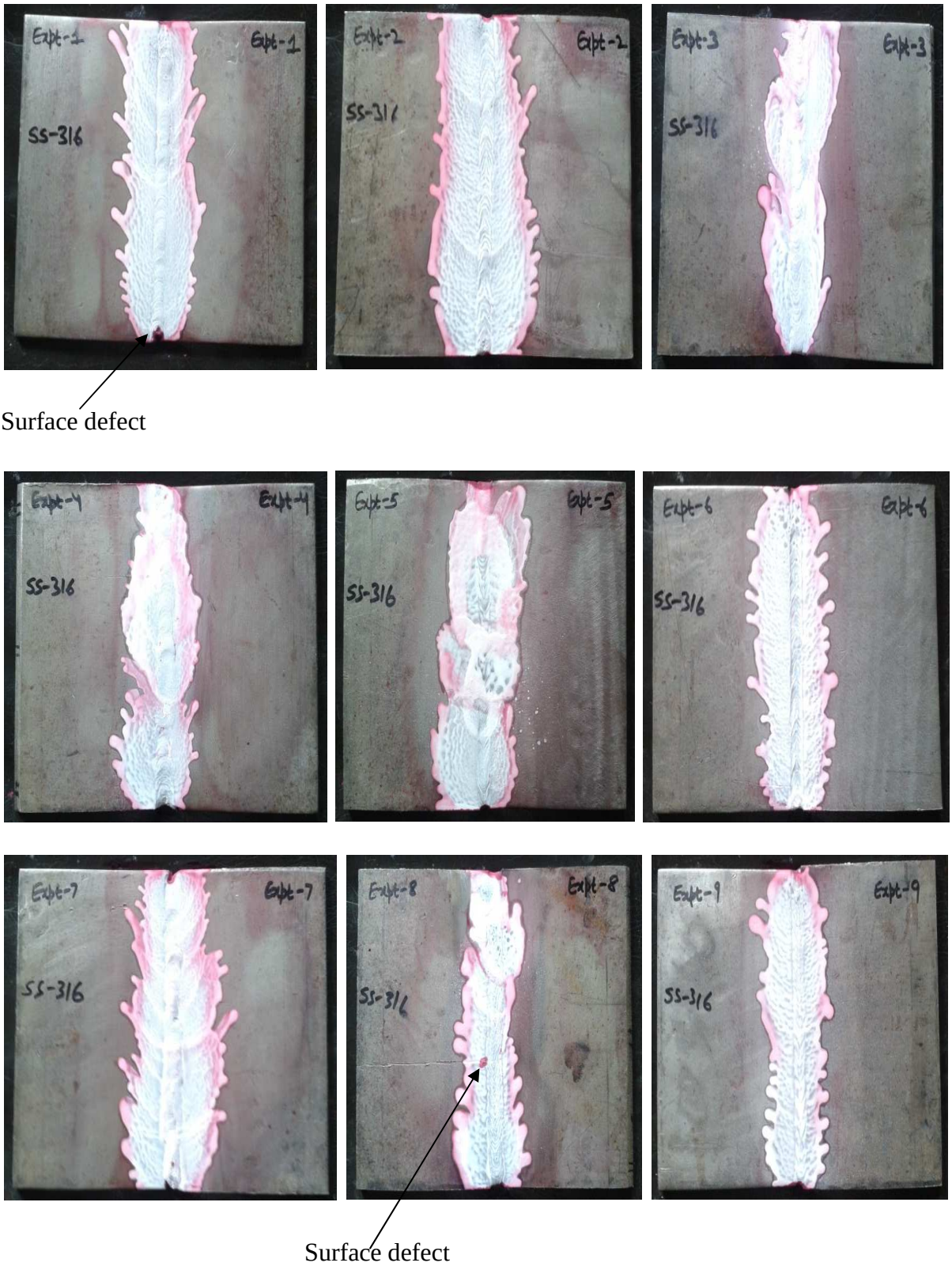

Figure 6.2: Result of dye penetration test on SS 316 specimens

As discussed earlier dye penetration test has been done in order to find soundness of the welded joints. This test has been carried out on each individual sample having particular values of process parameters as per orthogonal array L9. It is clear from above photographs that welding carried out was successful as there were minor surface cracks on few plates likewise specimen no. 7 of SS 310 and specimen no. 1 and 8 of SS 316. It is also to be mentioned over here that start or end of welding may show minor defects which are rejected as discussed earlier on account of start and end of weld. So it can be concluded that no major defects were found over effective length of the welded plates.

CHAPTER 7 RESULTS OF BULK HARDNESS TEST

7.1 RESULT OF ROCKWELL HARDNESS TEST ON SS 310

Table 7.1: Observations of Rockwell hardness test on SS-310 specimens

HRC values of SS 310	EXPERIMENT NUMBER								
	1	**2**	**3**	**4**	**5**	**6**	**7**	**8**	**9**
-60	53	53	53	55	54	54	55	56	55
-50	54	55	52.5	55	55	54	56	56	55
-40	53	53	53	55.6	55.6	55	59	57	56.7
-30	53	53	55.3	56	56.6	56.7	58	58	58
-25	55	55	55	56	56	57.3	59	58	58
-20	54	54	56	56.7	56.6	56.6	59	58	58.6
-15	54	54	57.7	57.3	57.3	57.3	59	57	57
-10	56	56.5	58.4	57	57	58	59.5	58.3	57.6
-5	56	56	58.4	57.5	58.6	58	57.7	58	58
-2	57	57.7	58.2	58	59.3	59.1	60	59.3	59.6
0	58	58.5	58.7	57.7	59	58.3	59.7	59	59
2	56.6	56.7	58	58.1	59.6	58.6	59.7	59.7	58.7
5	56.3	56.3	58.3	57.6	58.1	58.1	58.7	58.3	58
10	54	56.4	58.8	57.3	58.6	57.3	59.5	58	57
15	55	55	57.4	57.4	57	57	59	59	58
20	54	54	56.5	56.5	57.6	57.6	59	59	58
25	54.6	54.7	54.7	55.7	55.7	55.7	58	59.6	58.6
30	53	53	55	55	55	55.7	58	58	58
40	53	53	54	55.8	55.8	54.7	58	57	56
50	52.6	54	53.7	56.6	55	54	57	57	54
60	52	52	54	56	55	53	56	56	55

It is clear from tabular and graphical representations for SS 310 that no drastic variations have been observed in hardness in welded zone and heat affected zone and readings are approximately similar with respect to position nearby each other on either side.

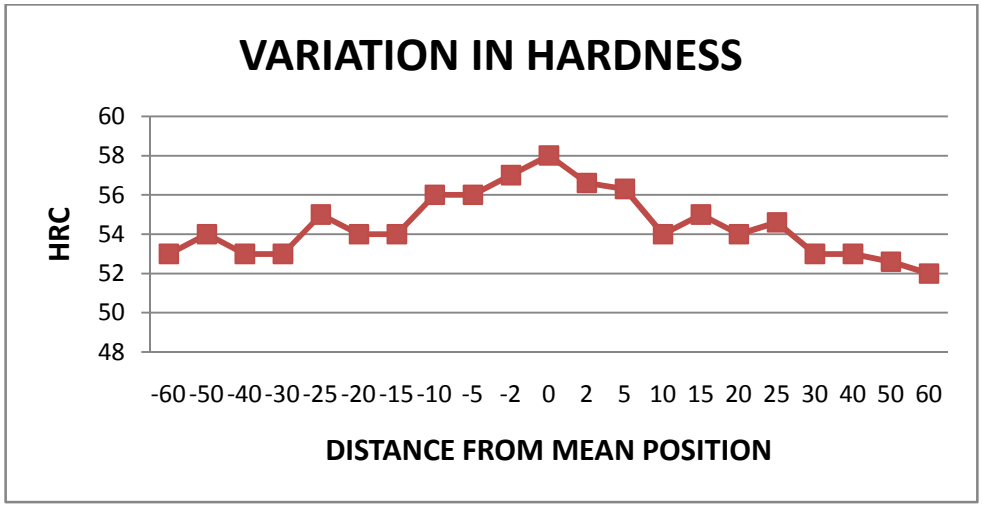

Figure 7.1: Graphical representation of variation of HRC in SS 310 of specimen-1

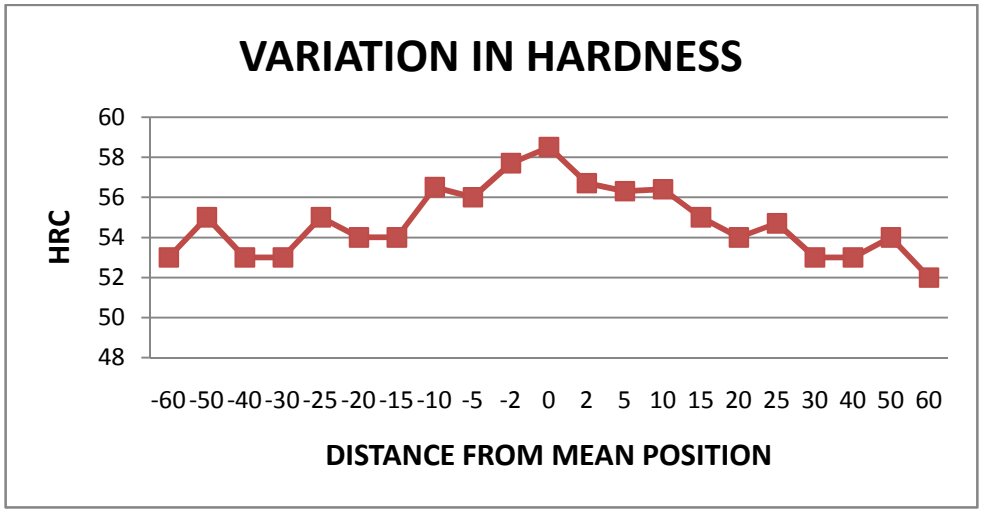

Figure 7.2: Graphical representation of variation of HRC in SS 310 of specimen-2

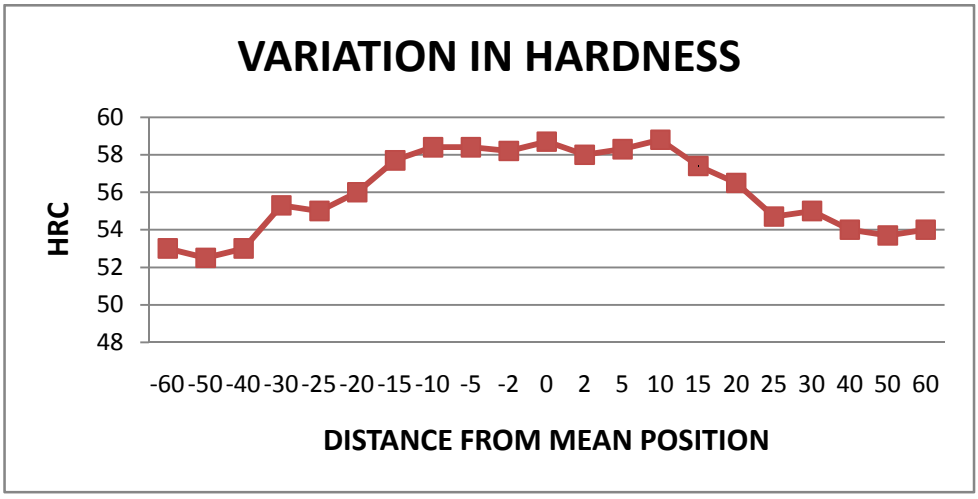

Figure 7.3: Graphical representation of variation of HRC in SS 310 of specimen-3

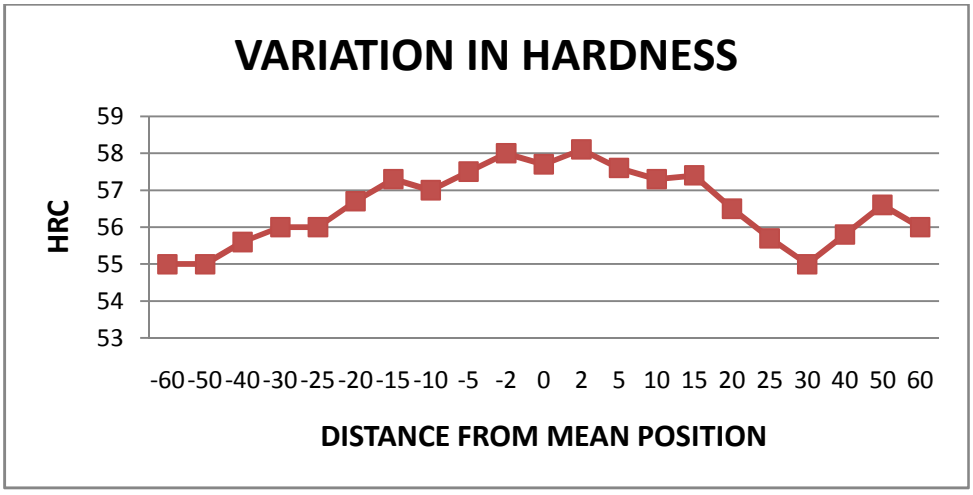

Figure 7.4: Graphical representation of variation of HRC in SS 310 of specimen-4

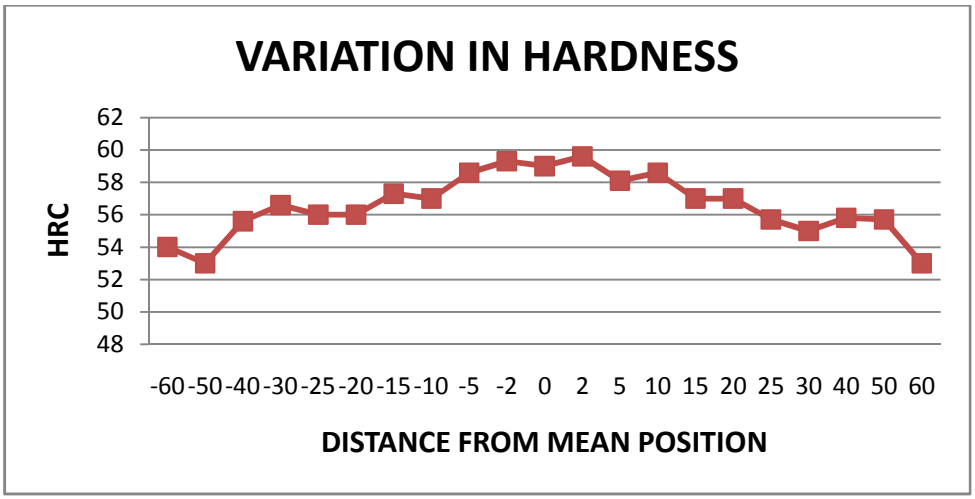

Figure 7.5: Graphical representation of variation of HRC in SS 310 of specimen-5

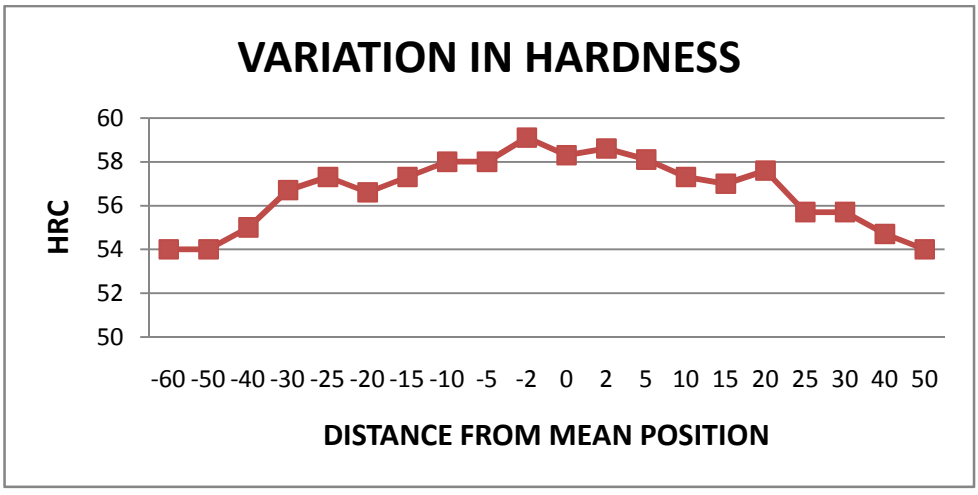

Figure 7.6: Graphical representation of variation of HRC in SS 310 of specimen-6

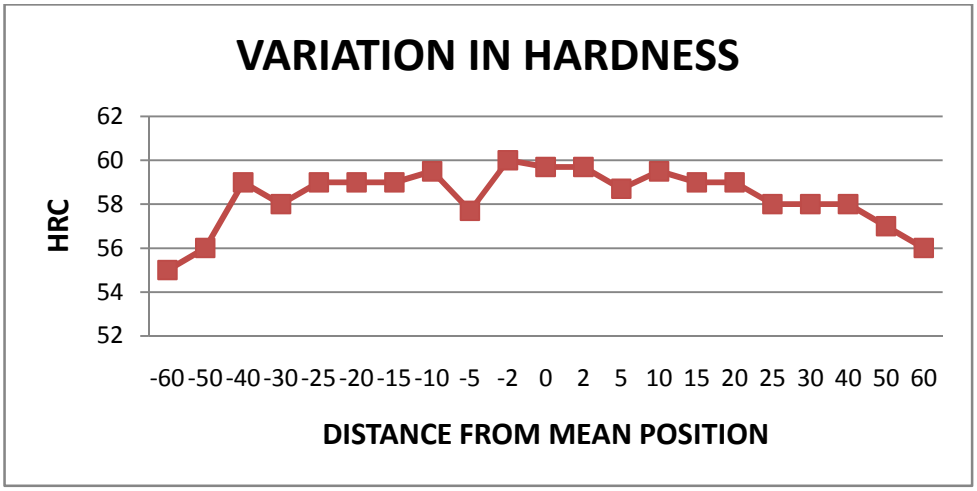

Figure 7.7: Graphical representation of variation of HRC in SS 310 of specimen-7

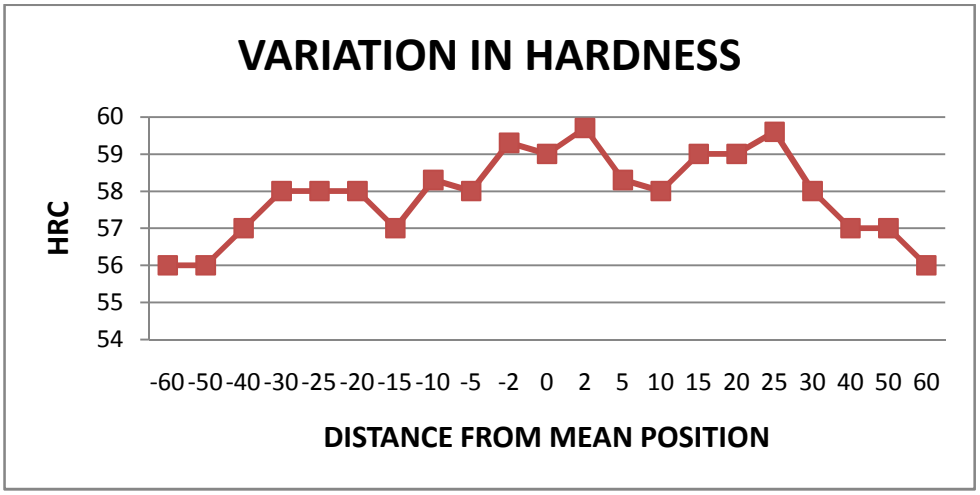

Figure 7.8: Graphical representation of variation of HRC in SS 310 of specimen-8

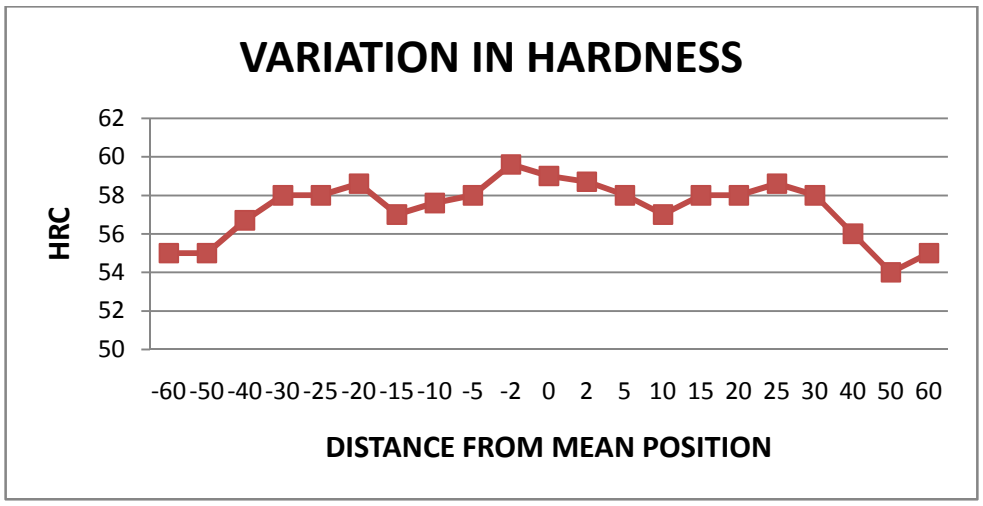

Figure 7.9: Graphical representation of variation of HRC in SS 310 of specimen-9

7.2 RESULT OF ROCKWELL HARDNESS TEST ON SS 316

Table 7.2: Observations of Rockwell hardness test on SS-316 specimens

HRC values of SS 316	EXPERIMENT NUMBER								
	1	**2**	**3**	**4**	**5**	**6**	**7**	**8**	**9**
-60	57	55	53	55	57	56	59	58	57
-50	57.6	56	54	56	58.3	55	60	57	57
-40	59	59	56	56.3	58	57	58	57	58
-30	58	58	55	57	59	57.7	59	58.3	58.7
-25	59	59	56	56	59	58	59	60	59
-20	59	59.6	56.3	58	60	57	59	59.5	59
-15	58.7	59	56	59	60	57	60	60	58.3
-10	59.5	59.5	57.3	59	59.7	58.3	59	60.5	58
-5	58.7	57.7	57	58.6	58.6	58	58	60	58
-2	60	60	58	59.7	59	59.3	58	59.7	59
0	59.7	59	58.3	57.7	60.3	58.7	59	60	58
2	59	59.7	59.3	59.3	59.3	59.7	58.7	60.7	59
5	58.7	58.7	58	58	58	58.3	57	59	58
10	59.5	59.5	58.3	58.3	60	58	60	61	57
15	59	59	58	59	59	59	59	59	58.3
20	59	59	59.3	58.7	58.7	59	58	59.3	58
25	58	58	57	58.7	59	59.6	59	60	58
30	58	58	56	56	59.3	58	60	58	57
40	57.6	57	56	56.6	58	57	58	58	57.3
50	57	57	54	55	59	56	59	57.7	57
60	57	56	54.3	55	58	56	56	57	55

It is clear from above tabular and graphical representations for SS 316 that no drastic variations have been observed in hardness in welded zone and heat affected zone. When moving away from weld bead, it has been also observed that readings are approximately similar with respect to position nearby each other.

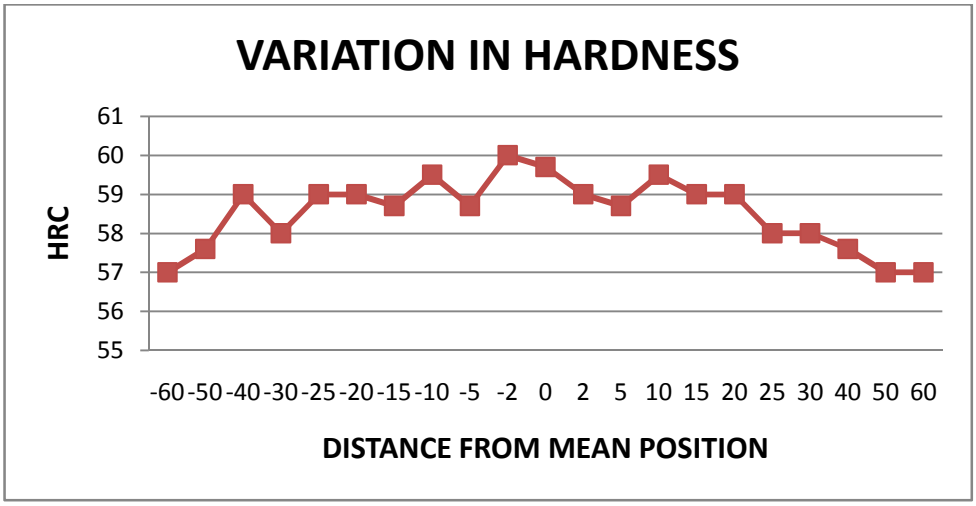

Figure 7.10: Graphical representation of variation of HRC in SS 316 of specimen-1

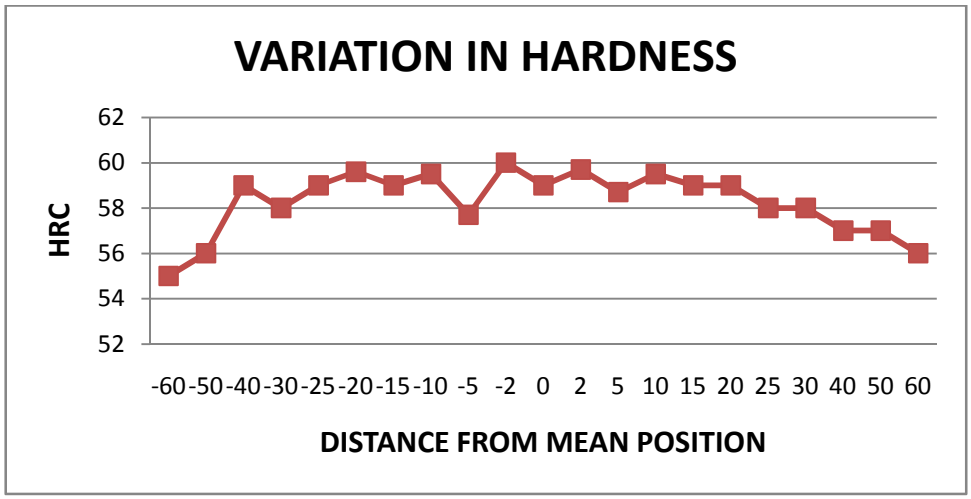

Figure 7.11: Graphical representation of variation of HRC in SS 316 of specimen-2

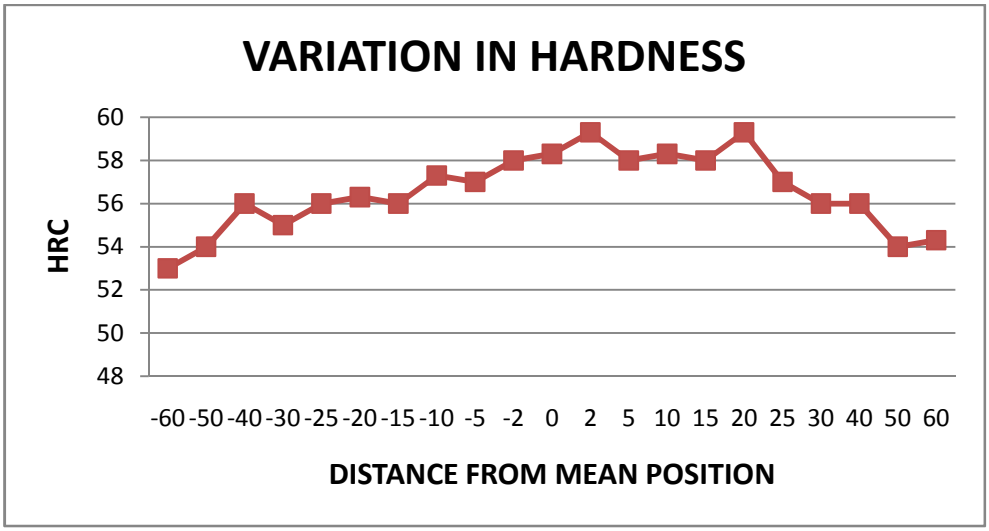

Figure 7.12: Graphical representation of variation of HRC in SS 316 of specimen-3

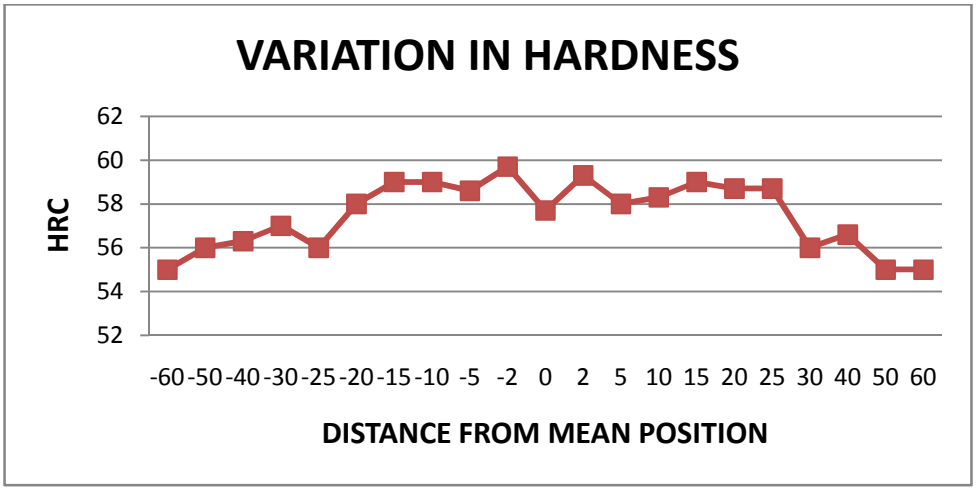

Figure 7.13: Graphical representation of variation of HRC in SS 316 of specimen-4

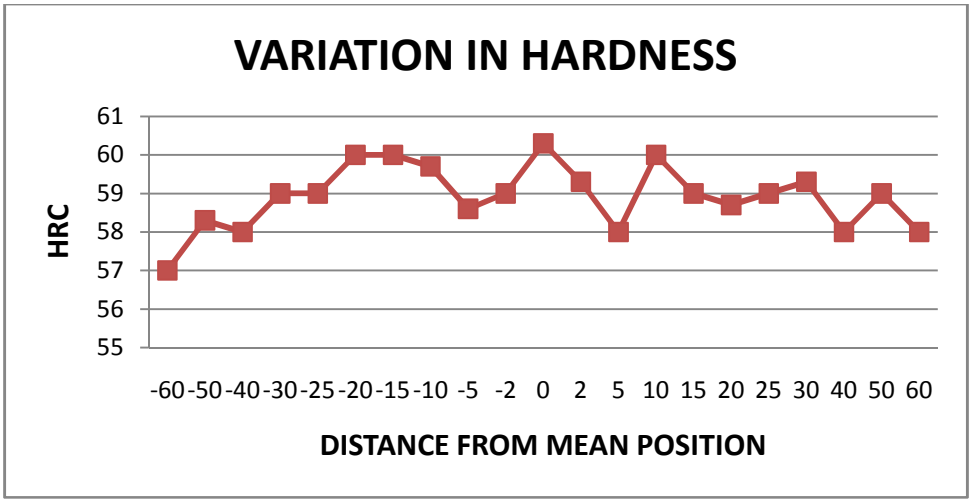

Figure 7.14: Graphical representation of variation of HRC in SS 316 of specimen-5

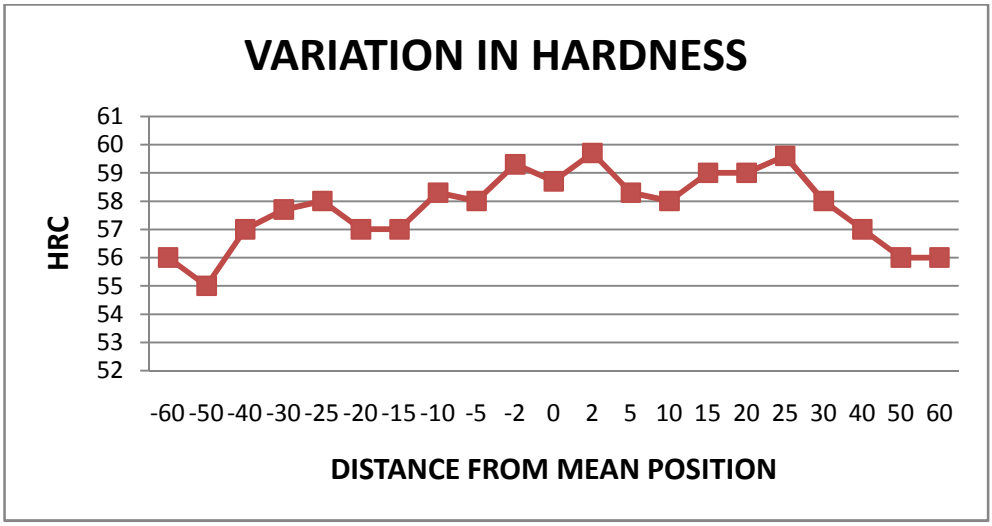

Figure 7.15: Graphical representation of variation of HRC in SS 316 of specimen-6

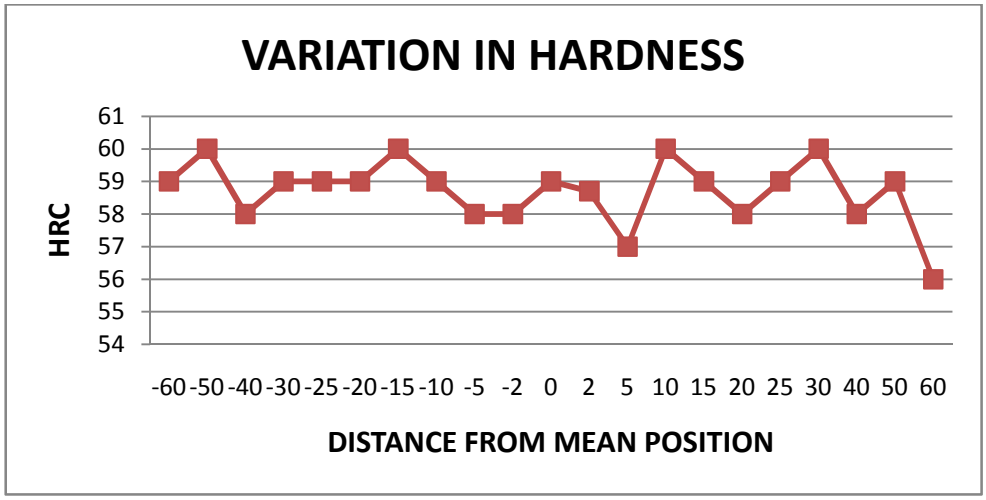

Figure 7.16: Graphical representation of variation of HRC in SS 316 of specimen-7

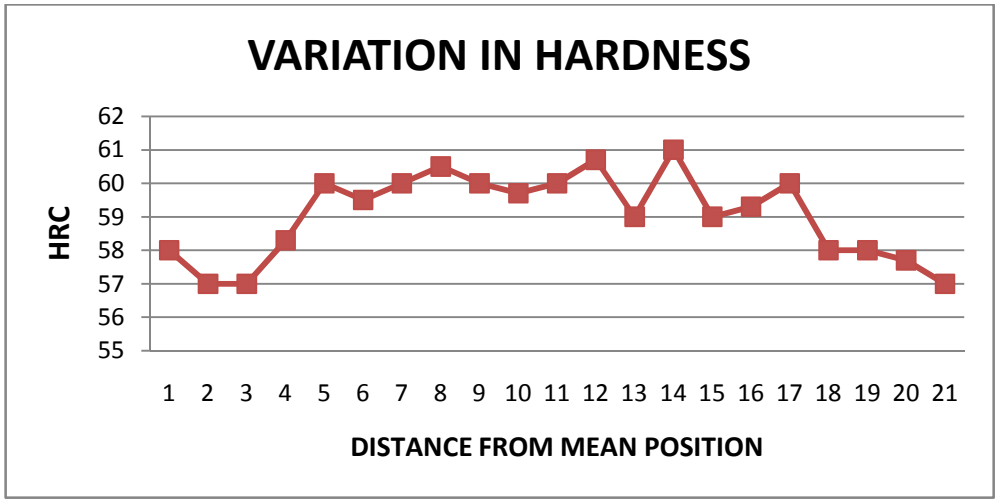

Figure 7.17: Graphical representation of variation of HRC in SS 316 of specimen-8

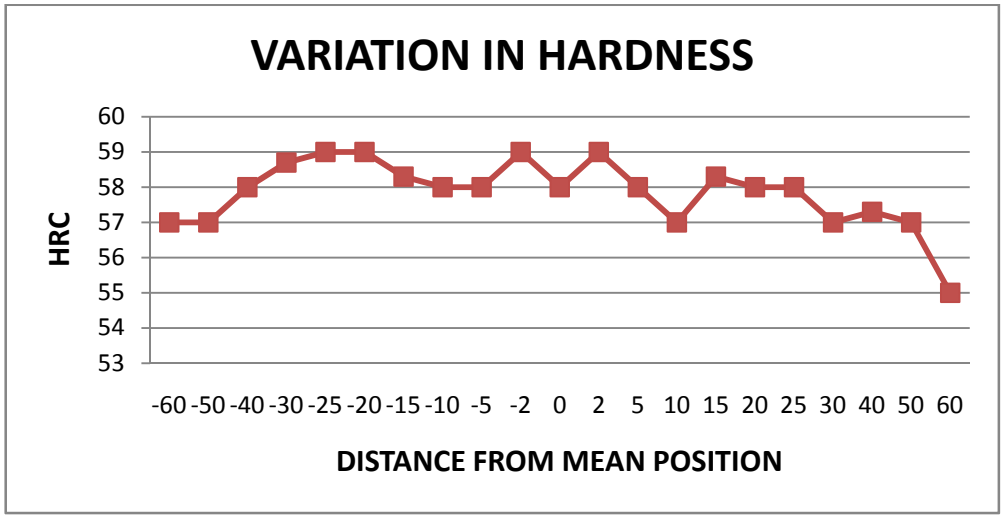

Figure 7.18: Graphical representation of variation of HRC in SS 316 of specimen-9

CHAPTER 8 RESULTS OF IMPACT TEST

The toughness of any material can be found by subjecting it to suddenly applied load. The experiments for particular parameter combinations as decided earlier in orthogonal array are repeated two times and the average values are shown in tables ahead. The test specimens after performing Charpy test are shown here under.

Figure 8.1: Charpy test on both SS 310 and SS 316 materials

8.1 RESULTS OF CHARPY TEST ON SS 310:

Table 8.1: Charpy impact test results of SS 310

Experiment number	Contributing parameters	Charpy test result at room temperature(28^{o}C) (joules)	Charpy test result at -20^{o} C (joules)
1	I_1,G_1,F_1,Θ_1	100.45	88.20
2	I_1,G_2,F_2,Θ_2	83.30	66.15
3	I_1,G_3,F_3,Θ_3	90.65	73.50
4	I_2,G_1,F_2,Θ_3	102.90	90.65
5	I_2,G_2,F_3,Θ_1	95.55	83.30
6	I_2,G_3,F_1,Θ_2	105.35	90.65
7	I_3,G_1,F_3,Θ_2	112.70	105.35
8	I_3,G_2,F_1,Θ_3	102.90	95.55
9	I_3,G_3,F_2,Θ_1	107.80	100.45

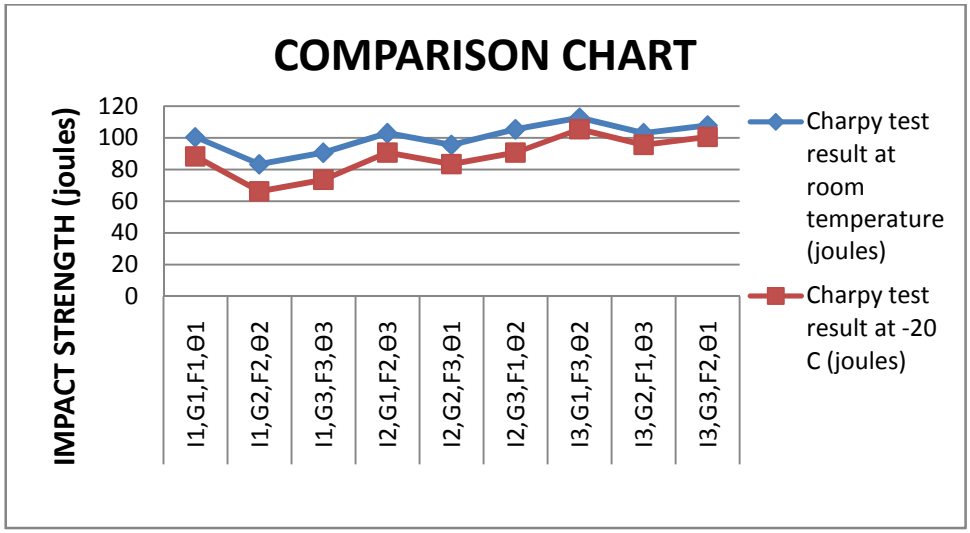

Figure 8.2: Comparison of toughness values of SS 310 at room temperature and at -20^0 C

The figure 8.2 shows the comparison of toughness values made on SS 310 material at room temperature i.e. 28^o C and -20^o C temperature. It can be noticed that since the current being most significant factor among all other factors, the value of toughness goes on increasing with increase in current. From comparison chart shown above it is clear that similar trend in value of toughness is followed but with decrease in temperature the toughness value decreases.

8.1.1 ANOVA FOR TOUGHNESS ON SS 310 AT ROOM TEMPERATURE

The result of Charpy test carried out on SS 310 at room temperature is shown in table 8.1 in which average of two values have been shown for each sample. The maximum toughness of about 112.7 J was obtained in experiment no. 7 at 210A current. The results so obtained have been analysed using ANOVA given in tables from table 8.2 to table 8.5. It is clear that current is the most significant factor affecting the toughness value. The nature of gas used has sub-significant affect on the same where as grove angle has least effect on toughness. The main effect plots for SS 310 on toughness shows that the value of toughness goes on increasing with increase in current. The F-ratio for current is greater than F-critical followed by nature of gas used. The use of argon results in maximum toughness whereas helium results in minimum toughness. Moreover, small gas flow rates results in achieving higher values of toughness. Grove angle has almost negligible effect as compared with other parameters.

Table 8.2 Analysis of variance for SN ratio of toughness of SS 310 at room temperature

Source	DOF	SS	Variance	F ratio	F (critical)	PC
Current	2	3.218	1.609	37.895	19	59.025
Gas type	2	1.640	0.820	19.321	19	29.310
Flow rate	2	0.364	0.182	4.290	19	5.264
Grove angle	2	0.084	0.042	1	19	6.401
Total	8	5.308				100
Error pooled	2	0.084	0.042			6.401

Table 8.3: Response table for SN ratio of toughness of SS 310 at room temperature

Level	Current	Gas type	Flow rate	Grove angle
1	39.18	40.42	40.23	40.09
2	40.09	40.08	39.75	39.94
3	40.63	39.39	39.92	39.86
Delta	1.45	1.03	0.49	0.23
Rank	1	2	3	4

Table 8.4: Analysis of variance for Means of toughness of SS 310 at room temperature

Source	DOF	SS	Variance	F ratio	F (critical)	PC
Current	2	405.502	202.751	43.424	19	60.612
Gas type	2	201.417	100.709	21.569	19	29.387
Flow rate	2	37.349	18.674	3.999	19	4.285
Grove angle	2	9.337	4.669	1	19	5.716
Total	8	653.606				100
Error pooled	2	9.337	4.669			5.716

Table 8.5: Response table for Means of toughness of SS 310 at room temperature

Level	Current	Gas type	Flow rate	Grove angle
1	91.47	105.35	102.90	101.27
2	101.27	101.27	98.00	100.45
3	107.80	93.92	99.63	98.82
Delta	16.33	11.43	4.90	2.45
Rank	1	2	3	4

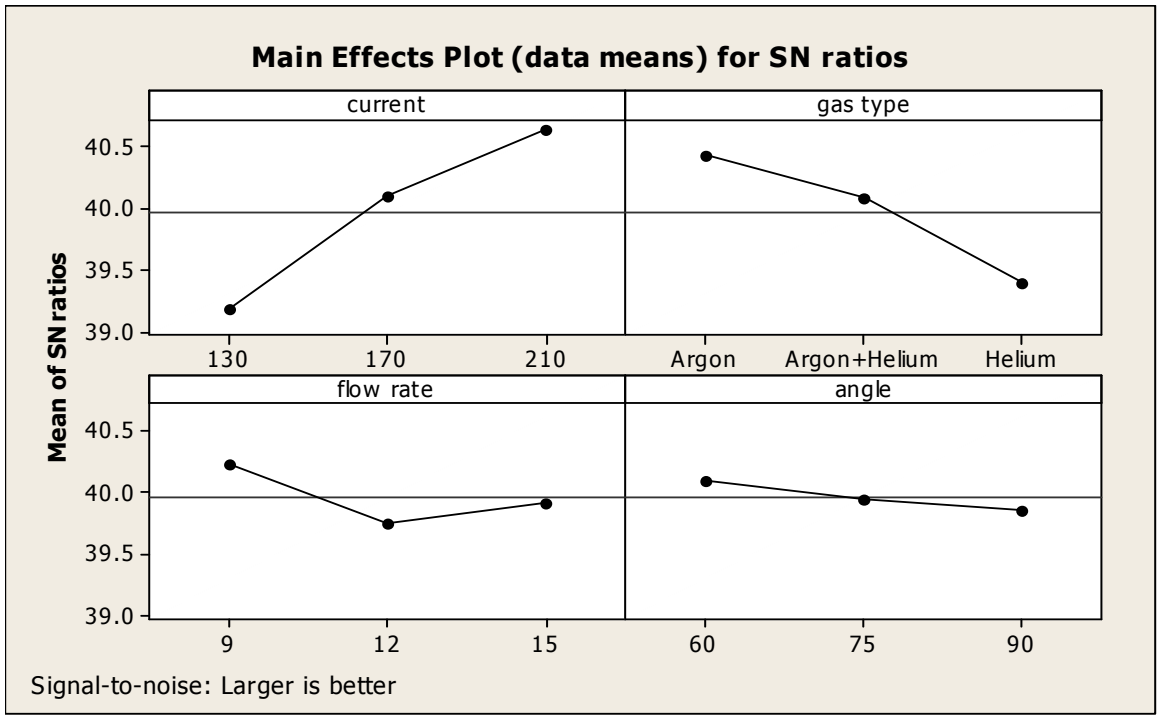

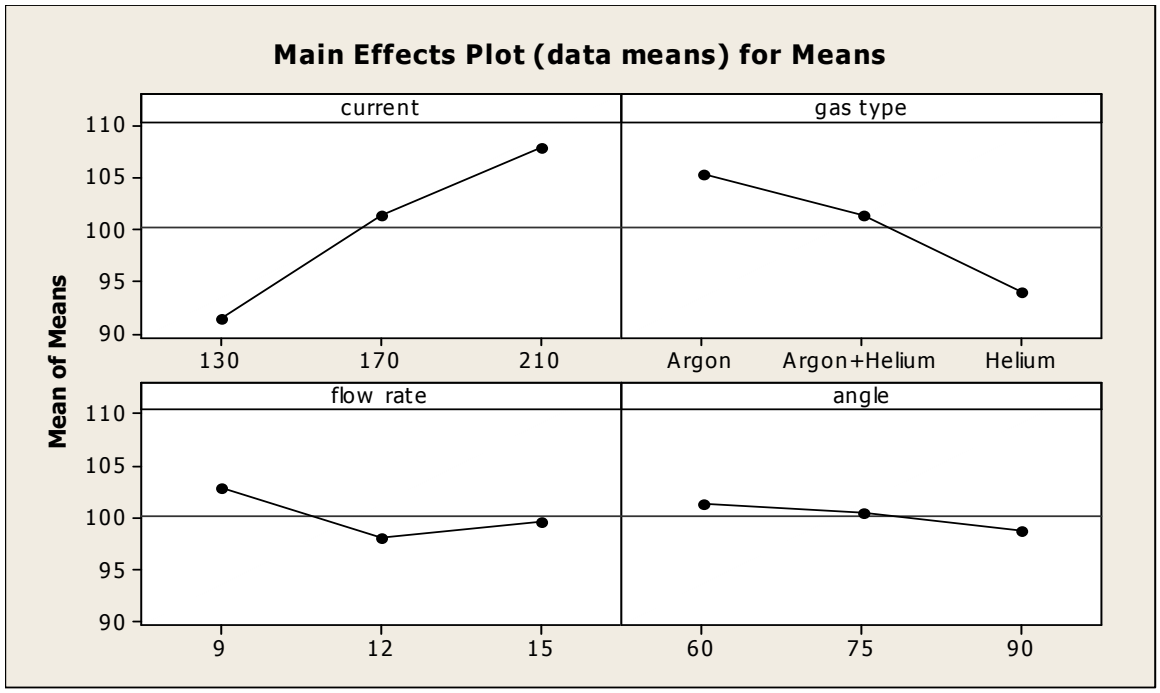

Figure 8.3: Main effect plot for SN ratios and means for toughness at room temp. of SS 310

8.1.1.1 OPTIMAL DESIGN FOR TOUGHNESS OF SS 310 AT ROOM TEMP.

It is clear from ANOVA table for means (table 8.4) that the F value of current and type of gas is greater than F critical. Main effect plot shows that toughness is maximum for third level current value i.e. 210 A and first level gas type i.e. argon. The confidence interval predict with 95 % confidence so that the value for SS 310 for toughness would be 112.98 ±6.929 joules.

Mean value of toughness is given by:

$\mu I_3G_1 = \overline{I_3} + \overline{G_1} - \overline{Y}$

$= 107.80 + 105.35 - 100.17$

$= 112.98$ joules

Confidence Interval around the Estimated Mean toughness

$$CI_1 = \sqrt{\frac{F_{\alpha,v_1,v_2} V_e}{n_{eff}}}$$

Where $F\alpha V_1V_2 = F0.05:1:2 = 18.51$

α = Risk (0.05), Confidence = 1-α

V_1 = DOF for mean which is always = 1

V_2 = DOF for error = Ve = 2

$\overline{Y}$ = Average toughness value

η_{eff} = Number of tests under that condition using the participating factors

$\eta_{eff} = N / (1+ DOF\mathbf{I_3G_1}) = 9/ 1+2+2 = 1.80$

CI = 6.929

So the confidence interval around the Estimated Mean toughness at room temperature is given by 112.98 ±6.929 joules

8.1.2 ANOVA FOR TOUGHNESS ON SS 310 AT -20^o C TEMPERATURE

The result of Charpy test carried out on SS 310 at -20^o C temperature is shown in table 8.1 in which average of two values have been shown for each sample. The maximum toughness of about 105.35 J was obtained in experiment no. 7 at 210A current value. The results have been analysed using ANOVA given in tables from table 8.6 to table 8.9. It is clear that current is the most significant factor affecting the toughness value. The nature of gas used has sub-significant affect on the same where as grove angle has least effect on toughness. The gas flow rate and grove angles had least significance. The main effects plot shows that the value of toughness goes on increasing with increase in current. The F-ratio for current is greater than F-critical. The use of argon results in maximum toughness whereas helium results in minimum toughness. Moreover, small gas flow rates results in achieving higher values of toughness. Grove angle has almost negligible effect. From response table for means the optimum value of toughness at -20^{O}C should be 100.45 joules

Table 8.6 Analysis of variance for SN ratio of toughness of SS 310 at -20^{O}C temperature

Source	DOF	SS	Variance	F ratio	F (critical)	PC
Current	2	9.872	4.936	22.502	19	66.993
Gas type	2	2.995	1.497	6.827	19	18.157
Flow rate	2	0.774	0.387	1.766	19	2.387
Grove angle	2	0.438	0.219	1	19	12.463
Total	8	14.081				100
Error pooled	2	0.4387	0.219			12.463

Table 8.7: Response table for SN ratio of toughness of SS 310 at -20^{O}C temperature

Level	Current	Gas type	Flow rate	Grove angle
1	37.46	39.48	39.18	39.09
2	38.86	38.79	38.47	38.59
3	40.02	38.07	38.69	38.67
Delta	2.56	1.41	0.70	0.50
Rank	1	2	3	4

Table 8.8: Analysis of variance for Means of toughness of SS 310 at -20^{O}C temperature

Source	DOF	SS	Variance	F ratio	F (critical)	PC
Current	2	900.38	450.188	32.142	19	70.55
Gas type	2	256.11	128.053	9.142	19	18.446
Flow rate	2	52.02	26.011	1.857	19	1.941
Grove angle	2	28.01	14.006	1	19	9.063
Total	8	1236.52				100
Error pooled	2	28.01	14.006			9.063

Table 8.9: Response table for Means of toughness of SS 310 at -20^{O}C temperature

Level	Current	Gas type	Flow rate	Grove angle
1	75.95	94.73	91.47	90.65
2	88.20	88.20	85.75	87.38
3	100.45	81.67	87.38	86.57
Delta	24.50	13.07	5.72	4.08
Rank	1	2	3	4

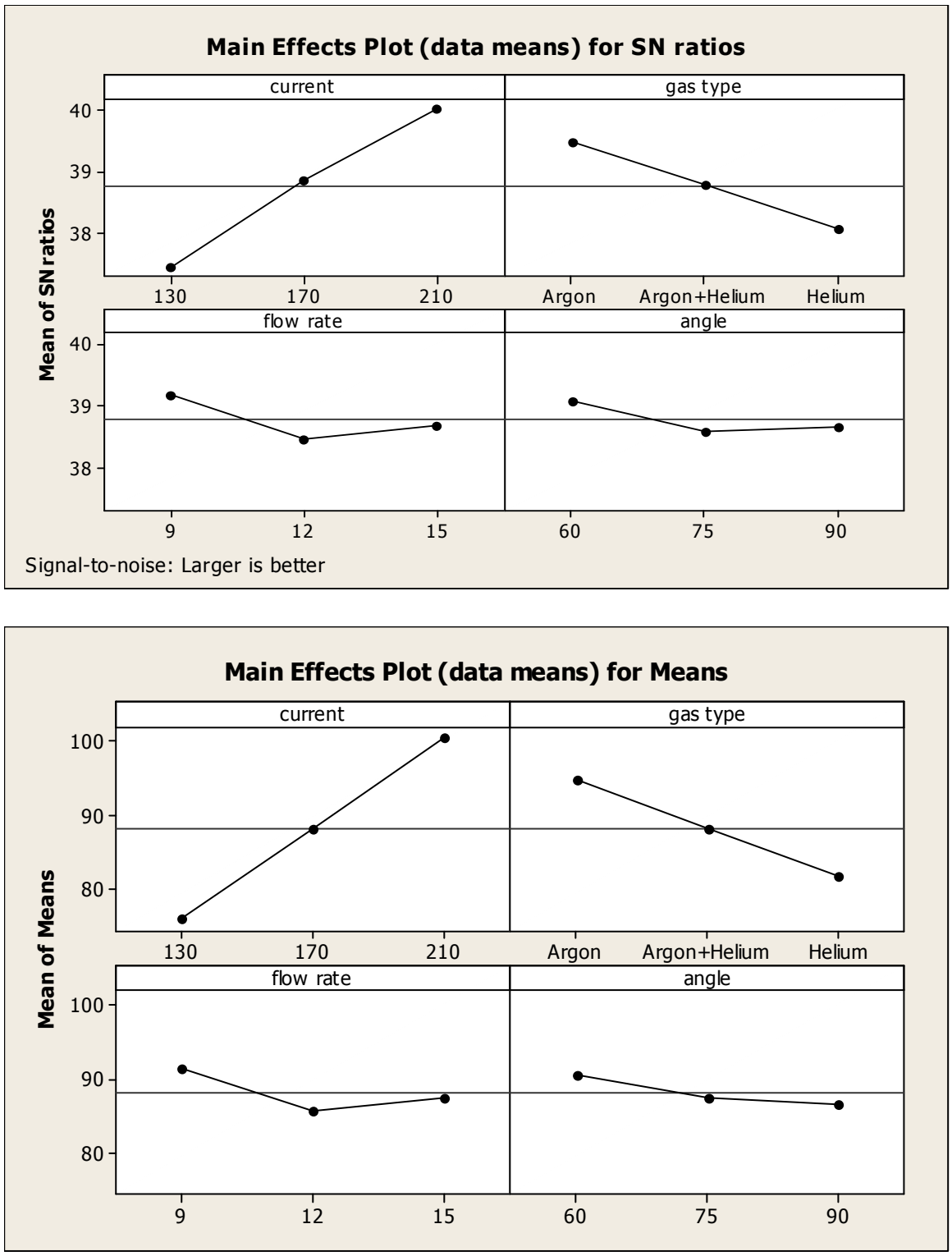

Figure 8.4: Main effect plot for SN ratios and means for toughness at -20^{O}C temp. of SS 310

8.2 RESULTS OF CHARPY TEST ON SS 316

Table 8.10: Charpy impact test results of SS 316

Experiment number	Contributing parameters of particular specimens	Charpy test readings at surrounding atmospheric temperature (28^o C) (joules)	Charpy test readings at -20^o C (joules)
1	I_1,G_1,F_1,Θ_1	90.65	88.20
2	I_1,G_2,F_2,Θ_2	73.50	71.05
3	I_1,G_3,F_3,Θ_3	80.85	78.40
4	I_2,G_1,F_2,Θ_3	95.55	90.65
5	I_2,G_2,F_3,Θ_1	75.95	71.05
6	I_2,G_3,F_1,Θ_2	93.10	85.75
7	I_3,G_1,F_3,Θ_2	105.35	102.90
8	I_3,G_2,F_1,Θ_3	98.0	95.55
9	I_3,G_3,F_2,Θ_1	100.45	98.0

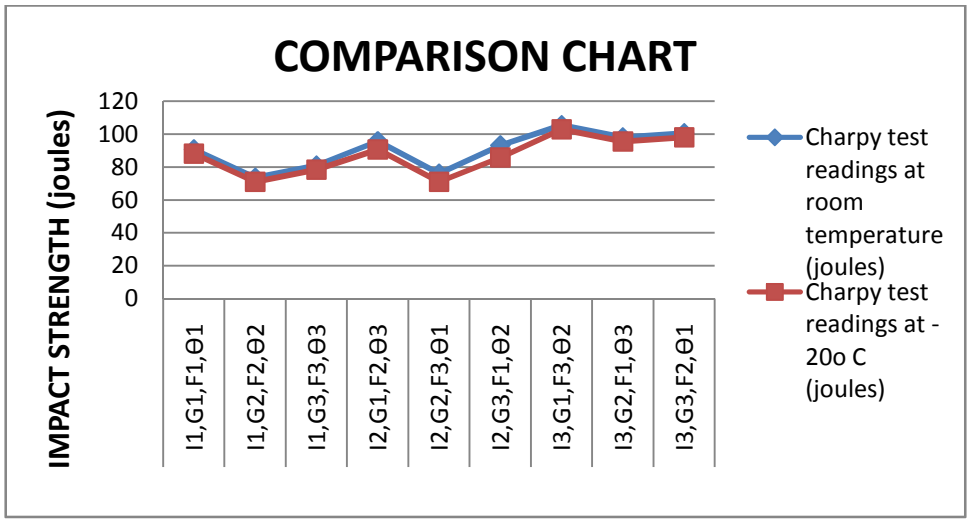

Figure 8.5: Comparison of toughness values of SS 316 at room temperature and at -20^0 C

The figure 8.5 shows the comparison of toughness values made on SS 316 material at room temperature of about 28^o C and -20^o C temperature. It can be noticed that since the current being most significant factor among all other factors, the value of toughness goes on increasing

with increase in current. From comparison chart shown above it is clear that similar trend in value of toughness is followed but with decrease in temperature the toughness value decreases.

8.2.1 ANOVA FOR TOUGHNESS ON SS 316 AT ROOM TEMPERATURE

The result of Charpy test carried out on SS 316 at room temperature is shown in table 8.10 in which average of two values have been shown for each sample. The maximum toughness of about 105.35 J was obtained at higher current level of 210A. The results so obtained have been analysed using ANOVA given in tables from table 8.11 to table 8.14. It is clear that current is the most significant factor affecting the toughness value. The nature of gas used has sub-significant affect on the same where as grove angle has least effect on toughness. The main effect plots for SS 316 on toughness shows that the value of toughness goes on increasing with increase in current. The use of argon results in maximum toughness. Moreover, small gas flow rates results in achieving higher values of toughness but from percentage contribution point of view the flow rate has negligible effect. Grove angle has almost negligible effect as compared with other parameters.

Table 8.11: Analysis of variance for SN ratio of toughness of SS 316 at room temperature

Source	DOF	SS	Variance	F ratio	F (critical)	PC
Current	2	5.739	2.869	41.868	19	54.185
Gas type	2	3.614	1.807	26.369	19	33.635
Flow rate	2	0.847	0.423	6.185	19	6.875
Grove angle	2	0.137	0.068	1	19	5.30
Total	8	10.339				100
Error pooled	2	0.137	0.068			5.30

Table 8.12: Response table for SN ratio of toughness of SS 316 at room temperature

Level	Current	Gas type	Flow rate	Grove angle
1	38.18	39.73	39.44	38.89
2	38.81	39.17	38.97	39.02
3	40.10	38.19	38.69	39.19
Delta	1.92	1.53	0.74	0.30
Rank	1	2	3	4

Table 8.13: Analysis of variance for Means of toughness of SS 316 at room temperature

Source	DOF	SS	Variance	F ratio	F (critical)	PC
Current	2	597.58	298.791	63.994	19	58.721
Gas type	2	329.47	164.735	35.282	19	31.957
Flow rate	2	65.36	32.680	6.999	19	5.592
Grove angle	2	9.34	4.669	1	19	3.730
Total	8	1001.75				100
Error pooled	2	9.34	4.669			3.730

Table 8.14: Response table for Means of toughness of SS 316 at room temperature

Level	Current	Gas type	Flow rate	Grove angle
1	81.67	97.18	93.92	89.02
2	88.20	91.47	89.83	90.65
3	101.27	82.48	87.38	91.47
Delta	19.60	14.70	6.53	2.45
Rank	1	2	3	4

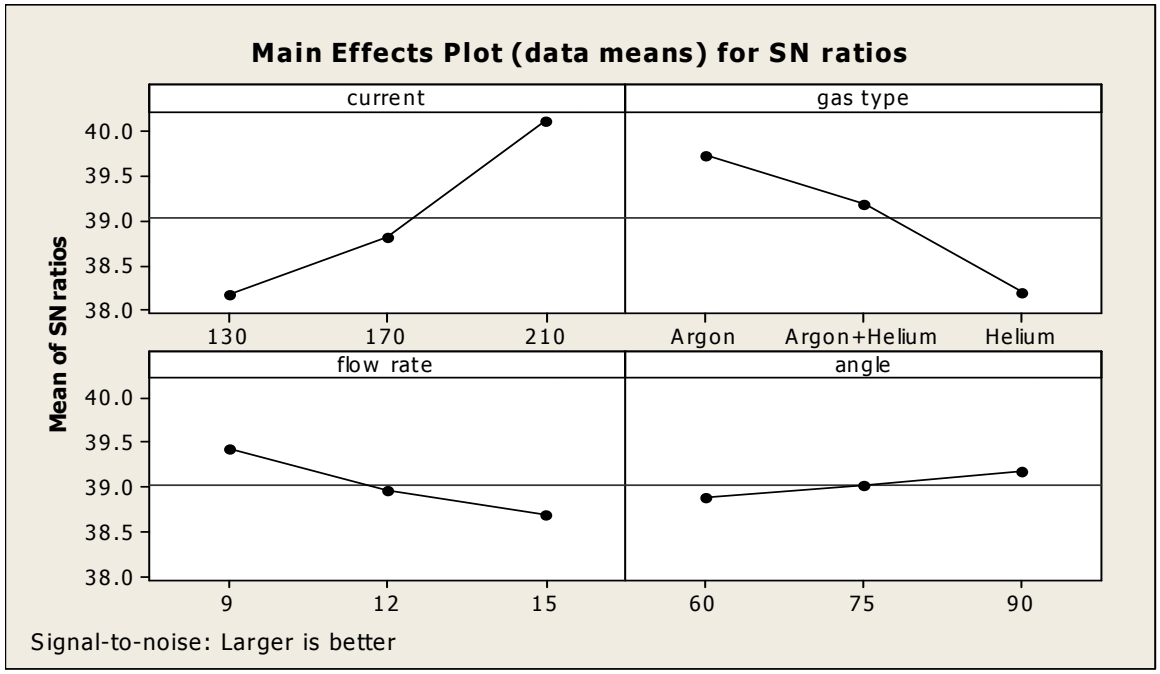

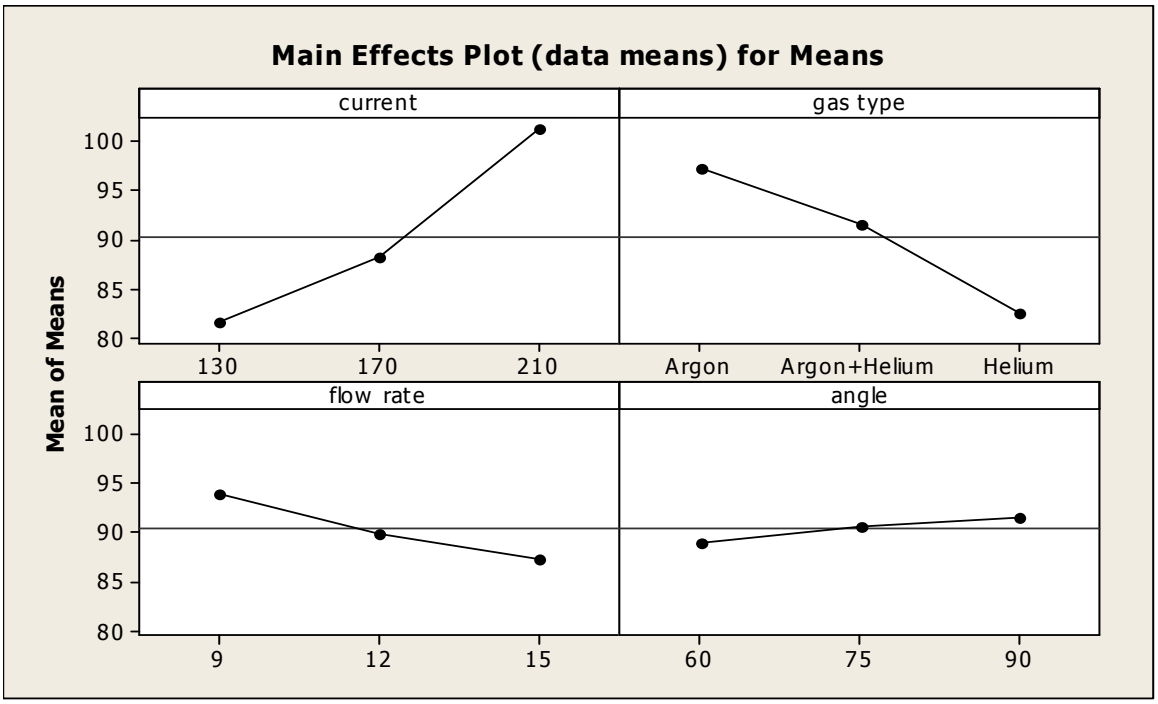

Figure 8.6: Main effect plot for SN ratios and means for toughness at room temp. of SS 316

8.2.1.1 OPTIMAL DESIGN FOR TOUGHNESS OF SS 316 AT ROOM TEMP

It is clear from ANOVA table for means (table 8.13) that the F value of current and type of gas is greater than F critical. Main effect plot shows that toughness is maximum for third level current value i.e. 210 A and first level gas type i.e. argon. The confidence interval predict with 95 % confidence so that the value for SS 316 for toughness would be 108.08 ± 6.929 joules

Mean value of toughness is given by:

$$\mu I_3 G_1 = \overline{I_3} + \overline{G_1} - \overline{Y}$$

$$= 101.27 + 97.18 - 90.37$$

$$= 108.08 \text{ joules}$$

Confidence Interval around the Estimated Mean toughness

$$CI_1 = \sqrt{\frac{F_{\alpha, v_1, v_2} V_e}{n_{eff}}}$$

Where $F\alpha V_1 V_2 = F0.05:1:2 = 18.51$

α = Risk (0.05), Confidence = 1-α

V_1 = DOF for mean which is always = 1

V_2 = DOF for error = Ve = 2

$\overline{Y}$ = Average toughness value

η_{eff} = Number of tests under that condition using the participating factors

η_{eff} = N / (1+ DOF$\mathbf{I_3G_1}$) = 9/ 1+2+2 = 1.80

CI = 6.929

So the confidence interval around the Estimated Mean toughness is given by 108.08 ±6.929 joules

8.2.2 ANOVA FOR TOUGHNESS ON SS 316 AT - 20^O C TEMPERATURE

The result of Charpy test carried out on SS 316 at -20^o C temperature is shown in table 8.10 in which average of two values have been shown for each sample. The maximum toughness of about 102.9 J was obtained. The results have been analysed using ANOVA given in tables from table 8.15 to table 8.18. The result shows that current is the most significant parameter affecting the toughness value. The nature of gas used has sub-significant affect on the same where as grove angle has least effect on toughness. The gas flow rate and grove angle has least significance effect. The main effects plot shows that the value of toughness goes on increasing with increase in current. Maximum toughness was obtained when argon was used as a shielding gas and small gas flow rates also results in achieving higher values of toughness. Grove angle has almost negligible effect as compared with other parameters. The value of toughness decreases with decrease in temperature.

Table 8.15: Analysis of variance for SN ratio of toughness of SS 316 -20^O C temperature

Source	DOF	SS	Variance	F ratio	F (critical)	PC
Current	2	6.477	3.238	44.423	19	57.844
Gas type	2	3.624	1.812	24.856	19	31.778
Flow rate	2	0.698	0.349	4.790	19	5.048
Grove angle	2	0.145	0.072	1	19	5.330
Total	8	10.946				100
Error pooled	2	0.145	0.072			5.330

Table 8.16: Response table for SN ratio of toughness of SS 316 -20^{O} C temperature

Level	Current	Gas type	Flow rate	Grove angle
1	37.94	39.42	39.05	38.58
2	38.27	38.79	38.66	38.63
3	39.88	37.88	38.37	38.87
Delta	1.94	1.55	0.68	0.29
Rank	1	2	3	4

Table 8.17: Analysis of variance for Means of toughness of SS 316 -20^{O} C temperature

Source	DOF	SS	Variance	F ratio	F (critical)	PC
Current	2	661.61	330.804	70.851	19	62.372
Gas type	2	325.47	162.734	34.854	19	30.229
Flow rate	2	49.35	24.677	5.285	19	3.826
Grove angle	2	9.34	4.669	1	19	3.573
Total	8	1045.77				100
Error pooled	2	9.34	4.669			3.573

Table 8.18: Response table for Means of toughness of SS 316 at -20^{O} C temperature

Level	Current	Gas type	Flow rate	Grove angle
1	79.22	93.92	89.83	85.75
2	82.48	87.38	86.57	86.57
3	98.82	79.22	84.12	88.20
Delta	19.60	14.70	5.72	2.45
Rank	1	2	3	4

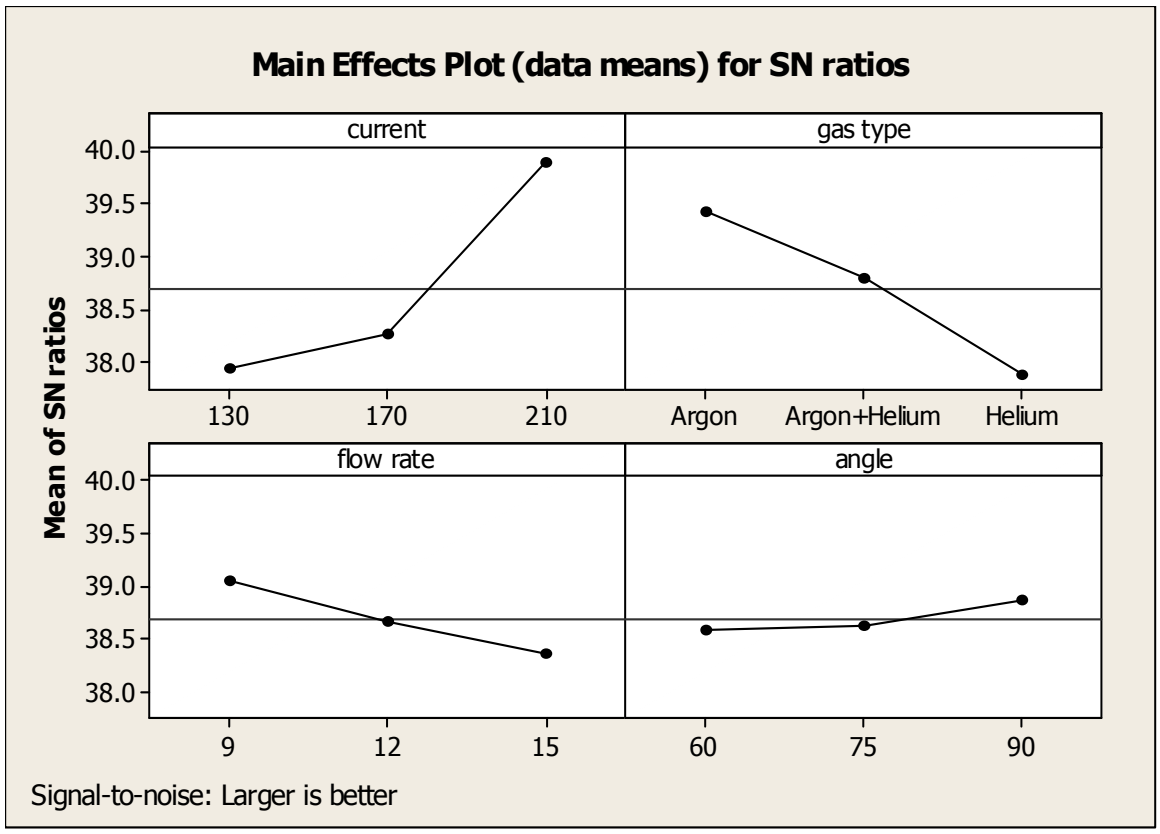

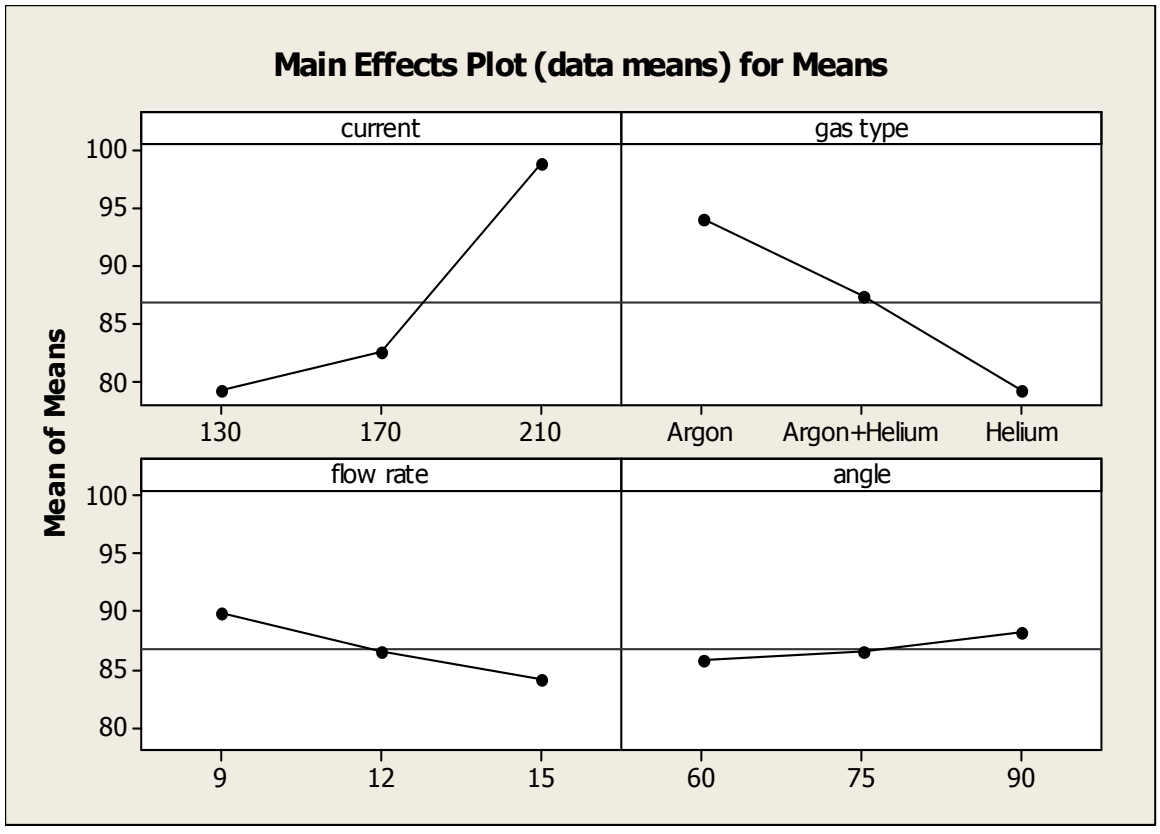

Figure 8.7: Main effect plot for SN ratios and means for toughness at -20^{O}C temp. of SS 316

8.2.2.1 OPTIMAL DESIGN FOR TOUGHNESS OF SS 316 AT -20^{O} C TEMP

It is clear from ANOVA table for means (table 8.17) that the F value of current and nature of gas is greater than F critical. Main effect plot shows that toughness is maximum for third level current value i.e. 210 A and first level gas type i.e. argon. The confidence interval predict with 95 % confidence so that the value for SS 316 for toughness would be 105.91 ±6.929 joules.
Mean value of toughness is given by:

$\mu I_3G_1 = \overline{I_3} + \overline{G_1} - \overline{Y}$

$= 98.82 + 93.92 - 86.83$

$= 105.91$ joules

Confidence Interval around the Estimated Mean toughness

$$CI_1 = \sqrt{\frac{F_{\alpha,v_1,v_2} V_e}{n_{eff}}}$$

Where $F\alpha V_1V_2 = F0.05:1:2 = 18.51$

α = Risk (0.05), Confidence = 1-α

V_1 = DOF for mean which is always = 1

V_2 = DOF for error = Ve = 2

$\overline{Y}$ = Average toughness value

η_{eff} = Number of tests under that condition using the participating factors

$\eta_{eff} = N / (1+ DOF\mathbf{I_3G_1}) = 9/ 1+2+2 = 1.80$

CI = 6.929

So the confidence interval around the Estimated Mean toughness is given by 105.91 ±6.929 joules

CHAPTER 9 RESULTS OF MICRO-HARDESS TEST

As decided earlier, micro-hardness (Vickers) was carried out on all the specimens of both materials SS 310 and SS 316 respectively. The observations obtained during test are shown hereunder.

9.1 RESULTS OF MICROHARDNESS TEST ON SS 310

Table 9.1: Result of Microhardness test performed on SS 310

Experiment Number	Contributing parameters of particular specimens	Microhardness number (HVN)
1	I_1,G_1,F_1,Θ_1	85.87516
2	I_1,G_2,F_2,Θ_2	88.77108
3	I_1,G_3,F_3,Θ_3	86.60661
4	I_2,G_1,F_2,Θ_3	103.8632
5	I_2,G_2,F_3,Θ_1	116.6102
6	I_2,G_3,F_1,Θ_2	97.96848
7	I_3,G_1,F_3,Θ_2	91.84255
8	I_3,G_2,F_1,Θ_3	104.9062
9	I_3,G_3,F_2,Θ_1	104.0908

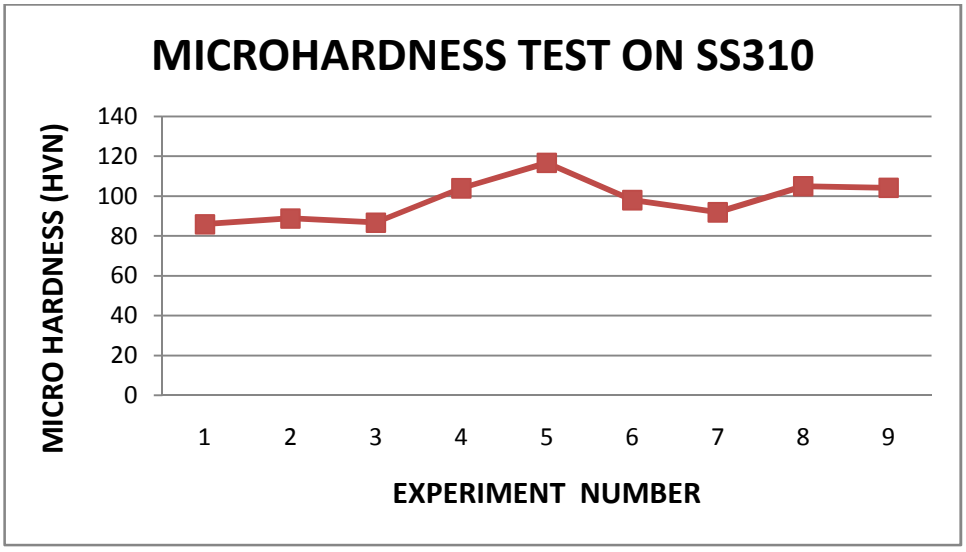

Figure 9.1: Graphical representation of microhardness (vicker's) on SS 310

9.1.1 ANOVA FOR MICROHARDNESS ON SS 310

The result obtained after carrying out microhardness test on all samples as shown in table 9.1 has been analysed using ANOVA compiled from table 9.2 to table 9.5. The maximum value of microhardness obtained is 116.6 (HVN) for experiment no.5. From ANOVA table of means it can be concluded that the current is the most significant factor affecting the microhardness in a particular way as shown in the results. The current alone contributes about 67.5% among all parameters. The other parameters like nature of the shielding gas and flow rate have somewhat less effect whereas the grove angle has almost negligible effect. It is clear from main effect plots that value of hardness is maximum at 170 A. Among all the gases used in the study, helium gas results in maximum microhardness. Response table of means suggests the optimum value for SS 310 is 106.15 HVN.

Table 9.2: Analysis of variance for SN ratio for microhardness (HVN) of SS 310

Source	DOF	SS	Variance	F ratio	F (critical)	PC
Current	2	4.566	2.283	47.629	19	67.576
Gas type	2	1.043	0.521	10.885	19	14.328
Flow rate	2	0.095	0.047	1	19	5.799
Grove angle	2	0.909	0.454	9.484	19	12.297
Total	8	6.615				100
Error pooled	2	0.095	0.047			5.799

Table 9.3: Response table for SN ratio for microhardness (HVN) of SS 310

Level	Current	Gas type	Flow rate	Grove angle
1	38.80	39.42	39.63	40.12
2	40.49	39.64	39.88	39.35
3	40.00	40.23	39.78	39.82
Delta	1.70	0.81	0.25	0.77
Rank	1	2	4	3

Table 9.4: Analysis of variance for Means for microhardness (HVN) of SS 310

Source	DOF	SS	Variance	F ratio	F (critical)	PC
Current	2	571.948	285.974	48.488	19	64.743
Gas type	2	149.083	74.542	12.636	19	15.867
Flow rate	2	11.799	5.899	1	19	5.457
Grove angle	2	132.349	66.175	11.218	19	13.933
Total	8	865.179				100
Error pooled	2	11.799	5.899			5.457

Table 9.5: Response table for Means for microhardness (HVN) **of** SS 310

Level	Current	Gas type	Flow rate	Grove angle
1	87.08	93.86	96.25	102.19
2	106.15	96.22	98.91	92.86
3	100.28	103.43	98.35	98.46
Delta	19.06	9.57	2.66	9.33
Rank	1	2	4	3

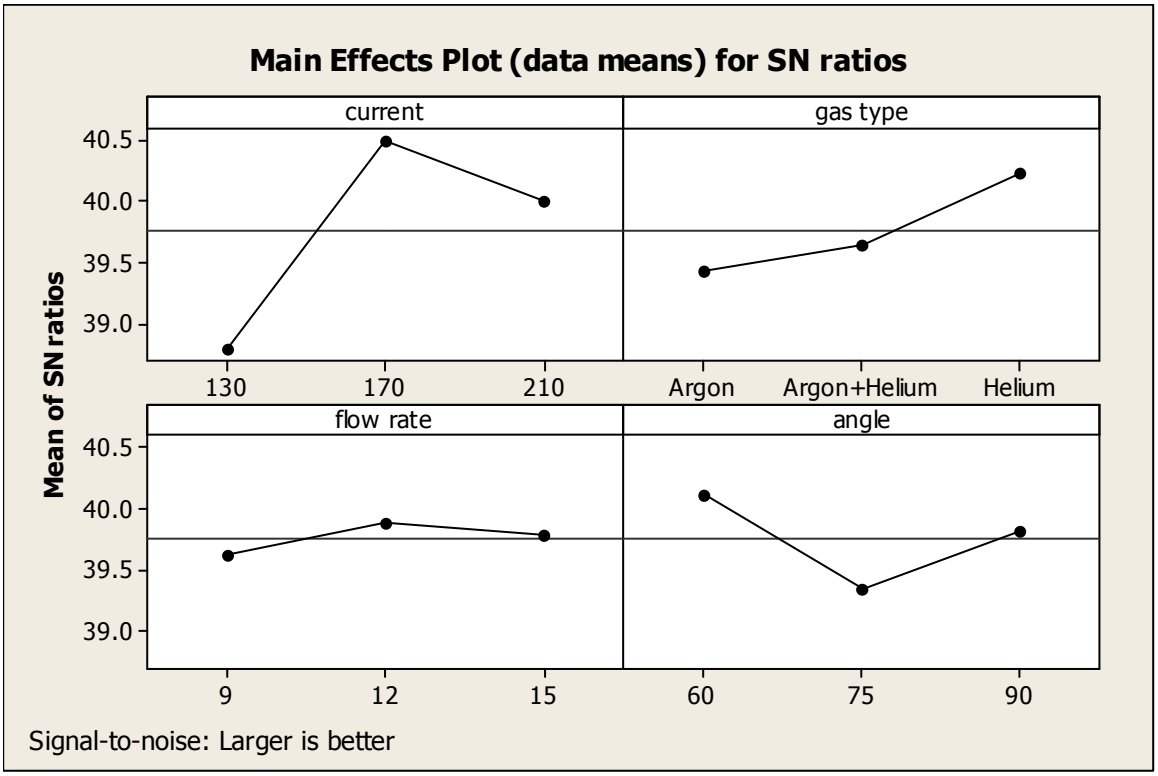

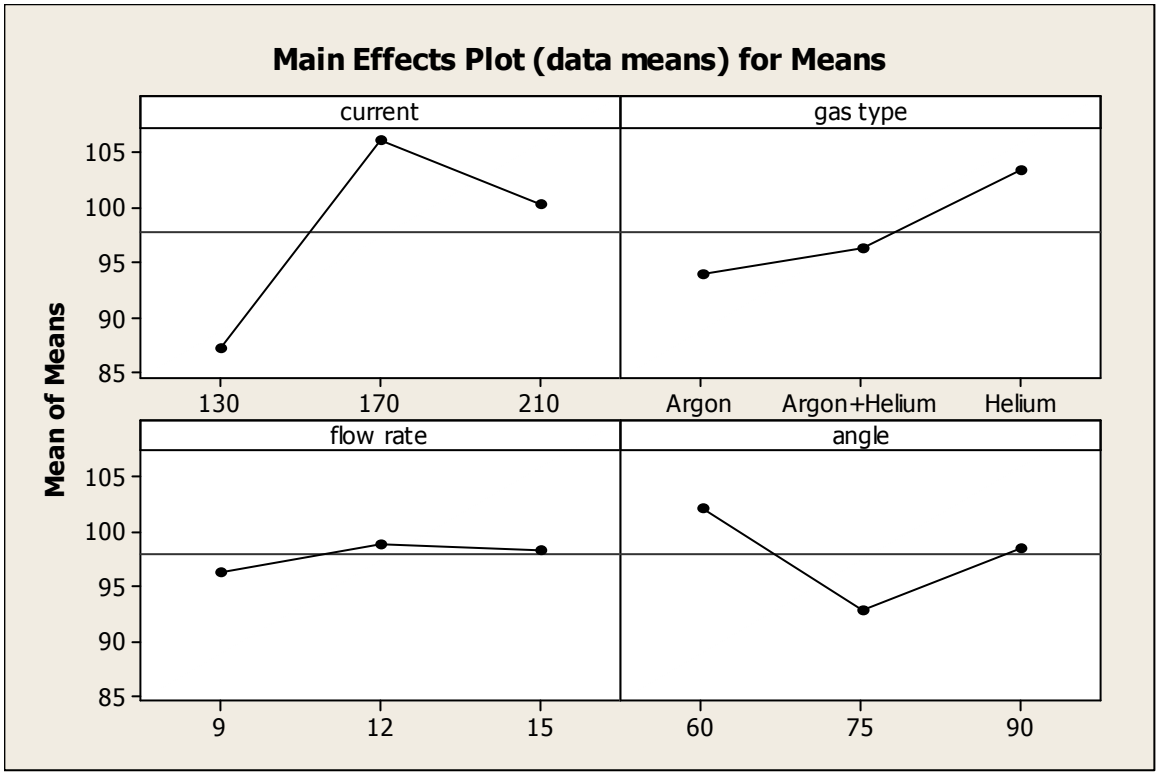

Figure 9.2: Main effect plot for SN ratios and means for microhardness (HVN) of SS 310

9.2 RESULTS OF MICROHARDNESS TEST ON SS 316

Table 9.6: Result of Microhardness test performed on SS 316

Experiment Number	Contributing parameters of particular specimens	Microhardness number (HVN)
1	I_1,G_1,F_1,Θ_1	94.271
2	I_1,G_2,F_2,Θ_2	95.753
3	I_1,G_3,F_3,Θ_3	99.503
4	I_2,G_1,F_2,Θ_3	101.441
5	I_2,G_2,F_3,Θ_1	111.971
6	I_2,G_3,F_1,Θ_2	104.130
7	I_3,G_1,F_3,Θ_2	102.476
8	I_3,G_2,F_1,Θ_3	105.967
9	I_3,G_3,F_2,Θ_1	102.682

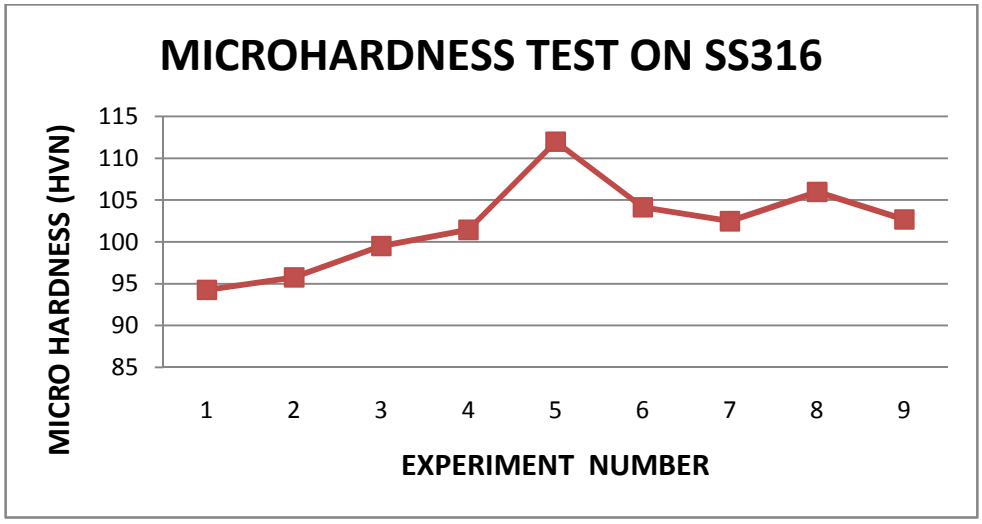

Figure 9.3: Graphical representation of microhardness (vicker's) on SS 316

9.2.1 ANOVA FOR MICROHARDNESS ON SS 316

The result obtained after carrying out microhardness test on all samples as shown in table 9.6 has been analysed using ANOVA compiled from table 9.7 to table 9.10. The maximum value of microhardness obtained is 111.97 (HVN) for experiment no.5. From ANOVA table of means it can be concluded that the current is the most significant factor affecting the microhardness in a particular way as shown in the results. The current alone contributes about 62.3 % among all parameters. The other parameters like nature of the shielding gas and flow rate have somewhat less effect. It is clear from main effect plots that value of hardness is maximum at 170 A. The value of microhardness increases with current till a critical value is reached after which it start decreasing. Among all the gases used in the study, helium gas results in maximum microhardness. Response table of means suggests the optimum value for SS 316 is 105.85 HVN.

Table 9.7 Analysis of variance for SN ratio of microhardness (HVN) of SS 316

Source	DOF	SS	Variance	F ratio	F (critical)	PC
Current	2	1.055	0.527	21.950	19	62.316
Gas type	2	0.273	0.136	5.691	19	13.956
Flow rate	2	0.239	0.119	4.977	19	11.830
Grove angle	2	0.048	0.024	1	19	11.898
Total	8	1.617				100
Error pooled	2	0.048	0.024			11.898

Table 9.8: Response table for SN ratio of microhardness (HVN) of SS 316

Level	Current	Gas type	Flow rate	Grove angle
1	39.69	39.94	40.11	40.23
2	40.48	40.18	39.99	40.06
3	40.31	40.37	40.38	40.19
Delta	0.80	0.43	0.39	0.17
Rank	1	2	3	4

Table 9.9: Analysis of variance for Means of weld bead width of SS 316

Source	DOF	SS	Variance	F ratio	F (critical)	PC
Current	2	143.612	71.806	19.04	19	60.295
Gas type	2	40.079	20.039	5.314	19	14.417
Flow rate	2	34.450	17.224	4.567	19	11.922
Grove angle	2	7.542	3.771	1	19	13.36
Total	8	225.683				100
Error pooled	2	7.542	3.771			13.36

Table 9.10: Response table for Means of microhardness (HVN) of SS 316

Level	Current	Gas type	Flow rate	Grove angle
1	96.51	99.40	101.46	102.98
2	105.85	102.11	99.96	100.79
3	103.71	104.56	104.65	102.30
Delta	9.34	5.17	4.69	2.19
Rank	1	2	3	4

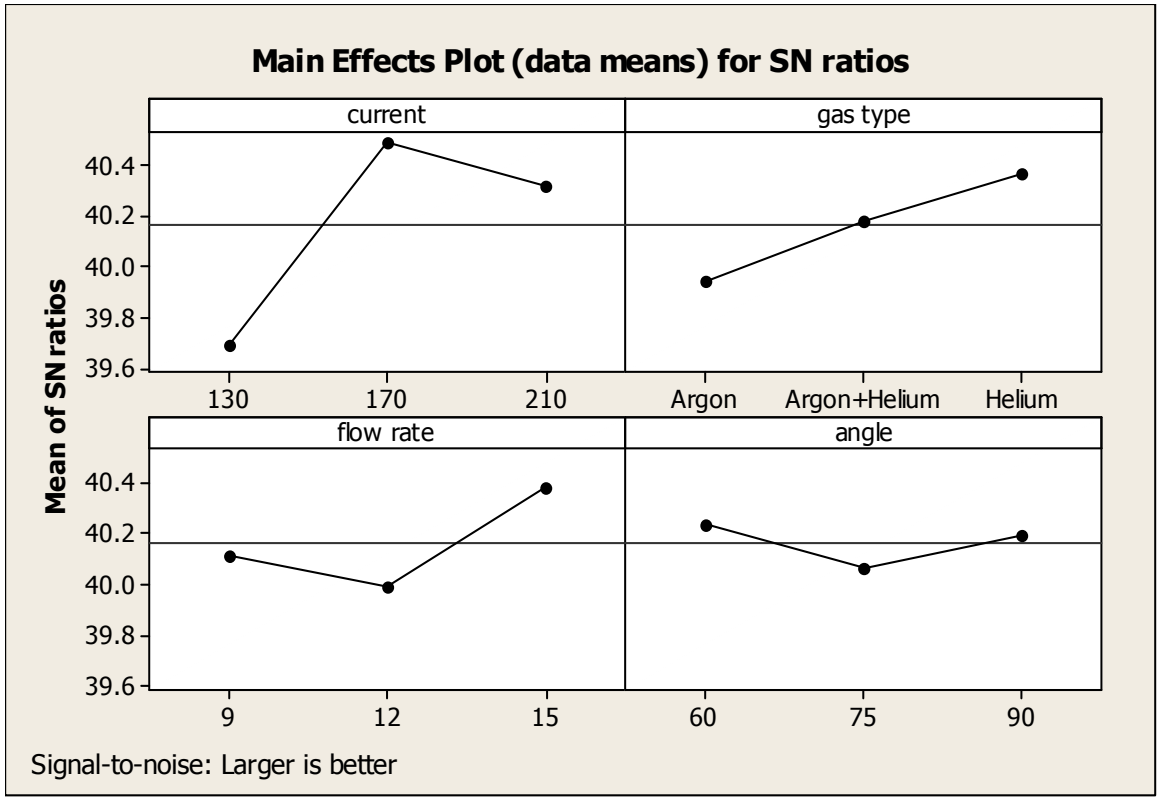

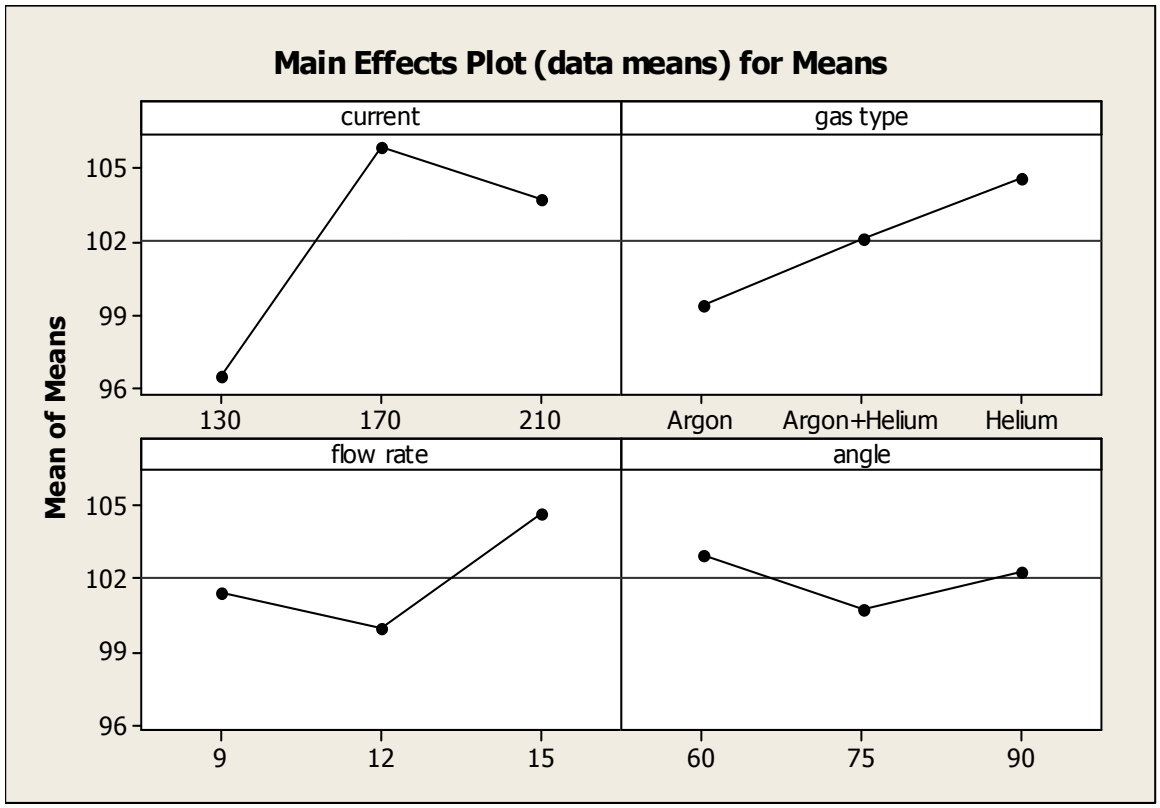

Figure 9.4: Main effect plot for SN ratios and means of Microhardness (HVN) of SS 316

CHAPTER 10 RESULTS OF CHEMICAL COMPOSITION TEST

The chemical composition of weld bead was examined by making use of atomic absorption spectrometer. The main purpose of carrying out this test was to find increase or decrease of any of the constituents in weld joint on account of formation of compounds or dissociation of elements taking place after welding.

Figure 10.1: Chemical composition on all samples of SS310 grade

10.1 RESULT OF CHEMICAL COMPOSITION ON SS 310:

Table 10.1: Values of Chemical Composition of SS 310

CONSTITUENT ELEMENTS	EXPERIMENT NUMBER →									BASE METAL
	1	2	3	4	5	6	7	8	9	
Fe	51.3	51.5	51.7	51.5	51.6	51.9	51.6	51.9	51.8	51.4
C	0.22	0.24	0.22	0.24	0.18	0.25	0.23	0.24	0.2	0.25
Si	1.49	1.52	1.54	1.53	1.54	1.56	1.55	1.54	1.57	1.50
Mn	2.01	2.03	2.03	2.02	2.01	2.01	2.03	2.02	2.04	2.0
P	0.044	0.046	0.03 96	0.03 99	0.046	0.044	0.048	0.047	0.048	0.045
S	0.03	0.03	0.03	0.03	0.03	0.03	0.03	0.03	0.03	0.03
Cr	24.3	24.2	24.2	24.1	24.0	24.1	23.9	23.8	23.8	24.4
Ni	19.1	19.3	19.2	19.6	19.7	19.5	19.7	19.4	19.8	19.1
Co	0.376	0.376	0.369	0.372	0.372	0.371	0.345	0.35	0.356	0.376
Cu	0.258	0.26	0.261	0.26	0.263	0.262	0.263	0.263	0.262	0.258
Remaining (V,Ti,W,Nb,Al)	Bal.	Bal.	Bal.	Bal.	Bal.	Bal.	Bal.	Bal.	Bal.	Bal.

The enormous amount of localised heat generated during welding may trigger either formation of new compounds or dissociation of elements thereby varying chemical composition of weld bead. An average of two readings was taken on all the samples as shown above in table 10.1 and for more clarification of the variations, various graphs are plotted hereunder:

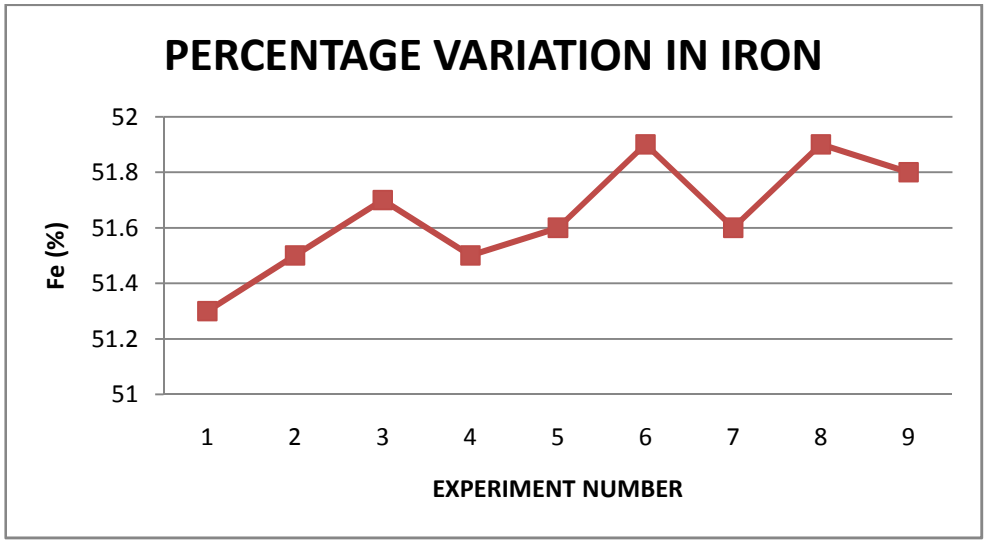

Figure 10.2: Percentage variation of 'Fe' in welded region of SS 310

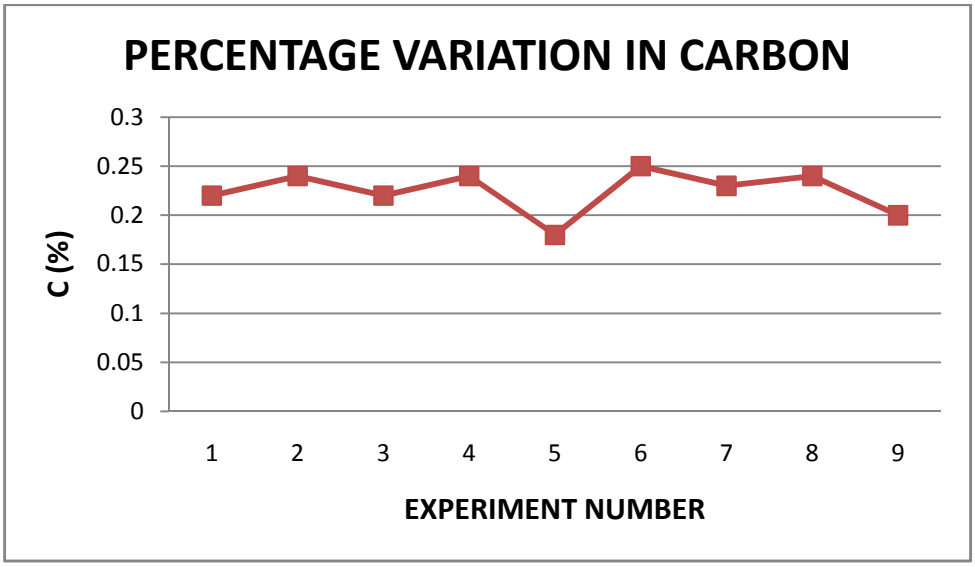

Figure 10.3: Percentage variation of 'C' in welded region of SS 310

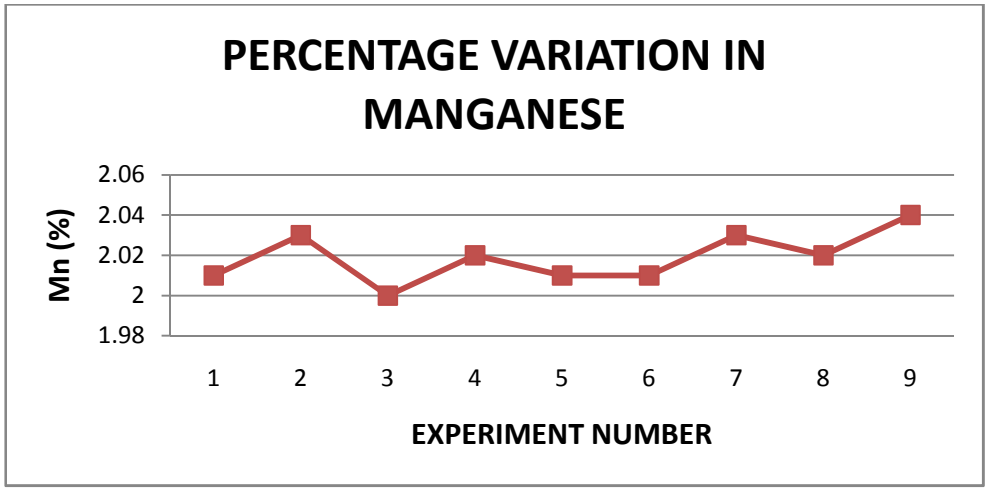

Figure 10.4: Percentage variation of 'Mn' in welded region of SS 310

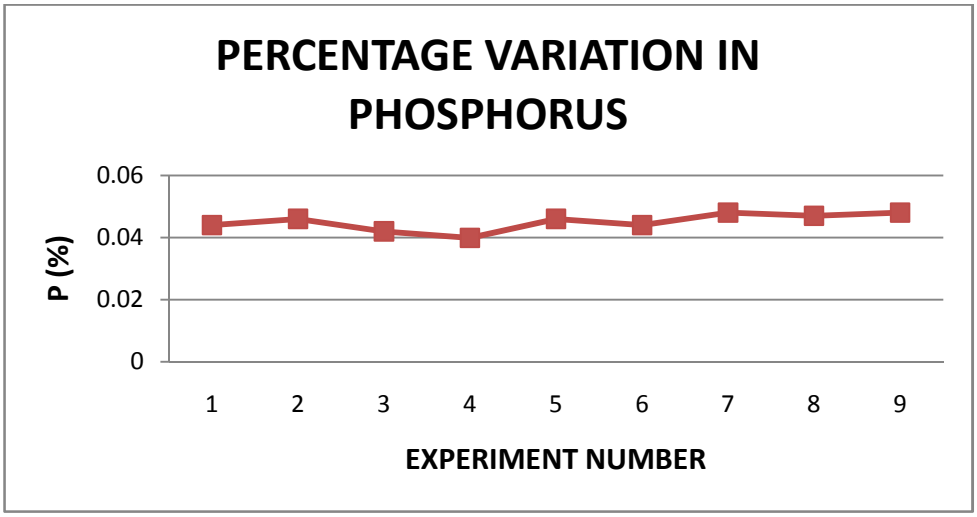

Figure 10.5: Percentage variation of 'P' in welded region of SS 310

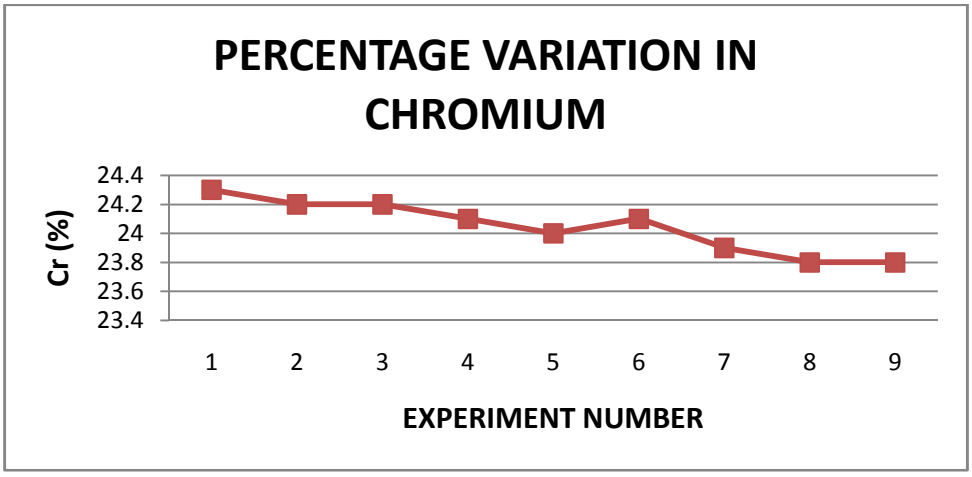

Figure 10.6: Percentage variation of 'Cr' in welded region of SS 310

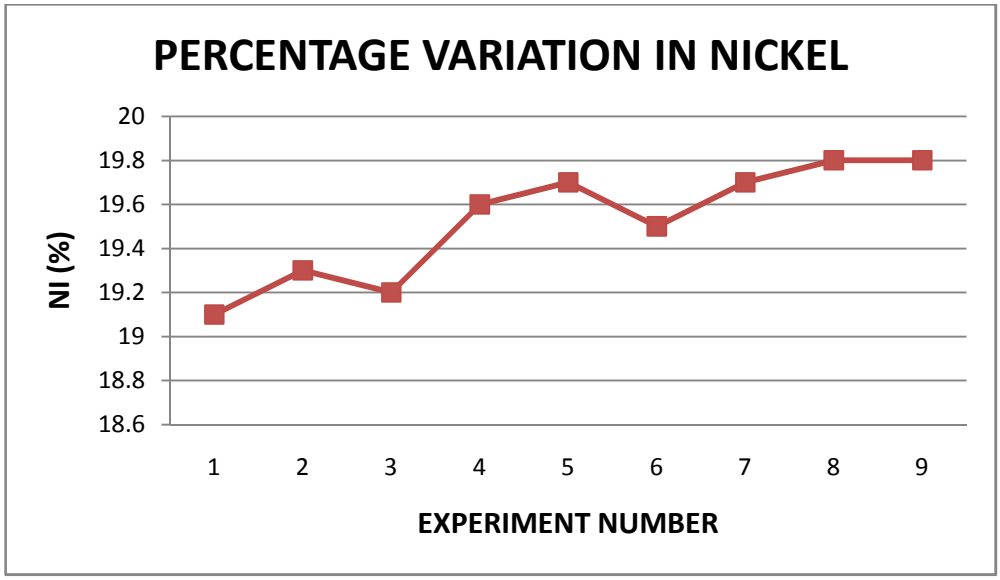

Figure 10.7: Percentage variation of 'Ni' in welded region of SS 310

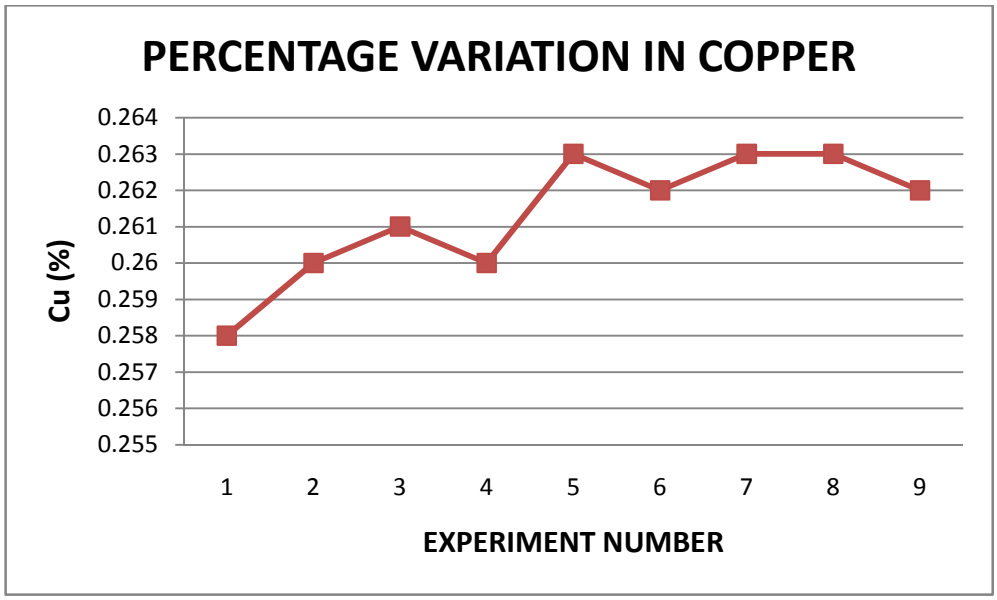

Figure 10.8: Percentage variation of 'Cu' in welded region of SS 310

From the graphical representation showing percentage variations of constituent elements of all specimens for SS 310 shown above, it can be concluded that there is a small increase in the percentage of nickel and iron in weld bead as compared to base metal where as the decrease in composition of chromium has been noticed. This may be due to formation of some compounds in welded region on account of enormous heat generated.

10.2 RESULT OF CHEMICAL COMPOSITION ON SS 316:

Figure 10.9: Chemical composition on all samples of SS310 grade

Table 10.2: Values of Chemical Composition of SS 316

CONSTITUENT ELEMENTS ↓	EXPERIMENT NUMBER →									BASE METAL SS 316 ↓
	1	**2**	**3**	**4**	**5**	**6**	**7**	**8**	**9**	
Fe	62.1	62.3	62.5	62.4	62.6	62.8	62.5	62.7	62.9	62.2
C	0.0787	0.0789	0.0787	0.0785	0.0787	0.0788	0.0786	0.0787	0.0784	0.08
Si	0.751	0.75	0.752	0.752	0.753	0.755	0.752	0.754	0.755	0.749
Mn	2.22	2.24	2.25	2.23	2.24	2.25	2.24	2.26	2.24	2
P	0.046	0.047	0.050	0.048	0.051	0.052	0.047	0.049	0.045	0.045
S	0.03	0.03	0.03	0.03	0.03	0.03	0.03	0.03	0.03	0.03
Cr	17.2	17	16.8	16.9	16.7	16.2	16.3	16.2	16	17.4
Ni	12.18	12.25	12	11.85	11.69	11.80	11.77	11.68	11.60	12.6
Mo	2.55	2.54	2.54	2.54	2.54	2.54	2.55	2.54	2.54	2.54
Cu	0.218	0.219	0.216	0.219	0.217	0.218	0.223	0.220	0.222	0.218
Remaining (V,Ti,W,Nb,Al, Co)	Bal.	Bal.	Bal.	Bal.	Bal.	Bal.	Bal.	Bal.	Bal.	Bal.

It can be concluded that slight increase in the composition of iron and manganese has been observed whereas there is decrease in percentage composition of carbon, nickel and chromium as compared to the values of the base metal. An average of two readings was taken on all the

samples as shown above in table 10.2 and for more clarification of the variations, various graphs are plotted hereunder:

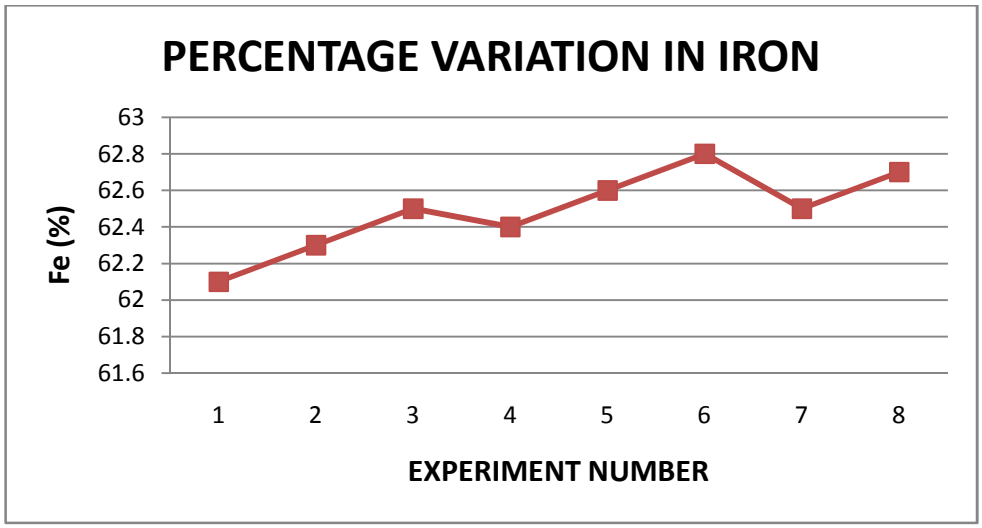

Figure 10.10: Percentage variation of 'Fe' in welded region of SS 316

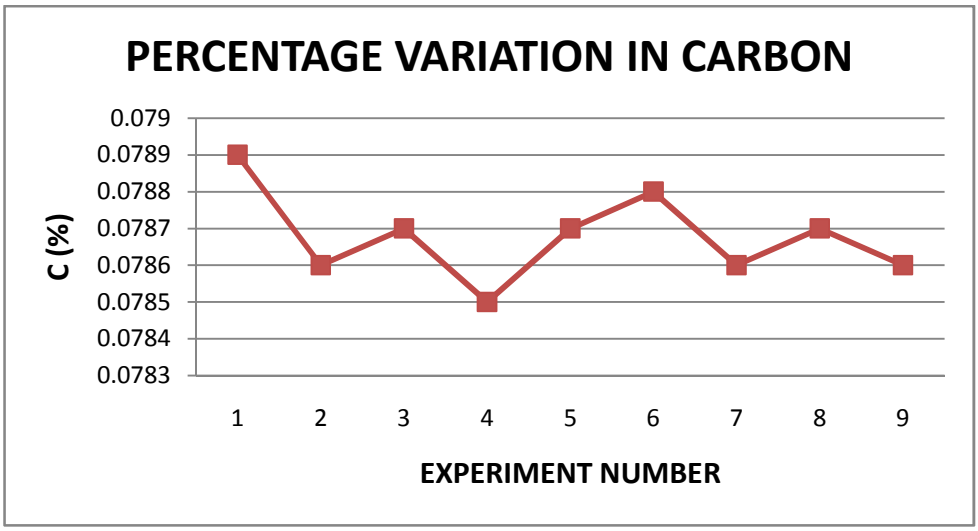

Figure 10.11: Percentage variation of 'C' in welded region of SS 316

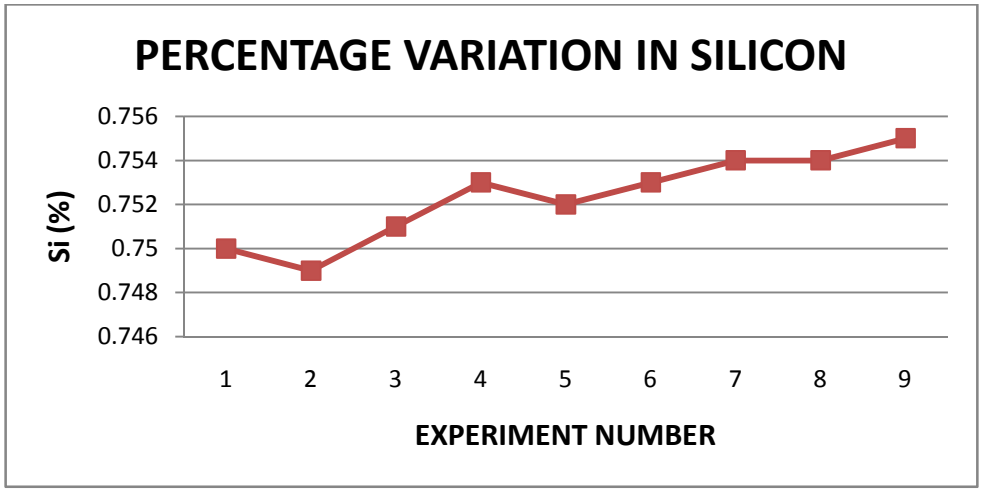

Figure 10.12: Percentage variation of 'Si' in welded region of SS 316

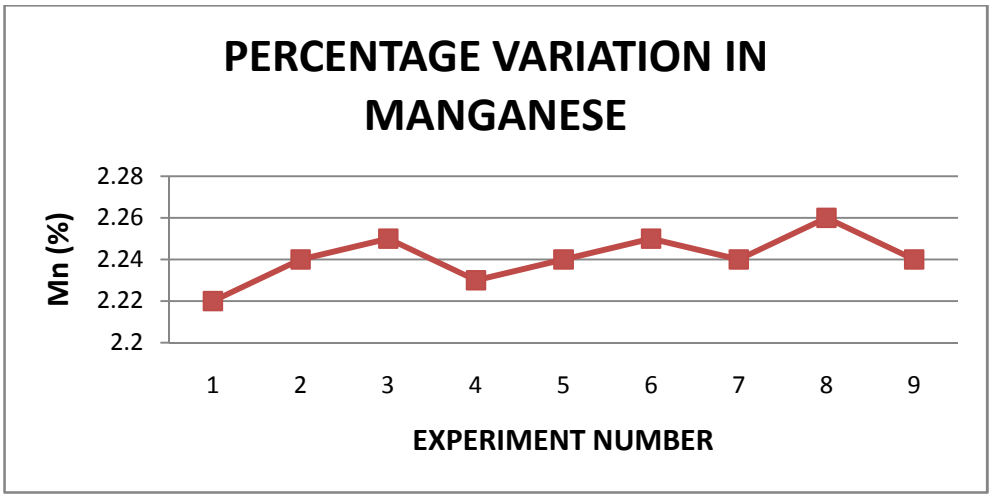

Figure 10.13: Percentage variation of 'Mn' in welded region of SS 316

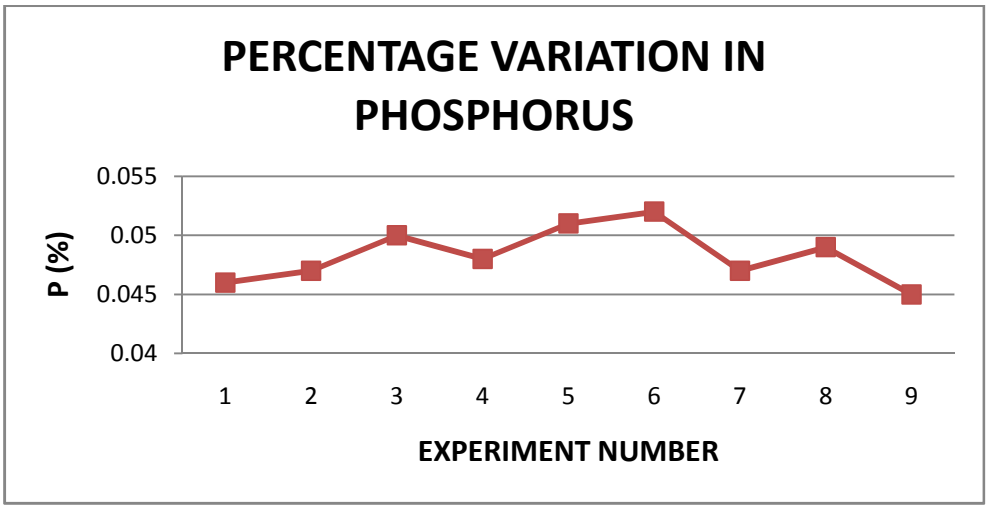

Figure 10.14: Percentage variation of 'P' in welded region of SS 316

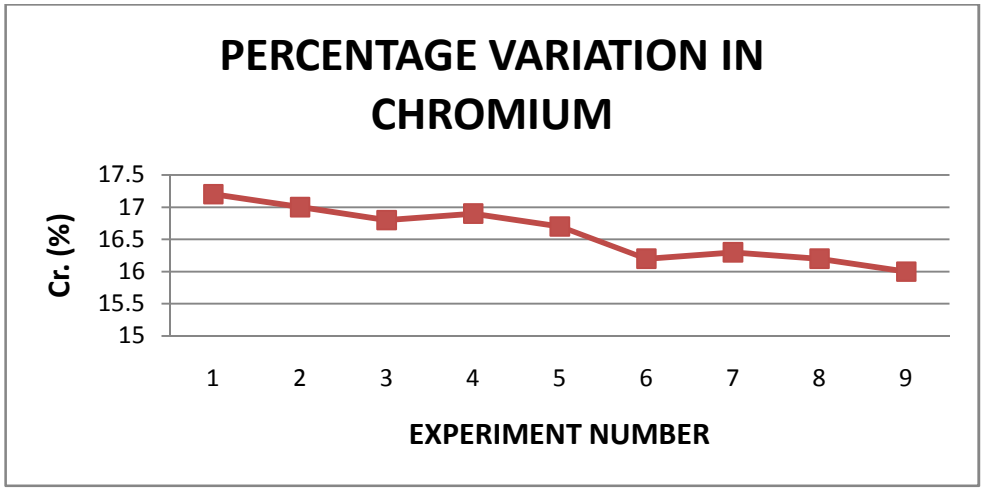

Figure 10.15: Percentage variation of 'Cr' in welded region of SS 316

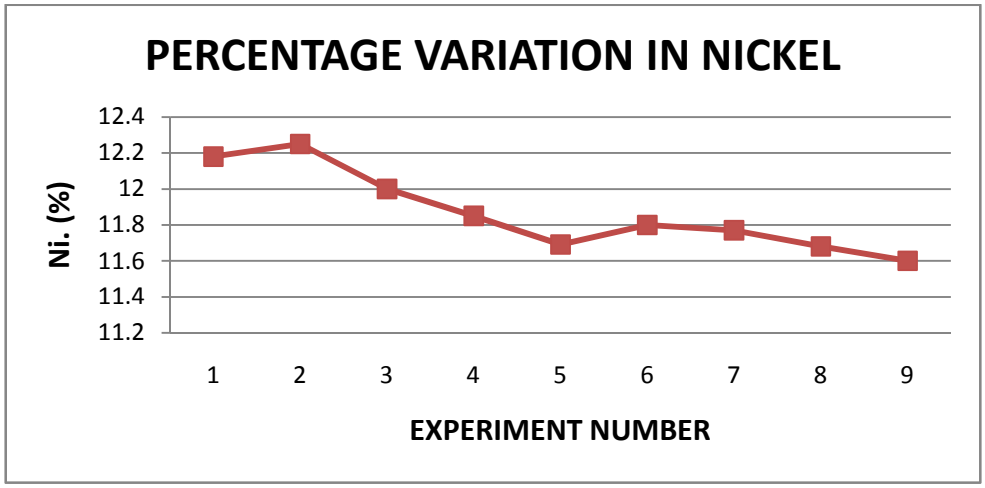

Figure 10.16: Percentage variation of 'Ni' in welded region of SS 316

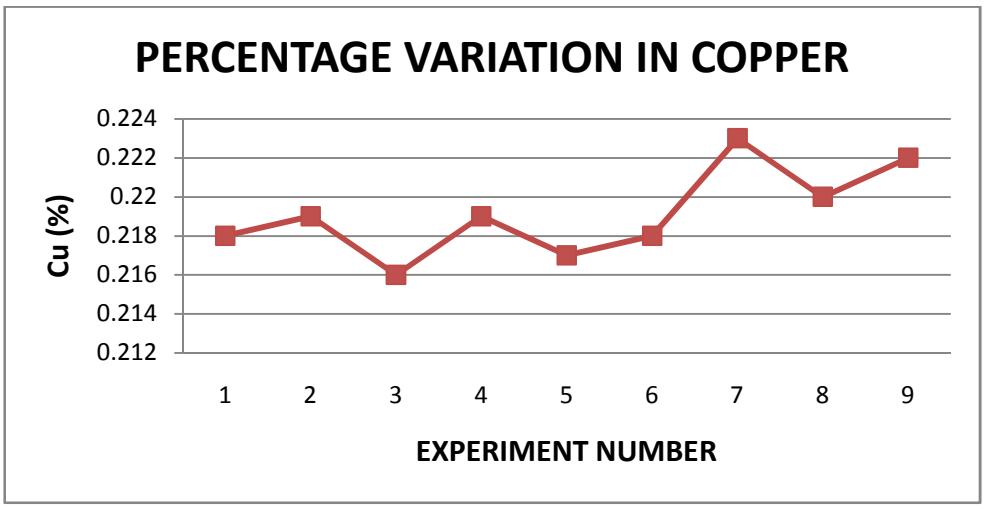

Figure 10.17: Percentage variation of 'Cu' in welded region of SS 316

CHAPTER 11 RESULTS OF TENSILE TEST

The tensile test was performed on all the specimens for both materials. The shape and size of the specimen chosen was in accordance with ASTM specification E8/E8M-11. The tensile test was carried out at Indiana Lab, Mohali with constant testing speed of 8 mm/min.

Figure 11.1: Tensile test specimens of both SS 310 and SS 316

11.1 TENSILE TESTING OF SS 310

Table 11.1: Tensile test results of ss 310

EXPERIMENT NUMBER	TENSILE STRENGTH (Mpa)	YIELD STRESS (Mpa)	ELONGATION (%)
1	342.680	264.713	2.90
2	569.971	325.873	31.04
3	395.495	341.540	6.24
4	479.139	374.437	8.88
5	394.667	305.778	6.48
6	492.495	342.250	13.74
7	381.573	321.561	8.34
8	575.617	365.517	31.46
9	534.024	340.877	17.64

Tensile tests were performed on the samples cut perpendicular to the weld line as shown in the figure 11.1.The table 11.1 shows the result of tensile testing done on stainless steel grade SS 310 having 50 mm gauge length and 12.55 mm width. The maximum tensile strength of 575.617 Mpa was obtained in experiment number 8 with current value of 210A, 9L/min gas flow rate, grove angle of 90^{o} and gas used was helium. It can be concluded that under these parameters maximum tensile strength is obtained. Although many of the specimens show good tensile strength but few failed with very less percentage elongation. The reason for this behaviour is unknown. Internal defects or discontinuities inherent within in the raw material

might be the possible cause of such a result as every care was undertaken during welding so that surface plates must be free from grease, oil, dirt etc before carrying out tacking and welding the pieces together. The clean weld specimen were used, hence some inherent defects in stainless steel plate must be the factor that resulted so in few of the welded plates. The graphs of stress vs. strain for all samples are shown below.

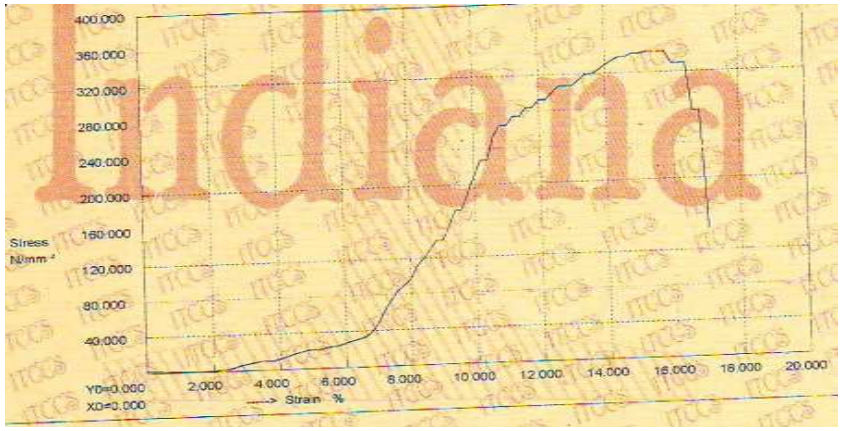

Figure 11.2: Graphical representation of stress vs. strain of SS 310 of specimen no.-1

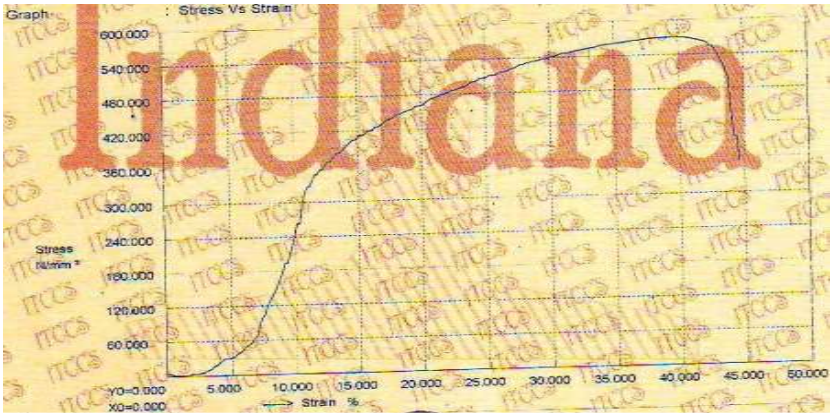

Figure 11.3: Graphical representation of stress vs. strain of SS 310 of specimen no.-2

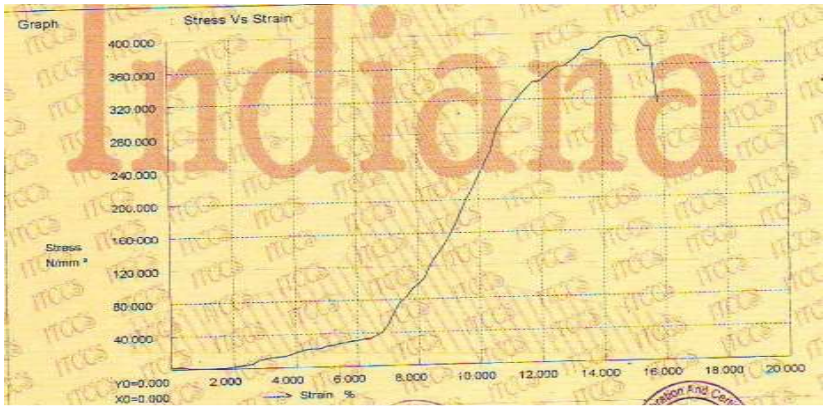

Figure 11.4: Graphical representation of stress vs. strain of SS 310 of specimen no.-3

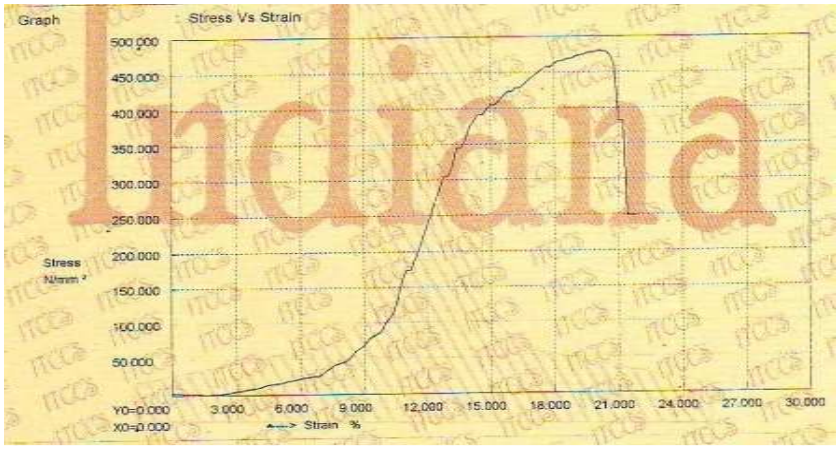

Figure 11.5: Graphical representation of stress vs. strain of SS 310 of specimen no.-4

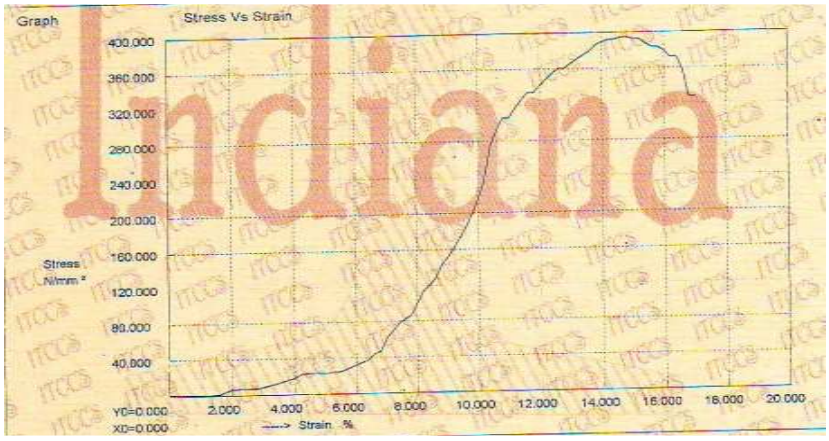

Figure 11.6: Graphical representation of stress vs. strain of SS 310 of specimen no.-5

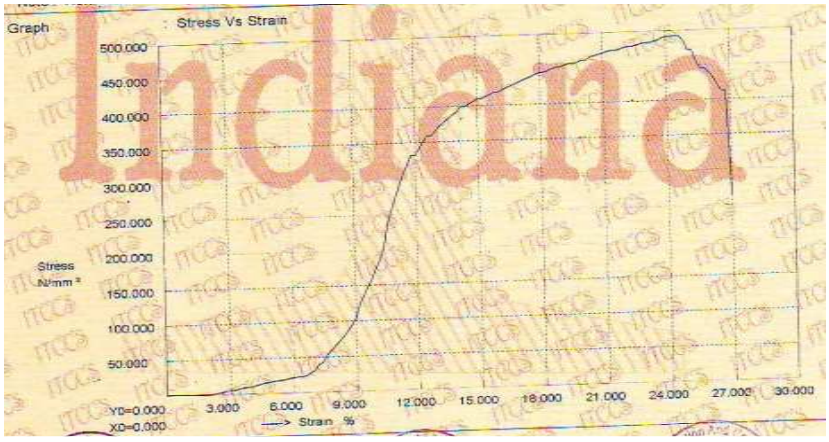

Figure 11.7: Graphical representation of stress vs. strain of SS 310 of specimen no.-6

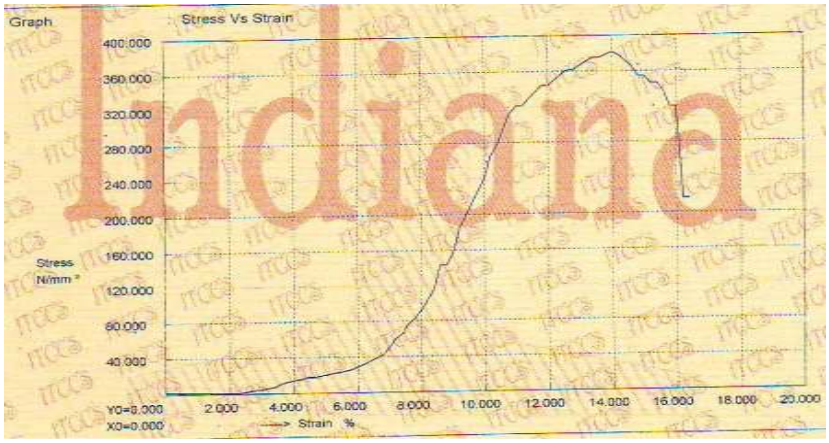

Figure 11.8: Graphical representation of stress vs. strain of SS 310 of specimen no.-7

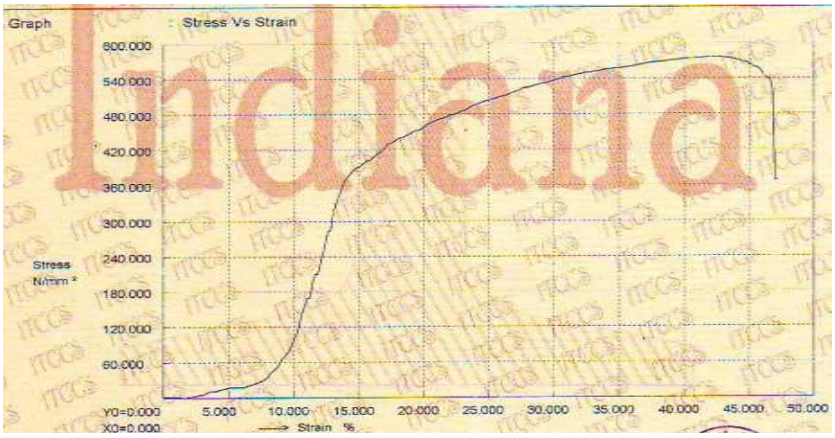

Figure 11.9: Graphical representation of stress vs. strain of SS 310 of specimen no.-8

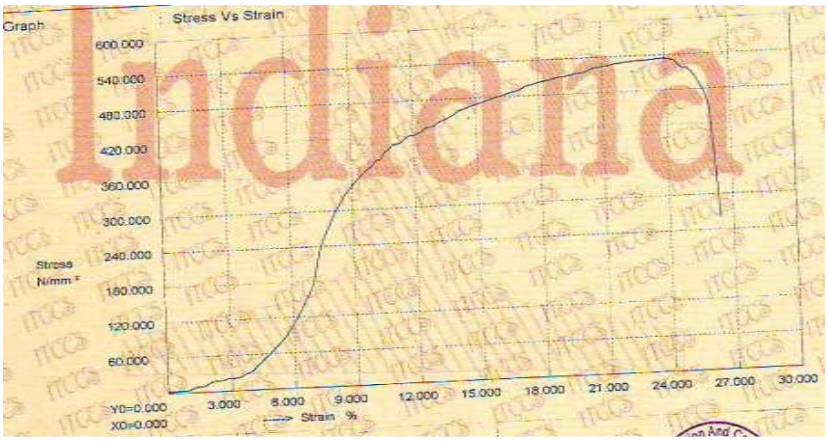

Figure 11.10: Graphical representation of stress vs. strain of SS 310 of specimen no.-9

11.2 TENSILE TESTING OF SS 316

Table 11.2: Tensile test results of ss 316

EXPERIMENT NUMBER	TENSILE STRENGTH (Mpa)	YIELD STRESS (Mpa)	ELONGATION (%)
1	334.688	319.688	5.28
2	587.508	417.053	29.52
3	607.810	383.277	40.46
4	487.083	429.285	5.98
5	590.551	401.334	29.20
6	606.328	397.396	31.50
7	350.490	319.082	3.14
8	583.350	398.284	29.44
9	484.423	391.165	8.80

Tensile tests were performed on the samples cut perpendicular to the weld line as shown in the figure 11.1.The table 11.2 shows the result of tensile testing done on stainless steel grade SS 310 having 50 mm gauge length and 12.55 mm width. The maximum tensile strength of 607.810 Mpa was obtained in experiment number 3 with current value of 130A, 15L/min gas flow rate, grove angle of 90^{o} and gas used was mixture of argon-helium. It can be concluded that under these parameters maximum tensile strength is obtained.

Although many of the specimens show good tensile strength but few failed with very less percentage elongation. The reason for this kind of behaviour is unknown. Internal defects or discontinuities inherent within in the raw material may be the possible cause of such a result as every care was undertaken during welding so that surface plates must be free from grease, oil, dirt etc before carrying out tacking and welding the pieces together. The clean weld specimen were used, hence some inherent defects in stainless steel plate must be the cause that resulted so in few of the welded plates. The graphs of stress vs. strain are shown below.

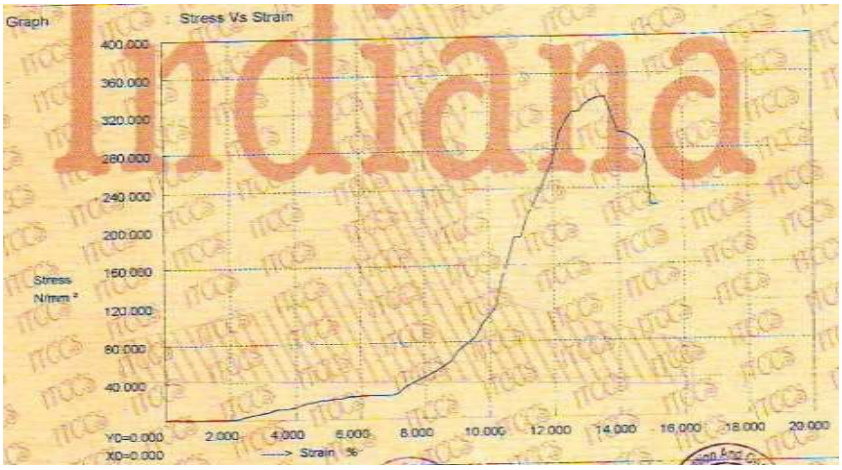

Figure 11.11: Graphical representation of stress vs. strain of SS 316 of specimen no.-1

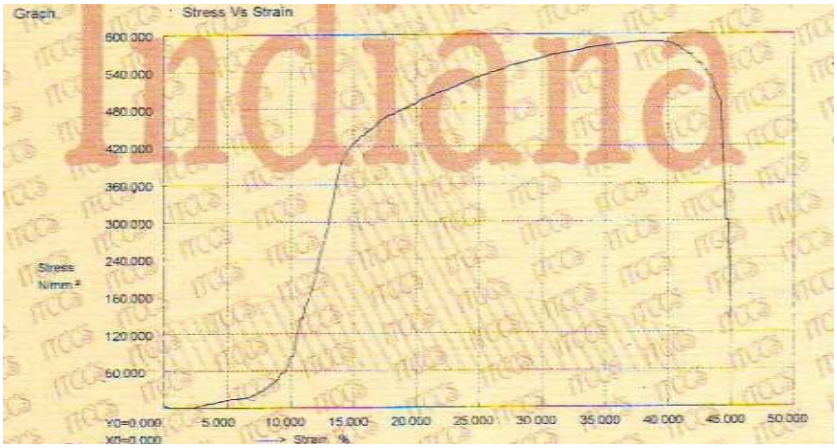

Figure 11.12: Graphical representation of stress vs. strain of SS 316 of specimen no.-2

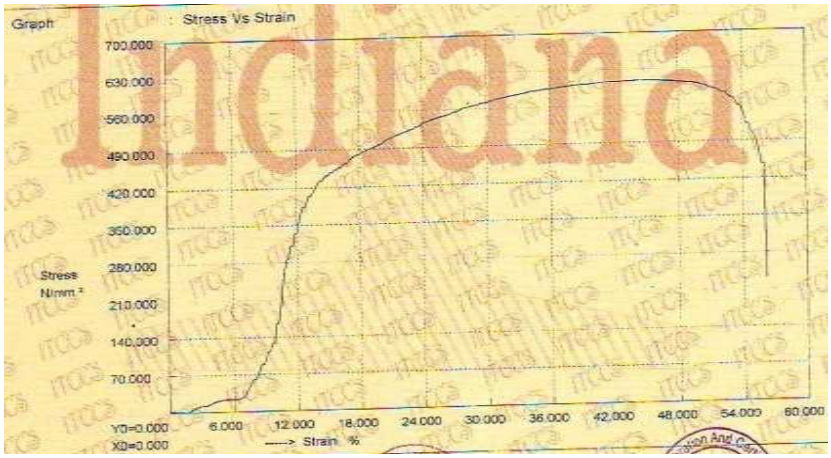

Figure 11.13: Graphical representation of stress vs. strain of SS 316 of specimen no.-3

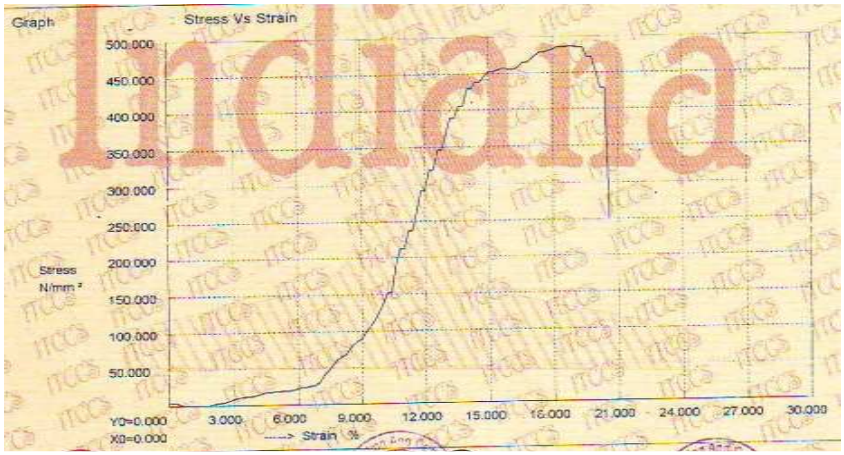

Figure 11.14: Graphical representation of stress vs. strain of SS 316 of specimen no.-4

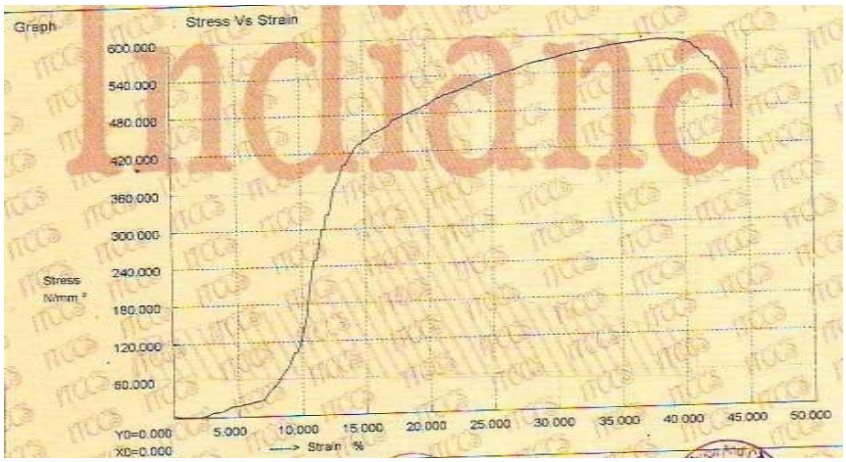

Figure 11.15: Graphical representation of stress vs. strain of SS 316 of specimen no.-5

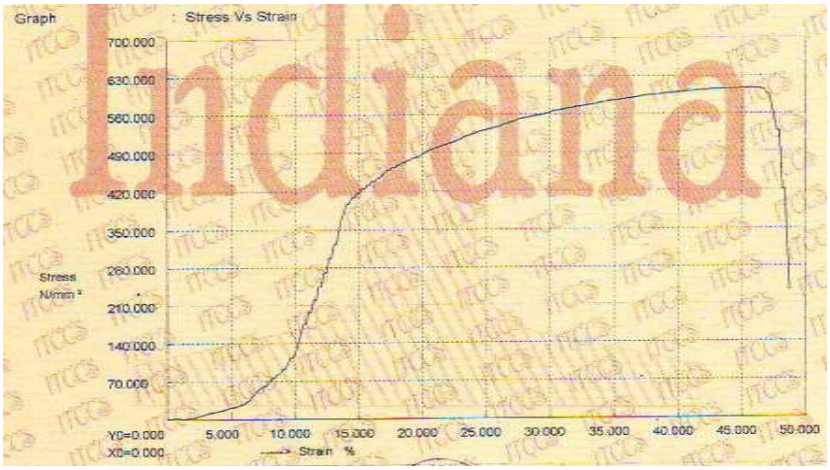

Figure 11.16: Graphical representation of stress vs. strain of SS 316 of specimen no.-6

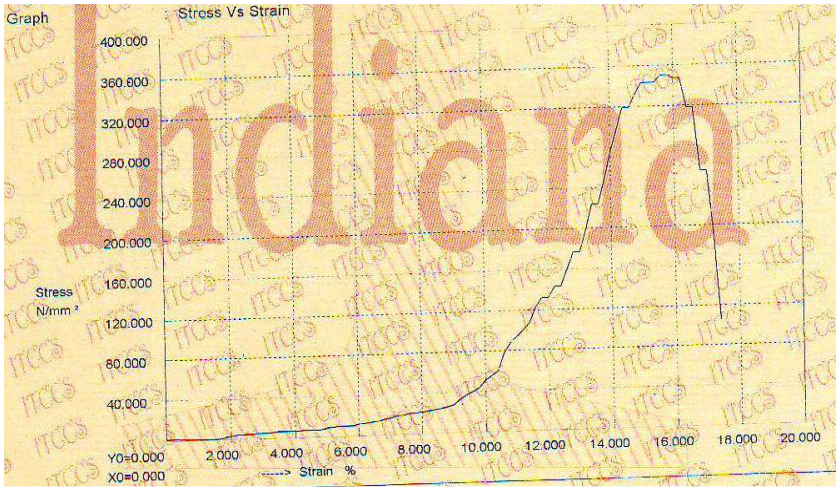

Figure 11.17: Graphical representation of stress vs. strain of SS 316 of specimen no.-7

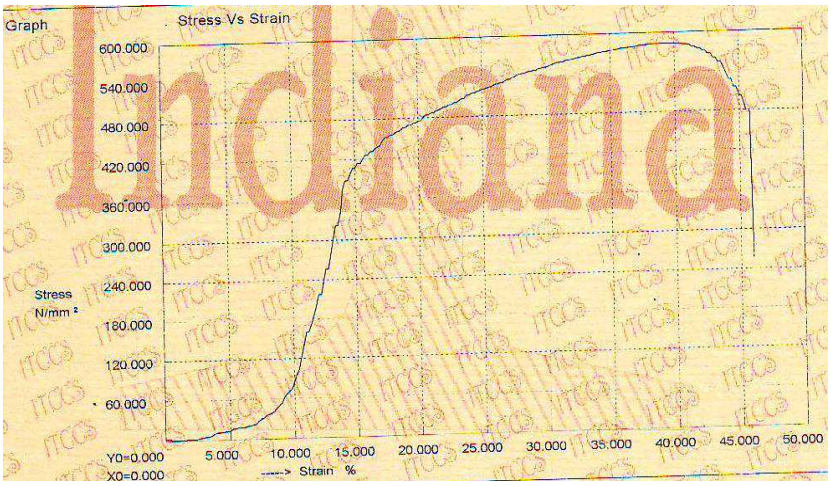

Figure 11.18: Graphical representation of stress vs. strain of SS 316 of specimen no.-8

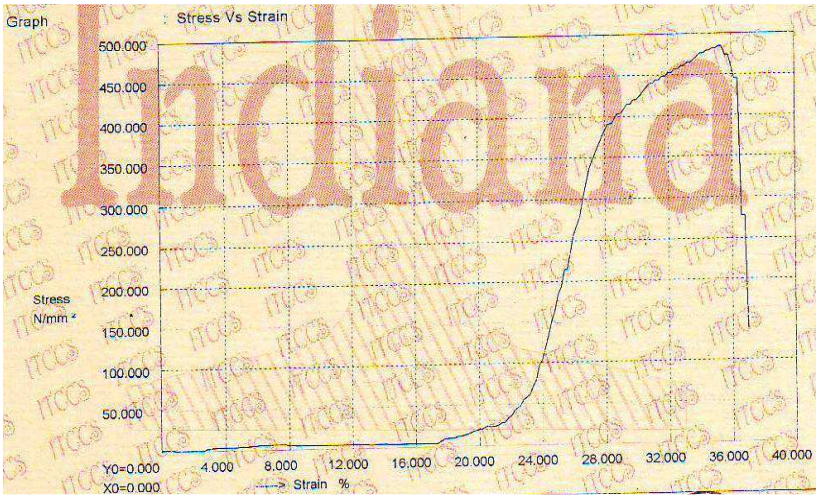

Figure 11.19: Graphical representation of stress vs. strain of SS 316 of specimen no.-9

CHAPTER 12 CONLUSION AND FUTURE SCOPE

The effect of process parameters i.e. Current, Gas type, Gas flow rate and Grove angle on austenitic stainless steel SS310 and SS316 have been studied along with a statistical technique. ANOVA was used to predict important parameters resulting into desired outputs. Some results consolidated from ANOVA and plots based on L9 orthogonal array are given below:

12.1 CONCLUSIONS

12.1.1 WELD BEAD GEOMETRY

- The weld bead width of SS 310 depends mainly on current and the type of shielding gas used for welding. It has been noticed that bead width increases with increase in current as current is seen to be contributing approximately 55% among all other parameters under study. The argon gas results in less bead width which is desired. The plot for main effect shows the combination of parameters 130A, Argon gas, 12 L/min. gas flow rate and grove angle of 75^{o} gives minimum bead width in practice.
- Bead height of SS 310 depends mainly on the grove angle. The minimum bead height is desired in most of the cases. It has been seen that bead height increases with increase in current but determining factor is grove angle. The plot for main effect shows the combination of parameters 130A current, helium gas with intermittent level flow rates of 9 L/min. and grove angle 90^{o} gives minimum bead height in practice.
- The optimised mean value of bead width and bead height at 95 % confidence for SS 310 is 7.977 ± 0.745 mm and 0.880 ± 0.077 mm respectively.
- The weld bead width of SS 316 depends mainly on current and the type of shielding gas used for welding. It increases with increase in value of current. The plot for main effect shows the combination of parameters 130A current, argon gas, intermittent gas flow rates of 12 L/min. at 75^{o} grove angle gives minimum bead width in practice. It also shows that the use of helium gas is results in increased bead width.
- Bead height of SS 316 depends mainly on the grove angle and value of current. It has been seen that bead height increases with increase in current but determining factor is grove angle. The plot for main effect shows the combination of parameters 130A, helium gas, 9 L/min. gas flow rate and grove angle of 75^{o} gives minimum bead width in practice for SS316 grade.
- The optimised mean value of bead width and bead height at 95 % confidence for SS 316 is 7.834 ± 0.848 mm and 0.887 ± 0.077 mm respectively.

12.1.2 DYE PENETRATION TEST

The dye penetration test results shows that welding carried out was successful as there were minor surface cracks on few plates likewise specimen no. 7 of SS 310 and specimen no. 1 and 8 of SS 316. It has been observed that start or end of welding may show minor defects at corners which were considered as rejection as discussed earlier on account of start and end of weld. So it can be concluded that no major defects were found over effective length of the welded plates.

12.1.3 BULK HARDNESS (ROCKWELL) TEST

Rockwell hardness test carried out on C-scale with a diamond indenter shows that there is no considerable variation in the values of hardness in the defined zone. When moving away from weld bead, it has been also observed that readings are approximately similar with respect to position nearby each other in weld metal, heat affected zone and base metal for both SS 310 and SS 316 grades.

12.1.4 CHARPY IMPACT TEST

- The result of Charpy impact test for SS 310 at room temperature shows that the value of toughness depends mainly on current and type of the gas used. The effect of gas flow rate and angle is almost negligible. The value of toughness is higher when the value of current is higher as the current contributes about 60.6 % among all other parameters. The maximum toughness of about 112.7 J (210A, argon, 9 L/min and 75^{o}) was obtained in experiment no. 7. The plot for main effect shows the combination of parameters 210 A, argon gas, 9 L/min. gas flow rate and grove angle of 60^{o} gives maximum toughness in practice for SS316 grade.
- The result of Charpy impact test for SS 310 at -20^{o} C temperature shows that the value of toughness depends mainly on current and type of the gas used. The maximum toughness of about 105.35 J (210A, argon, 9 L/min and 75^{o}) was obtained in experiment no. 7. The plot for main effect shows the combination of parameters 210 A, argon gas, 9 L/min. gas flow rate and grove angle of 60^{o} gives maximum toughness in practice for SS316 grade. The figure 8.2 shows by comparing results of SS 310 at room temperature and at -20^{o} C that value of toughness decreases with decrease in surrounding temperature.
- The optimised mean value of toughness at 95 % confidence for SS 310 at room temp. is 112.98 ± 6.929 joules.

- From response table for means the optimum value of toughness at -20^{O}C can be estimated as 100.45 joules as no optimisation can be done since current is the only significant factor.
- The result of Charpy impact test for SS 316 at room temperature shows similar result that the value of toughness depends mainly on current and type of the gas used. The effect of gas flow rate and angle is almost negligible. The value of toughness is higher when the value of current is higher. The plot for main effect shows the best combination of parameters 210 A, argon gas, 9 L/min. gas flow rate and grove angle of 90^{o} gives maximum toughness in practice for SS316 grade.
- The result of Charpy impact test for SS 316 at -20^{o} C temperature shows that the value of toughness depends mainly on current and type of the gas used. From percentage contribution point of view the grove angle is least significant among all parameters. The maximum toughness of about 102.9 J was obtained at 210A current value. It can be concluded by comparing results of SS 316 at room temperature and at -20^{o} C that toughness decreases with decrease in surrounding temperature.
- The optimised mean value of toughness at 95 % confidence for SS 316 at room temperature is 108.08 ± 6.929 joules
- The optimised mean value of toughness at 95 % confidence for SS 316 at -20^{o} C is 105.91 ±6.929 joules

12.1.5 MICROHARDNESS (VICKER'S) TEST

- Microhardness test on both SS 310 and SS 316 shows that the current is the most significant factor affecting the microhardness in a particular way as shown in the results. The maximum value of microhardness was obtained at 170 A current. Among different type of gases used in present study, helium results in higher hardness at 60^{o} grove angle. The maximum hardness value for SS 310 obtained was 116.61 HVN and for SS 316 was 111.97 HVN.
- The optimised mean value of microhardness at 95 % confidence for SS 310 is 106.15 HVN
- The optimised mean value of microhardness at 95 % confidence for SS 316 is 105.85 HVN

12.1.6 CHEMICAL COMPOSITION ANALYSIS

- Chemical composition result analysis for SS 310 shows that there is a slight increase in the percentage of nickel and iron in weld bead as compared to base metal on the other hand decrease in composition of chromium has been noticed. This may be due to formation of different compounds in welded region.
- Chemical composition result analysis for SS 316 shows that there is a slight increase in the composition of iron and manganese whereas there is decrease in percentage composition of carbon, nickel and chromium as compared to the values of the base metal This may be due to formation of different compounds in welded region on account of enormous heat generated.

12.1.7 TENSILE TEST

The result obtained after carrying out tensile testing on both SS 310 and SS316 shows some kind of unpredictable behaviour due to unknown reasons for few samples. Discontinuities or internal defects in the raw material may have resulted so. In case of SS 310 the maximum tensile strength of 575.617 Mpa was obtained in experiment number 8 with current value of 210A, 9L/min gas flow rate, grove angle of 90^{o} and gas used was helium. On the other hand in case of SS316 the maximum tensile strength of 607.810 Mpa was obtained in experiment number 3 with current value of 130A, 15L/min gas flow rate, grove angle of 90^{o} and gas used was mixture of argon-helium.

12.1.8 EFFECT OF TYPE OF SHIELDING GAS

- The pilot study done by using all gases each at one time without using any filler material shows that use of pure helium and mixture of argon-helium resulted in an increased welding speed when compared with argon gas. This gives an edge in welding conditions whenever integrity of weld is required along with saving in time is desirable too.
- The helium results in obtaining minimum weld bead height but darkens the region around weld and moreover higher flow rates are required because of its lighter nature. The cleansing action is lowest with helium.

12.2 FUTURE SCOPE

In continuation of present work, further work can be carried out in future in following directions:

- The study can be carried out by using different inert gases available in different proportions on various properties of steel.
- The study of effect of different grades filler material on mechanical properties of steel can be done.
- Parameters like current, voltage, welding speed, diameter of electrode/filler, electrode extension can be varied either individually to see their individual effect or combined together to see their combined effect on properties of material.
- Microstructure analysis may be carried out on welded plates by using S.E.M, XRD etc.
- In addition of destructive mechanical testing, other non-destructive testing like ultrasonic welding, radiography etc can be done.

CHAPTER 13 REFERENCES

[1] "A Textbook of Production Technology", P.C. Sharma, S.Chand, 2004 edition.

[2] http://en.wikipedia.org/wiki/Gas_tungsten_arc_welding

[3] http://www.millerwelds.com/pdf/gtawbook.pdf

[4] http://www.itl.nist.gov/div898/handbook/pmd/section3/pmd31.htm

[5] Wang, Sun, Na, Zhou, .Han,Wang, "Effects of TIG Welding Parameters on Morphology and Mechanical Properties of Welded Joint of Ni-base Superalloy." Procedia Engineering 10 (2011) 37–41.

[6] Kumar, Shahi, "Effect of heat input on the microstructure and mechanical properties of gas tungsten arc welded AISI 304 stainless steel joints." Materials and Design 32 (2011) 3617–3623.

[7] Goyal, Sandhya, Valsan, Bhanu Sankara Rao, "The effect of thermal ageing on low cycle fatigue behaviour of 316 stainless steel welds." International Journal of Fatigue 31 (2009) 447–454.

[8] Lu, Fujii , Nogi "Arc ignitability, bead protection and weld shape variations for He–Ar–O2 shielded GTA welding on SUS304 stainless steel. " journal of materials processing technology 2 0 9 (2 0 0 9) 1231–1239.

[9] Bayraktar, Moiron, Kaplan, "Effect of welding conditions on the formability characteristics of thin sheet steels: Mechanical and metallurgical effects." Journal of Materials Processing Technology 175 (2006) 20–26.

[10] Dhas ,Hexley Dhas , "A review on optimization of welding process." Procedia Engineering 38(2012) 544-554.

[11] Nagesh, Datta, "Genetic algorithm for optimization of welding variables for height to width ratio and application of ANN for prediction of bead geometry for TIG welding process." Applied Soft Computing 10 (2010) 897–907

[12] Benyounis, Olabi, “Optimization of different welding processes using statistical and numerical approaches – A reference guide.” Advances in Engineering Software 39 (2008) 483–496.

[13] Juang, Tarng, “Process parameter selection for optimizing the weld pool geometry in the tungsten inert gas welding of stainless steel.” Journal of Materials Processing Technology 122 (2002) 33–37

[14] Traidia, Roger, “Numerical and experimental study of arc and weld pool behaviour for pulsed current GTA welding.” International Journal of Heat and Mass Transfer 54 (2011) 2163–2179.

[15] Correa, Costa, Santos, “Studies on weldability of iron-based powder metal alloys using pulsed gas tungsten arc welding process.” journal of materials processing technology 2 0 9 (2 0 0 9) 3937–3942

[16] Balasubramanian, Jayabalan, Balasubramanian, “Effect of pulsed gas tungsten arc welding on corrosion behaviour of Ti–6Al–4V titanium alloy.” Materials and Design 29 (2008) 1359–1363.

[17] Lothongkum, Viyanit, Bhandhubanyong, “TIG pulse welding of 304L austenitic stainless steel in flat, vertical and overhead positions.” Journal of Materials Processing Technology 89-90 (1999) 410-414

[18] Li, Lu, Dong, Dianzhong Li, Yiyi Li, “Study of the law between the weld pool shape variations with the welding parameters under two TIG processes” Journal of Materials Processing Technology 212 (2012) 128– 136

[19] Arivazhagan, Surendra Singh, Satya Prakash, G.M. Reddy, “Investigation on AISI 304 austenitic stainless steel to AISI 4140 low alloy steel dissimilar joints by gas tungsten arc, electron beam and friction welding.” Materials and Design 32 (2011) 3036–3050.

[20] J.J. del Coz Díaz , P. Menéndez Rodríguez , P.J. García Nieto , D. Castro-Fresno, “Comparative analysis of TIG welding distortions between austenitic and duplex stainless steels by FEM.” Applied Thermal Engineering 30 (2010) 2448-2459.

[21] Cabello Mun˜ oza, Ruckert , Huneaua, Sauvageb, Marya, “Comparison of TIG welded and friction stir welded Al–4.5Mg–0.26Sc alloy” journal of materials processing technology 1 9 7 (2 0 0 8) 337–343

[22] Squillace, Fenzo,. Giorleo, Bellucci, “A comparison between FSW and TIG welding techniques: modifications of microstructure and pitting corrosion resistance in AA 2024-T3 butt joints” Journal of Materials Processing Technology 152 (2004) 97–105.

[23] Tseng, Hsu, “Performance of activated TIG process in austenitic stainless steel welds” Journal of Materials Processing Technology 211 (2011) 503–512.

[24] Huang, “Research on the Activating Flux Gas Tungsten Arc Welding and Plasma Arc Welding for Stainless Steel ” Met. Mater. Int., Vol. 16, No. 5 (2010), pp. 819~825.

[25] Xu , Dong, Wei, Yang, “Marangoni convection and weld shape variation in A-TIG welding process” Theoretical and Applied Fracture Mechanics 48 (2007) 178–186

[26] Kanga, Yarlagadda , Prasadb, Kanga, Kima, Kimc, “The effect of alternate supply of shielding gases in austenite stainless steel GTA welding” Journal of Materials Processing Technology 209 (2009) 4722–4727.

[27] Durgutlu, “Experimental investigation of the effect of hydrogen in argon as a shielding gas on TIG welding of austenitic stainless steel” Materials and Design 25 (2004) 19–23.

[28] Ming Gao, Zeng, Hu, “Effects of gas shielding parameters on weld penetration of CO2 laser-TIG hybrid welding” Journal of Materials Processing Technology 184 (2007) 177–183

[29] www.itl.nist.gov/div898/handbook/pri/section3/pri32.html

[30] http://mee-inc.com/rockhar.html

[31] Anirban Bhattacharya, Narnder Bansal, “An experimental investigation on welding aspects of stainless steel SS202 and SS 304 during GTAW” (December 2012)